ΠΟΛΥΤΕΧΝΕΙΟ ΚΡΗΤΗΣ / TECHNICAL UNIVERSITY OF CRETE

Accelerator mass spectrometry, principles and its use in environmental radioactivity research

Φασματοσκοπία μάζας με χρήση επιταχυντών, βασικές αρχές και εφαρμογές στην ραδιολογική έρευνα περιβάλλοντος

Master's diploma thesis
2024

Student:
Petros Leivadaros[1,2]

Supervising Professors:
Nikolaos Kallithrakas-Kontos[1]
Nikolaos Pasadakis[1]
Jan John[2]

[1]Technical University of Crete

[2]Czech Technical University in Prague

Acknowledgements

For the acknowledgements of this work, I would need to compile a long list of names of people who have truly been catalysts for its continuation. A list longer than the space I should occupy here. First and foremost the professors of my master's degree who allowed me during my PhD to migrate from Greece abroad in search of work, while fulfilling my obligations in the postgraduate program, especially Professor Kallithrakas Kontos Nikolaos who helped me, especially during the last years in the writing of my diploma thesis and Professors Pasadakis Nikolaos and Professor Despina Vamvouka who allowed me to continue my studies despite the extensive extension upon completion of my diploma thesis.

For the continuation of my research project, I have to mention project “RAMSES - Ultra-trace isotope research in social and environmental studies using accelerator mass spectrometry “funded by MEYS and European Union – European Structural and Investment Funds, Operational Programme Research, Development and Education.
Obviously, the department of Nuclear Chemistry of the Faculty of Nuclear Sciences and Physical Engineering of the Czech Technical University in Prague, which has supported me academically and financially, in the last few years.

I want to extend a heartfelt thank you to a group of people from my PhD department who continue to actively help me in the continuation of my research for my doctoral dissertation professors such as my professor and supervisor Jan John and Professor Mojmír Němec, but also my professors and doctoral colleagues Tomáš Prášek, Martin Daňo, Pavel Bartl, Miroslava Semelová, Miriam Mindová, Katerina Fenclova, and Stepanka Malinakova, who devoted valuable time from their daily lives during their work and beyond in order to help me fill my cognitive and technical gaps. And of course, all those people who helped me in partial periods of my research such as the team from NMBU in Norway, head and Professor Ole Christian Lind and my friends Karl Andreas Jensen and Simon Jerome.

But as in my previous work, so now I have to dedicate a few lines to the people who have not stopped standing by my side for a minute since the beginning of my first academic steps in 2011, since the first undergraduate program I enrolled in, are the same people who supported me in all my decisions and risks, are none others than my two parents, Pothitos Leivadaros and Ariadne Terlaki. As a minimum sign of gratitude, I try in my research works to always accompany my name with their names at the same time.
And, in the end, of course, a huge thank you to the people who have been by my side, not only academically, but also socially. I am grateful to my very good new friend, Ondřej Holas, and others who have shared interesting ideas and thoughts with me upon our fieldwork and beyond it.

To all these people and many more, I am expressing my deepest gratitude for everything I gained from them, and I know that soon I will write again about them on my future steps on my academic journey, and my research upon the existing…

Graphical Abstract

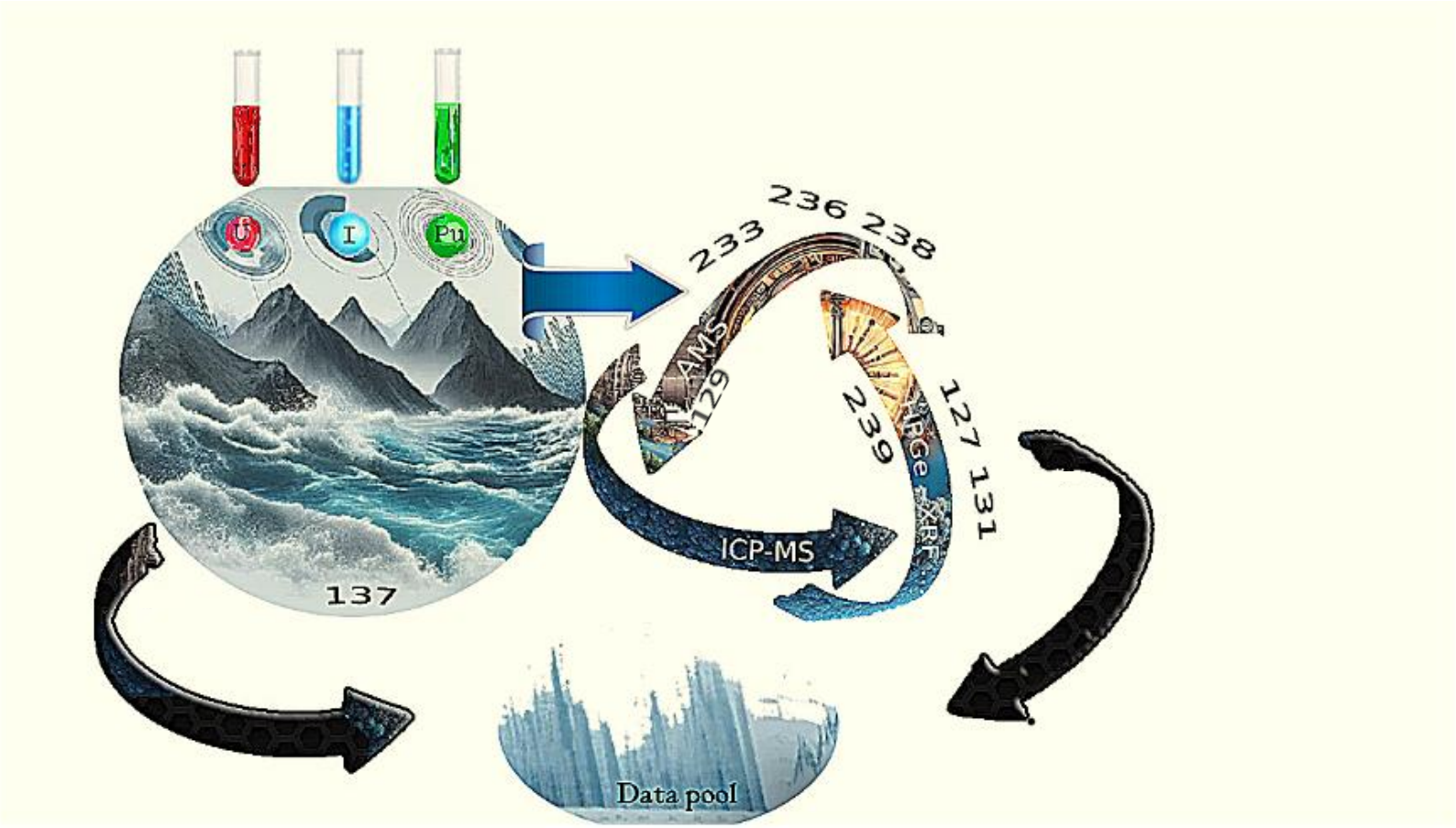

Abstract

Data from Norway and Greece, as well as from an opportunistic sampling case in Denmark, were collected and processed appropriately at laboratory level to provide information through three basic analytical methods. This thesis is not only part of a postgraduate thesis, but is part of an overall project for a complete and expanded research work in the context of environmental radiological studies. It is part of the "RAMSES" program as well as my PhD thesis which is currently in progress. In summary, it can be mentioned that the central objective in this text is not focused on the presentation of data as such (which, however, have been taken and analyzed from various longitudes and latitudes of the earth), but the demonstration of the methodology and analytical thinking on which our research is based, and the conflict of a new way of perceiving and using analytical tools in environmental studies and especially in oceanography. More specifically, the analyses of the ratios between selected radioisotopes of 3 different, but essential and interlinked elements in the environment, uranium, plutonium and iodine respectively, can well function as elements of analysis and detection of both the sea masses that carry them and their sediments.

The central methodologies described in this work and used are in turn AMS (Accelerator Mass Spectrometry) and ICP-MS (Inductively Coupled Plasma Mass Spectrometry) as well as XRF (X-ray Fluorescence methods). Both chemical treatment and further measurements and detection systems are described in separate chapters, while a comparative and combined attempt to illustrate our research hypothesis is attempted separately towards the end of the thesis with the controversy of further discussion. It is clear, as stated in individual sections of this work (with references to other research projects) that analytical procedures, especially in environmental studies, are not only not methodologically limited but instead seek to further expand these scientific tools and their methodologies. Both previous studies and promising proposals for future work are discussed and presented alongside the approved species, and tested methods widely used at present.

Περίληψη

Δεδομένα από τη Νορβηγία και την Ελλάδα, καθώς επίσης και από μία ευκαιριακή μόνο-δειγματοληπτική περίπτωση από τη Δανία, συλλέχθηκαν και επεξεργάστηκαν κατάλληλα σε εργαστηριακό επίπεδο ώστε να παρέχουν πληροφορίες μέσω τριών βασικών αναλυτικών μεθόδων. Η παρούσα εργασία δεν αποτελεί απλά ένα κομμάτι μιας μεταπτυχιακής διπλωματικής εργασίας, αλλά εντάσσεται εντός ενός συνολικότερου έργου για μία ολοκληρωμένη και διευρυμένη ερευνητική εργασία στα πλαίσια περιβαλλοντικών ραδιολογικών μελετών. Αποτελεί μέρος του προγράμματος «RAMSES» καθώς επίσης και της διδακτορικής διατριβής μου η οποία βρίσκεται εν εξελίξει. Συνοπτικά μπορεί να αναφερθεί ότι η κεντρική στοχοθεσία στο παρόν κείμενο δεν δίνει το κέντρο βάρους στην παρουσίαση των δεδομένων αυτών-καθαυτών (τα οποία ωστόσο έχουν ληφθεί και αναλυθεί από διάφορα μήκη και πλάτη της γης), αλλά στην κατάδειξη της μεθοδολογίας και της αναλυτικής σκέψης πάνω στην οποία βασίζεται η εν εξελίξει έρευνά μας, και η προσέγγιση ενός νέου τρόπου αντίληψης και χρήσης των αναλυτικών εργαλείων στις περιβαλλοντολογικές μελέτες, και ειδικότερα στην ωκεανογραφία. Πιο συγκεκριμένα, οι αναλύσεις των αναλογιών μεταξύ επιλεγμένων ραδιοϊσοτόπων από τρία διαφορετικά, αλλά ουσιαστικά «συγκοινωνούντα» ως στοιχεία στο περιβάλλον, του ουρανίου, του πλουτωνίου και του ιωδίου, μπορούν κάλλιστα να λειτουργήσουν ως στοιχεία ανάλυσης και ανίχνευσης τόσο τον θαλάσσιων μαζών που τα φέρουν όσο και των ιζηματαποθέσεών τους.

Οι κεντρικές μεθοδολογίες οι οποίες περιγράφονται σε αυτήν την εργασία και χρησιμοποιούνται είναι η AMS (Accelerator Mass Spectrometry), η ICP-MS (Inductively Coupled Plasma Mass Spectrometry) καθώς επίσης και η XRF (X-ray Fluorescence methods). Τόσο η χημική επεξεργασία όσο και οι περεταίρω μετρήσεις και τα ανιχνευτικά συστήματα περιγράφονται σε ξεχωριστά κεφάλαια, ενώ μια συγκριτική και συνδυαστική προσπάθεια απεικόνισης της ερευνητικής υπόθεσής μας, επιχειρείται ξεχωριστά προς το τέλος της εργασίας για τη διεξαγωγή μιας περαιτέρω συζήτησης. Είναι σαφές όπως αναφέρεται και σε επιμέρους τμήματα της εργασίας (με αναφορές και σε άλλα ερευνητικά έργα) ότι οι αναλυτικές διαδικασίες, ιδιαίτερα στις περιβαλλοντολογικές μελέτες, όχι μόνο δεν περιορίζονται μεθοδολογικά, αντ' αυτού επιδιώκεται η περεταίρω διεύρυνση αυτών των επιστημονικών εργαλείων και των μεθοδολογιών τους. Τόσο προγενέστερες μελέτες όσο και ελπιδοφόρες προτάσεις για μελλοντικές εργασίες συζητούνται και παρουσιάζονται παράλληλα με τις ήδη εγκεκριμένες και ελεγμένες μεθόδους που χρησιμοποιούνται ευρέως στην παρούσα περίοδο.

Prelude

At the prelude to this thesis, I would like to refer to the main reasons that led me to continue and complete this second postgraduate program in a period of particular personal and social instability with intense radical changes in my daily life and in my life in general. A cornerstone of my search for new research and academic skills has always been and always is the innate, I think innate, tendency of our species to seek and stir up the dust of reality - as a habit more or less childish and spontaneous - in an effort to overcome and defeat the mortality that binds us to the ground.

At a time when the social freedoms and cultural heritage of our species are being put into a maze of insanity, subordinate mediocrity, and dehumanization, at all levels of our social and individual lives. At a time when, especially in Greece, the social acquises of free education and beyond, seem to be precipitating under the weight of a darkened period (economically, socially and politically), it is our duty as parts of the academic and scientific community, but also active members of society, to suggest ways to ostracise and deconstruct demagoguery. By its very existence, the scientific ideal itself is an act of resistance against the mediocrity of the existing and the obfuscation of the mind. As Neil deGrasse Tyson has very characteristically stated in an interview "Science is humanity at its best". Indeed, this rallying around a common, universally accepted, lofty purpose, which will transcend our existence and individuality, on an ideal, moral and practical level, that of seeking our place and role in the universal becoming, is, I believe, and must always be centered as the cornerstone around which education and education should revolve.

From the shattered social fabric of the Greek reality and the privatization of the universities to occupied Palestine and the atrocities embodied there upon the Palestinian people, on a terrible decline of the human species, on an institutional, moral and social level, we are obliged to set new values and ideals in a world that needs a new perspective on an international level, against oppression and barbarism, for the total social and individual liberation of all. It was anyway the first glance from the moon to the earth that prompted the human species to perceive its entity as one, it was this first moment when the knowledge and perception of its existence was revealed in its entirety, as a single fragile but at the same time enchanting patchwork that gave birth even for a while to some essential ideas and raised new questions concerning what we are, who and where we are heading as beings.

∾*∾

Πρελούδιο

Στο προοίμιο αυτής της εργασίας θα ήθελα, να αναφερθώ στους βασικούς λόγους που με οδήγησαν να συνεχίσω και να ολοκληρώσω αυτό το δεύτερο μεταπτυχιακό πρόγραμμα, σε μία περίοδο ιδιαίτερης προσωπικής και κοινωνικής αστάθειας, με έντονες και ριζικές αλλαγές στην καθημερινότητά μου και στη ζωή μου γενικότερα. Ακρογωνιαίος λίθος πάντα στην αναζήτηση μου για νέες ερευνητικές και ακαδημαϊκές δεξιότητες υπήρχε και υπάρχει πάντα η, θεωρώ έμφυτη, τάση του είδους μας να αναζητεί και να αναμοχλεύει τη σκόνη της πραγματικότητας - σαν μία συνήθεια λίγο πολύ παιδική και αυθόρμητη - σε μία προσπάθειά του να υπερπηδήσει και να νικήσει τη θνητότητα που το δεσμεύει στο χώμα.

Σε μία περίοδο όπου οι κοινωνικές ελευθερίες και η πολιτισμική κληρονομιά του είδους μας βάλλεται, μέσα σε ένα κυκεώνα παραφροσύνης, υποβάλλουσας μετριότητας, και αποκτήνωσης, σε όλα τα επίπεδα του κοινωνικού και ατομικού μας βίου. Σε μία περίοδο που ιδιαίτερα στην Ελλάδα τα κοινωνικά κεκτημένα της δωρεάν παιδείας και όχι μόνο φαίνεται να κατακρημνίζονται υπό το

βάρος μιας συσκοτισμένης περιόδου (οικονομικά, κοινωνικά και πολιτικά), είναι χρέος μας σαν κομμάτια της ακαδημαϊκής και επιστημονικής κοινότητας, αλλά και ενεργά μέλη της κοινωνίας να υποδείξουμε τρόπους εξοστράκισης και αποδόμησης των δημαγωγιών. Με την ίδια του την ύπαρξη το επιστημονικό ιδεώδες, αυτό καθ' αυτό, αποτελεί μία πράξη αντίστασης απέναντι στη μετριότητα του υπάρχοντος και την συσκότιση του νου. Όπως πολύ χαρακτηριστικά έχει αναφέρει ο Neil deGrasse Tyson σε μία συνέντευξή του «η επιστήμη είναι η ανθρωπότητα στα καλύτερά της». Όντως αυτή η συσπείρωση γύρω από έναν κοινό, καθολικά αποδεχόμενο, υψηλόφρονα σκοπό, ο οποίος θα υπερβαίνει την ύπαρξη και την ατομικότητά μας, σε ιδεατό, ηθικό και πρακτικό επίπεδο, αυτόν την αναζήτησης της θέσης και του ρόλου μας στο συμπαντικό γίγνεσθαι, αποτελεί θεωρώ, και πρέπει να κεντροβαρεί πάντα ως το ακρογωνιαίο στοιχείο, γύρω από το οποίο η παιδεία και η εκπαίδευση θα πρέπει να περιφέρεται.

Από τον κατακρεουργημένο κοινωνικό ιστό της ελληνικής πραγματικότητας και την ιδιωτικοποίηση των πανεπιστημίων, μέχρι την κατεχόμενη Παλαιστίνη και τις κτηνωδίες οι οποίες ενσαρκώνονται εκεί, σε βάρος των παλαιστινίων, σε μια τρομακτική κατάπτωση του ανθρώπινου είδους, σε θεσμικό, ηθικό και κοινωνικό επίπεδο, είμαστε υποχρεωμένοι να θέσουμε νέες αξίες και ιδανικά σε έναν κόσμο ο οποίος έχει ανάγκη από μία νέα προοπτική σε διεθνές επίπεδο, ενάντια στην καταπίεση και την βαρβαρότητα, για την συνολική κοινωνική και ατομική απελευθέρωση όλων. Ήταν έτσι κι αλλιώς η πρώτη ματιά από τη σελήνη προς τη γη που ώθησε το ανθρώπινο είδος να αντιληφθεί την οντότητά του ως ένα, ήταν αυτή η πρώτη στιγμή που η γνώση και η αντίληψη της ύπαρξής του, φανερώθηκε στην ολότητά του, ως ένα ενιαίο εύθραυστο μα ταυτόχρονα μαγευτικό συνονθύλευμα που γέννησε έστω και για λίγο κάποιες ουσιαστικές ιδέες αντιλήψεις και έθεσε νέα ερωτήματα σε σχέση ως προς το τι είμαστε, ποιοι και ως προς το πού οδεύουμε ως όντα.

~*~*~*~*~~*~*~*~*~~*~*~*~*~~*~*~*~*~

Table of Contents

Introduction

In every environmental system, diverse and interrelated dynamics develop and communicate with their neighbouring ecological levels. In order to understand those dynamics and understand the mechanisms hidden behind the phenomena, an integrated analysis is necessary. And for that, natural sciences are the most suitable from every aspect. Field research and data representation and interpretation form the base of the natural sciences. Corresponding to that, the global scientific community has developed for generations comprehensive and integrated methods to examine phenomena and observations throughout a continuous spectrum of scientific fields and disciplines. As such, the need is to constantly try to develop and push the boundaries of interdisciplinarity until the panacea is found to unite the disciplines.

Nuclear chemistry is a specialized branch of chemistry that combines the science of radioactivity and chemistry. It uses chemical knowledge to study radioactivity and radioactive substances for chemical research. This field delves into the properties, behaviours, and reactions of atomic nuclei, as well as their interactions with subatomic particles such as protons, neutrons, electrons, and antiparticles. This field of study has numerous practical applications in various fields, including materials science, energy production, and medicine. Radioactivity is a fundamental concept in nuclear chemistry, referring to the spontaneous emission of energy or particles from unstable atomic nuclei. Radioactive decay can occur through different processes, such as alpha, beta, and gamma decay.

It also involves the study of nuclear reactions, which involve changes in the number of protons and/or neutrons in an atom's nucleus. Such reactions can release massive amounts of energy and have practical applications in nuclear power plants, medical imaging, and nuclear weapons. Stable isotopes are another important aspect of nuclear chemistry and refer to atoms of the same element with varying numbers of neutrons. Isotopes (both radioactive and stable) play significant roles in diverse fields such as environmental science, geology, and medicine. Overall, nuclear chemistry is a complex and captivating field with important implications for our understanding of the world.

By adapting the nuclear chemistry methods into marine sciences and oceanographic research we can create a comprehensive research field with a clear depiction of what we call reality. Oceanography is mistakenly considered usually as a discipline that contributes and focuses only on the vast oceanic environment and the phenomena occurring there and only there. In reality, it is a way wider area where the water, as a global mean of connection between the vivo and non-vivo, interacts, transforms and recirculates in a non-ending cycle. From the biological cycles to the elemental porous adsorption and from tectonic movements to the global circulation and climate, oceanography and marine sciences exist and contribute to the overall understanding of our world and existence.

From material extraction, handling and reformation, to the vital sustainable maintenance of our ecosystem and social structure, environmental monitoring and process understanding represent the hammer of Hephaestus. It is not only crucial to understand the complexity of the world that surrounds us but also to figure out the ways to integrate our existence in the most sufficient way.

This is where the natural sciences appear to be the pinnacle of our species' efforts. Throughout those processes, we develop and evolve society and bio in an absolute interconnection.

1. General

In this research work, the primary focus developed around oceanographic research was sustained by the use of advanced tools from the scientific area of nuclear chemistry. Physicochemical

characteristics and radio-isotopic ratios have already proved valuable tools and future advances seem more than promising. Those techniques and approaches we will try to analyze and unfold in front of an integrated and comprehensive ongoing research.

Sediment, soil and water samples from different areas in the Northern hemisphere are anticipated to give information about the current state of these regions as well as their influencers' origins and in time their overall place in the global interconnected physicochemical circulation network.

1.1. Oceanography

Marine science and oceanography can be considered the same field with different nomenclature, part of a vast family of environmental sciences. Is such the nature of this field that almost every scientific field meets in the center of an integrated environmental science. The endless cycle of destruction and recreation of the oceanic tectonic plates refills our world with material that boosts a huge physicochemical circle that penetrates living and non-living things.

Both mid-ocean spreading ridges and subduction zones are among Earth's most important tectonic features. Those huge structures have momentous influence on the planets' evolution and transformation. The lithosphere that forms at ridges is recycled eventually into the mantle through subduction processes. The geophysical characteristics of subduction zones vary and are influenced by factors such as plate velocity, direction and angle of convergence, thickness and age of the lithosphere, convection to the mantle's overlying wedge, liquids and melted materials moving through the subduction zone, and time. These factors determine the evolution of subduction zones and the subsequent formation of volcanic arcs, which ultimately contribute to the development of continental masses (Blanco-Quintero et al., 2011). As a subducting oceanic plate moves towards a subduction-accretionary complex, materials get transferred or accreted, resulting in the formation of rock assemblages. These assemblages are made up of oceanic igneous rocks, which get progressively covered by pelagic sedimentary rocks such as chert and/or limestone, and trench-fill clastic sedimentary rocks that mostly consist of sandstone, shale/mudstone (Wakabayashi, 2017), together with the volcanic activity and the geomorphological and geothermal structure reformation, create the base for the base elementary flow and global thermohaline structure, modifying essentially the climate of our planet.

1.2. Nuclear chemistry

As mentioned above, nuclear chemistry is a branch of chemistry with some unique characteristics and advantageous practical uses. As we will describe further, radiochemistry as a field has contributed to the development of a series of analytical tools that can and already do find use in other fields or increase the efficiency of the results from a spectrum of field researches and studies.

Even only from an environmental perspective, one can easily observe the importance of an advanced chemical approach to any field study. The transfer of material from land to ocean plays a crucial role in determining the chemical composition of seawater and the global element cycles. This transfer is mainly influenced by the transport of particulate material from rivers to oceans. Numerous isotopic tracers such as $^{143/144}$Nd, $^{87/86}$Sr, $^{30/28}$Si, $^{56/54}$Fe & $^{232/230}$Th, provide evidence that a significant proportion of this particulate material dissolves in seawater once it reaches the oceans (Jeandel and Oelkers, 2015). The studies of those elemental cycles can be used both ways, to study the land-to-ocean transfer and the ocean-to-land (or organisms) transfer, with back-tracing being a tool for the tracking of the origin, path and influence of almost any possible chemical and molecular type, able to detect and analyse.

1.2.1. Radionuclides

Various ways have been proposed that can describe and classify nuclides into categories. This includes the one that ranks nuclides based on their half-life. In this way, the nuclides are divided into:

Stable nuclides. This category includes those nuclides that do not show radioactive decay. Initially, 264 stable nuclides were identified, but with the developing methods of analysis, the number is drastically reduced because it was found that some of them were not stable but decaying with a very long half-life. As an examples of stable nuclides, we may list e.g. the following: ^{12}C, ^{14}N and ^{16}O.

Primordial radionuclides. This category includes radioactive nuclides that have existed on Earth since the birth of the planet and that have a long half-life. All isotopes with half-life comparable to the age of the Earth (~4.54×10^9 years) belong to primordial nuclides, including ^{238}U ($t_{1/2}=4.47x10^9$ y), ^{40}K ($t_{1/2}=1.28x10^9$ y) and ^{89}Rb ($t_{1/2}=4.8x10^{10}$ y)(Dragović et al., 2006; "Primordial Radionuclides | nuclear-power.com," n.d.).

Secondary naturally occurring radionuclides. Those radionuclides are formed from the natural decays of the primordial radionuclides, with shorter half-lives. Among them, the best known are ^{226}Ra ($t_{1/2}=1600$ y), ^{222}Rn ($t_{1/2}=3.8$ d) or ^{234}Th ($t_{1/2}=24.1$ d).

Those produced by cosmic radiation. They are those nuclides that are constantly produced due to the effect of cosmic radiation on the atmosphere. This category includes tritium, ^{3}H ($t_{1/2}=12.3$ y) and ^{14}C ($t_{1/2}=5730$ y). Both of them are produced by the interaction of cosmic radiation with ^{14}N of the atmosphere.

Artificial radionuclides. Inside this category belong the nuclides produced in the reactors and/or experimental and other human activities. The best-known are ^{60}Co, ^{137}Cs and ^{24}Na.

It is also possible for nuclides to be grouped according to their atomic and mass numbers, as shown below:

Isotopes are nuclides that have the same atomic (Z) number and a different mass number (A=Z+n), i.e. a different number of neutrons. Carbon nuclei are cited as examples: $^{11}_{6}C$(radioactive), $^{12}_{6}C$(stable), $^{13}_{6}C$(stable) & $^{14}_{6}C$(radioactive).

Isobars are nuclides that have the same mass number (A), but a different atomic number (Z). Examples are carbon-14 and nitrogen-14: $^{14}_{6}C$ & $^{14}_{7}N$.

Isotons are nuclides that have the same number of neutrons (N), but a different number of protons, such as the nuclides carbon-13, nitrogen-14 and oxygen-15: $^{13}_{6}C$, $^{14}_{7}N$ & $^{15}_{8}O$, which have the same number of neutrons (A-Z=7).

Isomers are nuclides that have the same atomic and mass numbers, but different energy states. They are denoted by the letter m next to the mass number: ^{234m}Pa to distinguish them from the ground energy state, ^{234g}Pa where g is the ground state.

Isodifferential radionuclides are called radionuclides that have the same neutron proton difference, that is, they have the same n-p difference. In this category belong e.g. the radionuclides ^{174}Re, ^{176}Os, ^{13}N, ^{11}C, ^{17}O.

1.2.2. Decay processes

Unstable nuclei, driven by a spontaneous tendency to reach more stable structures which are characterized by smaller mass energies, start a process known as decay process. The time scale ranges from fractions of a second to billions of years. They are subject to the laws of the principle of

conservation of total energy, momentum and angular momentum, charge and mass number of the system.
The process of decay consists of two pathways, either the deterioration of the nuclear system of subatomic particles (the elementary particles that make up the nucleus of the atom, i.e. protons and neutrons, with the electrons occupying the energetic levels around it) to lower energy levels, or the change in the number of nucleons itself (A, Z) (i.e. change of atomic and/or mass number), in such a way that in the final chain reactions more stable nuclei result. These processes are always exoenergetic and are accompanied by the emission of electromagnetic radiation and/or particles.

Nuclides with Z>82 (elements after ^{208}Pb) that have been found on our planet or artificially prepared (until today up to Z=118) are metastable and deexcite by gradual decays through emission of alpha or beta radiation to stable nuclei with Z≤82. The unstable nuclei that exist today in nature come either from the initial nucleosynthesis (Big Bang), from cosmic explosive processes (e.g. supernovae), or from nuclear reactions that occur on Earth from natural and anthropogenic causes.

The largest percentage of naturally occurring radionuclides diffused in the earth's crust, with Z>82, are grouped into three series of natural radioactivity, which are: (a) the thorium series (4n) with parent ^{232}Th ($t_{1/2}$=1.39·10^{10}y) and final daughter ^{208}Pb, (b) the uranium series (4n + 2) with initial ^{238}U ($t_{1/2}$=4.51·10^{9}y) and final ^{206}Pb and (c) the actinium series (4n + 3) starting at ^{235}U ($t_{1/2}$=7.07·10^{8}y) and final product ^{207}Pb. The series of nuclei with a mass number A = 4n + 1 is missing, it was discovered after the creation of artificial radioisotopes in reactors. Today it does not exist in nature because its longest-lived nucleus, neptunium, has a half-life of 2.25·10^{6} years, which means that all nuclei created during cosmogony have decayed. This artificial series is the series of Neptunium (4n+1) with parent Neptunium ^{237}Np ($t_{1/2}$=2.25·10^{6} y) and final in ^{205}Tl ("Nuclear and Radiochemistry," n.d.; Vértes et al., 2010). The main characteristics of the four radioactive series are given in Table 1.2.1.1 below, while the decay chains of the three natural radioactivity series are shown in Figure 1.2.1.1. The neptunium series is no longer significant for the earthly environment for the reason that the species involved is characterised by comparable short half-lives (OpenStax, 2016).

Table 1.2.2.1: The four radioactive series (OpenStax, 2016).

Row	Name	Longest-lived isotope	$T_{1/2}$ (y)	Final decay product
4n	**Thorium**	**^{232}Th**	**1.39 x 10^{10}**	**^{208}Pb**
4n+1	**Neptunium**	**^{237}Np**	**2.25 x 10^{6}**	**^{205}Tl**
4n+2	**Uranium**	**^{238}U**	**4.51 x 10^{9}**	**^{206}Pb**
4n+3	**Actinium**	**^{235}U**	**7.07 x 10^{8}**	**^{207}Pb**

Apart from natural radiation, which is responsible for the largest percentage (~90%) average annual dose to men, medical procedures are the most important of the anthropogenic factors. These mainly include X-rays and, in some cases, irradiation by protons, β, neutrons and various radiotracers. The most important radionuclides in cases of nuclear weapons use are ^{131}I, ^{95}Zr, ^{90}Sr and ^{137}Cs. In nuclear power plants, ^{85}Kr gas is normally emitted at low activities, while in cases of nuclear accidents, there are large leaks of ^{133}Xe (Three Miles Island, USA) and ^{137}Cs (Chornobyl, northern Ukraine).

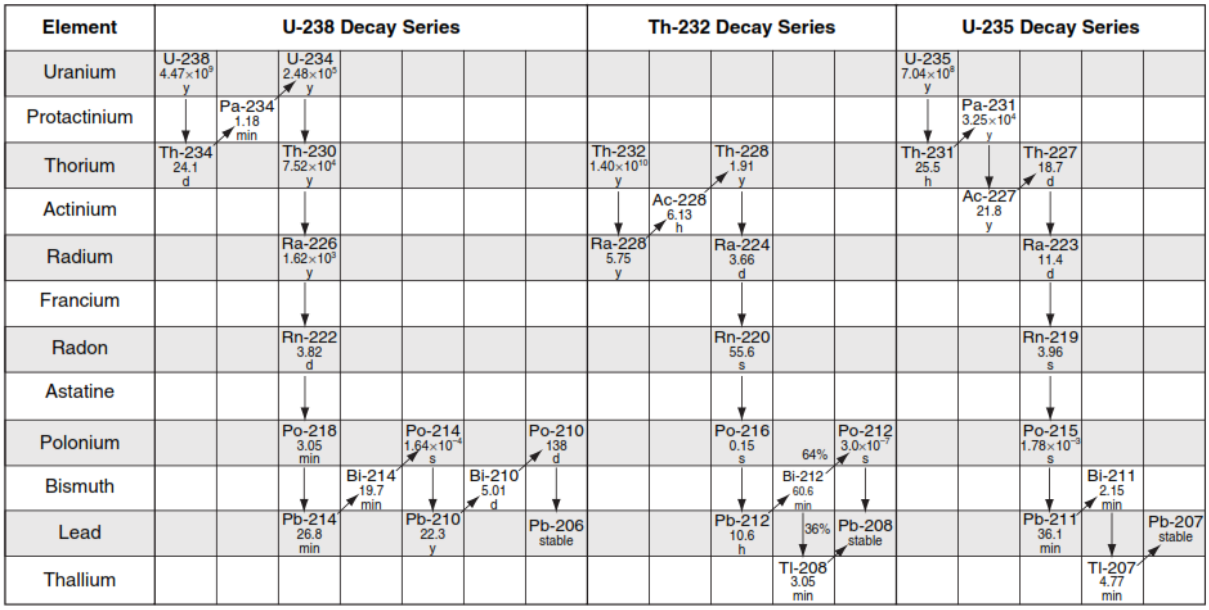

Graph. 1.2.2.1: Decay chains of the three natural radioactivity series and half-lives of individual isotopes. The vertical arrows designate deexcitation of the parent nucleus by α-decay, and the diagonal arrows by β-decay (Emerson and Hedges, 2008a, 2008b).

Nuclear deexcitation - Law of Sequential deexcitations

It has been established to call unstable nuclei radioactive and the quantity expressing the rate of deexcitation for a set of nuclei is called radioactivity (or activity). The exact time when a given radionuclide will decay is not possible to predict, but for a large number of nuclei, the law of statistical decay is accurate, and known and is the law of radioactive decay. The calculation of the decay rate of radioactive nuclei is governed by a common law for all kinds of radioactive decays and nuclei. The *Law of Radioactive Decay* by Rutherford and Soddy was established experimentally in the early 20th century and describes the exponential decrease over time in the activity of a radioactive sample (Leo, 1987).

The rate of deexcitation per unit time (the so-called radioactivity) is:

$$\frac{dN}{dt} = -\lambda N$$

where N is the number of radioactive nuclei present. By integrating the above equation, we conclude the following:

$$N_t = N_0 \exp(-\lambda t)$$

where N_0 is the number of nuclei at t=0 sec and λ (s^{-1}) is the decay constant characteristic of each nucleus, and if the nucleus decays in more than one way, then the constant λ is the sum of the decay constants for each process. The λ-decay constant gives the probability of nucleus decay in the unit of time. The statistical probability of decay of each radioactive atom, of a group of atoms, in the unit of time expressed by the numerical value of λ. For instance, if λ of an isotope is λ=0.01 s^{-1}, each atom of the isotope in a second has a 1% probability of decay and a 99% chance of not decaying. Thus, when a nucleus will decay is not predictable, nonetheless through the decay constant, the probability of decay is known.

The exponential dependence of N unbroken nuclei with time (t) is shown in the following figure:

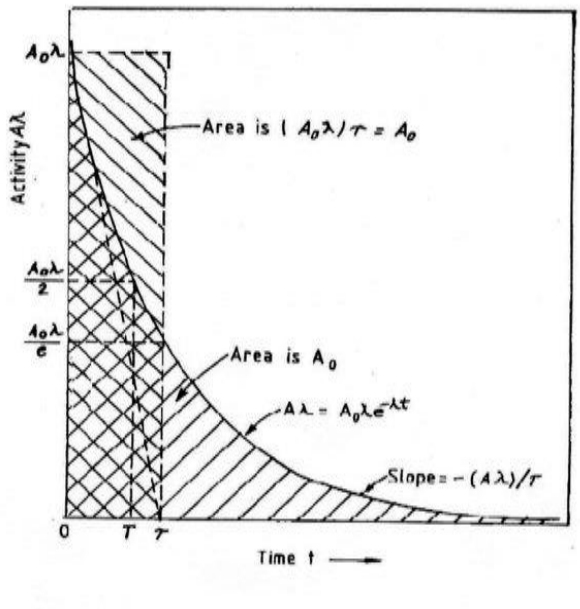

Graph. 1.2.2.2: Temporal evolution of a radioactive sample with an average lifetime $T_{1/2}$. Graphical relationship in the decay of a single radioactive nuclide. T=half-life, λ = decay constant, A_0 = number of atoms at time t=0, A=number of decays at t. The initial slope (dotted line) is extended, intersecting the time axis at the mean lifespan (T) (Bhaumik, 2014).

The half-life of a nucleus' decay, $t_{1/2}$, is the time during which half of the original radioactive nuclei have decayed. When $t = t_{1/2}$ will be $N = N_o/2$ so the law of radioactive decay will result:

$$No/2 = No\exp(-\lambda t_{1/2}) \Rightarrow t_{1/2} = \ln 2/\lambda = 0.693/\lambda$$

Both $t_{1/2}$ and λ are characteristic constants of a radioactive isotope. The larger the λ, the smaller the $t_{1/2}$.

The unit of measurement of the activity of an element used to be defined as Curie (Ci) which equals $3.70 \cdot 10^{10}$ decays in one second. The equivalent of this amount is approximately equal to the activity of one gram of ^{226}Ra. The unit of activity in the international SI system is Becquerel (Bq) corresponding to one decay per sec and the relation linking Bq to Ci is: 1 Ci = $3{,}70 \cdot 10^{10}$ Bq.

There are several types of radioactive decay that often compete with each other or occur sequentially. The most common are referred to as α, β and γ-decay indicating the emission of the corresponding type of radiation. The study of nuclear deexcitation was first initiated by the French physicist Antoine Henri Becquerel in the late 19th century, who was the first to observe these three types of radiation.

1.2.2.1. **α-decay**

In deexcitation by alpha decay, a nucleus emits a particle consisting of two protons and two neutrons, i.e. a 4E nucleus. α-decay may or may not be accompanied by gamma-ray emission, i.e. electromagnetic radiation. **The alpha-lability condition – a mass of the parent nuclide greater than the sum of the masses of the daughter nuclide and the alpha particle – is usually satisfied only for nuclei with mass number "A" greater than 140**.

$$_zX^A \rightarrow {}_{Z-2}Z^{A-4} + {}_2He^{4\,2+}$$

Alpha particles are always emitted with discrete values of kinetic energy, which is determined by the principles of conservation of momentum and energy. However, the spectra of alpha particles in terms of their energy, although discrete, contain enlarged peaks, due to the principle of indeterminacy and experimental factors. Since they are large, they can travel a few centimetres or meters at best in the air, before they collide with air molecules, and they easily are absorbed in

denser molecular grids (e.g. sheet of paper), due to their intense interaction with the molecules of matter.

1.2.2.2. **B-decay**

In β-decay, the mass number A remains constant while atomic Z varies. The switchover between proton and neutron is due to the weak interaction, through which the two basic reactions take place:

$$p^+ \Leftrightarrow n^0 + e^+ + \nu \qquad (1)$$

where a proton is converted into a neutron by simultaneously emitting a positron (positive electron), and a neutrino, as well as:

$$n^0 \Leftrightarrow p^+ + e^- + \bar{\nu} \qquad (2)$$

where a neutron is converted into a proton by simultaneously emitting an electron and an antineutrino, which is an uncharged elementary particle with near-to-zero mass. In other words, these are two-way reactions. They result from the transfer of a particle from one strand to another with its simultaneous replacement by its antiparticle.

Finally, another transition is observed, from the interaction of an electron with a proton, which in practice is the capture of an orbital electron (e.g. the K layer – K capture) :

$$p^+ + e^- \rightarrow n^0 + \bar{\nu} \qquad (3)$$

The three equations (1), (2) and (3) describe the three cases of β-decay, respectively: "β-" decay, "β+" decay, and electron capture (EC).

Depending on the energy possessed, beta particles can travel several meters in the air and are absorbed in a thin layer of metal or plastic.

1.2.2.3. **γ-decay**

In gamma-decay, there is deexcitation of the excited nucleus, i.e. nucleus whose nucleons are for some reason at higher energy levels than the ground state. During the deexcitation, electromagnetic radiation is emitted as the nucleus falls to a lower or ground state. The general equation for gamma-decay, where M* denotes the higher energy state is:

$$^A_Z M^* \rightarrow {}^A_Z M + (\gamma - rays)$$

There are three modes of decay associated with gamma-ray emission:

I. net gamma-ray emission
II. internal conversion (IC)
III. Auger electrons emission

In the first mode we have the creation of an elementary electromagnetic field, a photon, that transfers energy, momentum and angular momentum between the initial and final states, as required by conservation rules. The second mode takes place through the field of an atomic electron in the neighbourhood of the nucleus, while the electron carries the required energy, momentum and angular momentum, this process also, is also usually accompanied by the emission of Auger electrons.

2. Radioactivity and the environment

As we mentioned already, the natural environment consists of many different and dynamic fields, all of them interconnected to some level. Describing radioactivity as a phenomenon expectedly we are driven into the analysis of its relation with the environmental structure and dynamics. The ionizing radiation, natural (cosmic radiation or terrestrial radiation) or Man-made, follows and interacts with the flow of the elements globally, and on top of it adds significant characteristics to the carrier entities it exists with.

The fundamental principle of characterisation tracing is predicated on the following two assertions:

- **Firstly, the concentrations of radionuclides introduced into the environment should be higher closer to the discharge sources than at greater distances.**

- **Secondly, the mixing and the precipitation processes follow the same paths as the rest physicochemical characteristics of the water masses (salinity, dissolved elements etc.)**

2.1. Radioactivity in the marine environment

Some of the applications that have been developed in recent years include radionuclide measurements in seawater and sediments. Both laboratory and in situ techniques are used. The main isotopes studied in research by gamma-ray spectroscopy are the natural isotopes of ^{238}U, ^{232}Th, ^{40}K and the anthropogenic ^{137}Cs due to nuclear testing and nuclear accidents. Also, important tracers for the study of groundwater and seawater are the daughter nuclei of radon (^{222}Rn) and thoron (^{220}Rn) because they are in the gaseous state and have high solubility in water.

In summary, the main sources of artificial radioactivity in marine ecosystems are nuclear weapons testing, leaks and deposits from nuclear power plants and reactors, improper storage and dumping of nuclear waste in marine horizons, Chernobyl (1986) and Fukushima (2011) nuclear accidents, and finally submarine and aircraft accidents.

For indicative purposes, the study of radionuclides in the marine environment can provide information for estimating the residence time and age of water from submarine estuaries (coastal zone), transport and mixing of marine masses (^{137}Cs), sedimentation and deposition rates (^{210}Pb, ^{137}Cs), estimation of the age and time of formation of marine masses ($^{3}He/^{3}H$ pair), quantification of transport processes involving particles ($^{238}U/^{234}Th$), radioactive contamination of the seabed of coastal industrial areas (e.g. plants' fertiliser facilities, petroleum industry) and information of background radioactivity in various areas.

For the needs of monitoring after an accident systems for online monitoring of deep-sea environmental radioactivity, such as DSER (Li et al., 2016), have developed with improved crystal probes to adapt to the deep-sea environment. In other cases such as Aegean and Mediterranean study cases, radioisotopic concentrations have been used in combination with dissolved oxygen, salinity and dynamic temperature, in order to track down the subsurface flows, marine masses formation and the precipitation processes, in a very geologically, complex system (Leivadaros et al., 2022; Tsabaris et al., 2020). Similar analyses have been developed in the Pacific and the models of prediction gave a very important precedence regarding the prediction of nuclear leaks after accidents such as Fukushima in 2011 where inverse models could be fed. This inverse modelling approaches in combination with environmental measurements efficiently reduce uncertainty and enhance assessment of atmospheric releases, and consequently are frequently used for source determination (Huang et al., 2016). Similarly, marine masses and sediments, both could carry an identification fingerprint for the source of any contamination or the origin of their flow. Thorium-234/uranium-238 ($^{234}Th/^{238}U$) ratio can quantify the biological pump, radium (Ra) isotopes can estimate the submarine groundwaters' discharge magnitude and iodine-129 (^{129}I) is a prodigious supplementary tool for investigating the large-scale ocean circulation (Qiao et al., 2023; Rodellas et al., 2023).

2.2. Uranium-Plutonium

Uranium and Plutonium are both actinides with remarkably similar chemical properties and environmental behaviours, their separation methodologies have many similarities and are usually combined, and due to that, they are both covered in one chapter.

2.2.1. Uranium

Two main oxidation states of uranium abounded under natural geochemical conditions, namely +4 and +6 (A. Yu. Romanchuk et al., 2020). Uranium is mainly present, in all aqueous solutions, typically

in its **utmost mobile form, the uranyl cation $U^{VI}O_2^{2+}$**, naturally in the form of hydroxyl and carbonate complexes (Deng et al., 2023; Priest et al., 2016). The mobility of uranium is affected by various factors, including redox conditions, the presence of cations such as Ca^{2+}, Fe^{2+} and Fe^{3+}, anions like carbonate, phosphate and sulfate, silica, organic substances, microorganisms and natural rock-forming minerals. In any reducing environment, such as the oxygen-free deep underground disposals and in the presence of microorganisms' activity, uranium can transform into a less mobile form of U(IV). However, U(IV) can easily be reoxidised if the conditions change. Additionally, uranium can be kinetically stabilized in "hot" particles (A. Y. Romanchuk et al., 2020). For instance, U(IV) was predominantly in the form of UO_2 in kinetically stable fuel particles that were released into the environment due to accidental fallout like the Chernobyl accident.

Pentavalent uranium (U(V)) was traditionally considered nonexistent in nature due to its instability in aqueous solutions. Recent discoveries, however, have challenged this notion. U(V) can indeed be detected, under the influence of Fe(II)/Fe(III) oxides especially, and oxy-hydroxides. Understanding the occurrence and behavior of U(V) has implications for environmental remediation and nuclear waste management (Deng et al., 2023; A. Yu. Romanchuk et al., 2020).

Uranium and Organic Matter: Interaction between uranium and natural organic matter (NOM) is particularly important in wetland environments. The behavior of uranyl in the presence of clay minerals (common environmental components) has also been studied. Uranium speciation can have a complex formation. Uranyl behavior in the presence of Ca^{2+} and CO^{2-}_3 has been investigated. In low concentrations and neutral pH the formation of the neutral aqueous $Ca_2UO_2(CO_3)_3$ complex increases uranium mobility. The ternary system of Ca^{2+}-U(VI)–CO^{2-}_3 covers diverse processes. Precipitation, sorption, and incorporation of uranium in the structure of calcium carbonate, on any ternary system and environmental formation, depending on the concentrations for each of the members appeared.

Uranium Immobilization: Various approaches for purification or leaching, and even for just the immobilization of uranium have been put under examination and refined. There are two reliable mechanisms for transforming mobile uranium into a solid phase, highlighted in field cases multiple times, **reduction and phosphate precipitation**. The increased mobility of uranium due to the complex formation can lead to its transport within the environment. It may move through soil, water, or other media, affecting nearby ecosystems.

If present near contaminated sites (such as nuclear waste storage facilities), the mobile uranium can migrate toward groundwater or surface water bodies. This migration poses risks of contaminating water sources. The complexed uranium becomes more bioavailable to organisms. It can be taken up by plants, animals, or microbes, potentially entering the food chain (A. Yu. Romanchuk et al., 2020). For environmental remediation efforts, understanding this mobility is crucial. It affects decisions on retention, removal, or immobilization strategies.

Studies show that the increased uranium mobility resulting from the $Ca_2UO_2(CO_3)_3$ complex formation has implications for environmental quality, human health, and remediation efforts. The $Ca_2UO_2(CO_3)_3$ complex plays a crucial role in uranium behaviour, and its impact depends on the specific conditions:
Precipitation: Under certain circumstances, the complex can lead to precipitation. When conditions favor the formation of solid compounds, uranium ions may combine with other elements (such as phosphates or hydroxides) to form insoluble precipitates. This process immobilizes uranium, preventing its mobility.

Dissolution: Conversely, in different conditions, the complex can contribute to dissolution. If the environment becomes more acidic or if competing ions are present, the complex may dissociate.

Dissolved uranyl ions (UO_2^{2+}) can then become more mobile and potentially migrate through soil or water. The $Ca_2UO_2(CO_3)_3$ complex can either lead to precipitation (immobilization) or dissolution (increased mobility), depending on the local environment.

Exploring the solvation and behavior of the $Ca_2UO_2(CO_3)_3$ complex in water and its potential impact on uranium mobility, we will find:

The neutral $Ca_2UO_2(CO_3)_3$ complex is the dominant uranium species in many uranyl-containing streams. This complex plays a crucial role in uranium speciation in seawater. The $Ca_2UO_2(CO_3)_3$ complex is very stable in water, as demonstrated by first-principles molecular dynamics simulations It remains intact over the simulation timeframe, and its key distances align with experimental data. The complex's structure and solvation have been investigated from first principles (Priest et al., 2016; Wu et al., 2016). Two Ca ions in the complex bind differently due to the hydrogen-bonding network around the whole complex. This unique arrangement influences the complex's behaviour and has implications for its dissociative equilibrium in water (Priest et al., 2016).

Seawater Context:

Uranium in seawater exists in minute concentrations (about 3.3 ppb) but has significant mass due to seawater volume (Priest et al., 2016). The $Ca_2UO_2(CO_3)_3$ complex can impact uranium mobility. Under certain conditions, it may lead to precipitation, immobilizing uranium. In different conditions, it can contribute to dissolution, increasing uranium mobility (Jo et al., 2019). In summary, the $Ca_2UO_2(CO_3)_3$ complex can both favour solubility in water and potentially contribute to uranium mobility. Its behaviour depends on environmental conditions and interactions.

It was previously believed that pentavalent uranium rarely occurs naturally, with a few exceptions. This is because the $U^{V}O^{+}_2$ cation is unstable in aqueous solution and undergoes disproportionation into U^{IV} species and $U^{VI}O^{2+}_2$. Moreover, detecting pentavalent uranium in samples presents a technical difficulty. However, recent studies suggest that uranium in its U(V) form should also be taken into account in the environment.
The leakage of uranium throughout liquid radioactive waste (LRW) from storage facilities and underground disposals occurs mainly through the release of uranyl species. In contaminated soils from uranium mining, uranium is primarily found in the uranyl form. The mobility of hydroxo and carbonato uranyl complexes in water systems is a significant issue for many nuclear legacy sites. Scientists are studying the mechanisms of uranyl retention through processes such as sorption, incorporation, precipitation, and reduction under simulated natural and waste disposal conditions. They are also identifying effective strategies for immobilizing uranium through field tests and case studies. However, remediating contaminated soils faces the challenge of selecting the right technical strategy, complicated by factors such as soil type, mineral composition, natural organic matter (OM), and the initial forms of uranium. To prevent uranium from entering groundwater in excessive amounts, two main methods can be used: monitoring natural attenuation or implementing remedial actions, especially in the case of uranium contamination in the vadose zone, particularly in arid and semiarid climates (Dresel et al., 2011; A. Yu. Romanchuk et al., 2020).
In-depth studies of uranyl behaviour in the presence of Ca^{2+} and CO^{2-}_3 have concluded that at a pH bigger than 8 the sorption of U(VI) on orthoclase and muscovite could be reduced up to 30% by the presence of Ca^{2+} at a concentration of millimolar, due to the formation of the $Ca_2UO_2(CO_3)_3$ complex (Richter et al., 2016), which is neutral aqueous complex. Studying such a ternary system (Ca^{2+}-U(VI)–CO^{2-}_3) is pertinent due to the diverse processes it covers, such as precipitation, sorption, and incorporation of uranium in the calcium carbonates' structures. Studies of uranyl behaviour in the presence of clay minerals showed the absorption of uranyl in alteration zones and the intergrowth of silicates and uranyl minerals (Gartman et al., 2015; A. Yu. Romanchuk et al., 2020).

The mobility of uranium decreases when it is exposed to polyphosphate solutions, leading to the formation of calcium uranyl phosphate. Research (Mehta et al., 2016; A. Yu. Romanchuk et al., 2020) has shown that the size, crystallinity, and composition of these precipitates affect the stability of uranyl solids affected by waste discharges. In the presence of phosphate, meta-ankoleite-like species have a significant impact on the speciation of uranium. Furthermore, the interaction between the uranyl-phosphate system at a pH of 6 and goethite and mica was studied to replicate environmental conditions. Polyphosphate solutions decrease the mobility of uranium and cause the precipitation of calcium uranyl phosphate. The composition and structure of the precipitates impact the stability of uranyl solids in acidic/neutral waste-discharged sediments.
The presence of phosphate controls the speciation of uranium and the accumulation of boltwoodite-like species. The sorption of goethite accelerates the transition between phases. Uranium bioavailability in contaminated sites is determined by phosphate forms of uranyl. The complexity of the uranyl-phosphate system supports the need for further study. Uranium can be slowed down upon treatment with bases or adsorbed by surface coatings, coprecipitation or adsorption. Thiol groups in NOM play a key role in bioremediation and immobilization of uranium. Microorganisms can reduce or reoxidize uranium, and biosorb, bioaccumulate, or biomineralize it. Uranium mobility is affected by various factors, including redox conditions, cations, anions, silica, organic substances, microorganisms, and minerals.

2.1.2. Plutonium

Plutonium exists in four oxidation states: Pu(III), Pu(IV), Pu(V), and Pu(VI). Under suitable environmental conditions, these states can coexist in a solution. Is the oxidation state of plutonium that demarcates its reactivity and its solubility. The migration of plutonium in the environment was investigated (Joseph et al., 2019) at the Nevada National Security Site (NNSS), where 828 underground nuclear tests were conducted. Over 95% of the plutonium in the groundwater well was associated with colloidal particles (mainly clays and zeolites).

Plutonium and Natural Organic Matter (NOM): During the Chernobyl accident, most of the released plutonium was linked to uranium particles. The movement of this plutonium in the environment was influenced by the spread of these particles. The concentration of plutonium in the groundwater of the Chernobyl Exclusion Zone is currently low (Bugai et al., 2020). Concentrations observed in experimental researches (Bugai et al., 2020; A. Yu. Romanchuk et al., 2020) were pointedly higher compared to those calculated using the distribution coefficient (Kd) concept. For the in-situ experiments, a relatively low Kd of plutonium was found compared to batch values. The cause of this exaggerated plutonium migration remains practically and scientifically unidentified, but then again is most likely due to facilitated transport via mobile colloids or complexes with NOM (natural organic matter), bearing in mind the characteristics of geochemistry locally. Levchuk et al. (2012) showed through ultrafiltration that a significant portion of the plutonium in the groundwater near the Chernobyl NPP is bound to low-molecular-weight NOM (<1 kDa), and to humic, and fulvic acids (Levchuk et al., 2012).

Such is the influence of organic substances on the migration of plutonium which has been discussed in several other works. For switching among the oxidation states of Pu, the redox potentials are very close to 1V for more than a few reactions, which produces an exceptional condition in which multiple oxidation states can coexist in the solution (Clark et al., 2006). The reactivity and solubility of plutonium are controlled by its oxidation state. When in the form of Pu(IV) and Pu(III), plutonium is less soluble in water compared to Pu(VI) and Pu(V). The behaviour of plutonium in the environment is influenced by vital reactions such as sorption, complexation, precipitation, and colloid formation. These reactions are greatly affected by the oxidation state. It's important to note that there is relatively less research on the environmental behaviour of plutonium compared to uranium.

Investigations at a NNSS site where nuclear tests were carried out, regarding the movement of plutonium in the environment, revealed its presence in two aquifers located 1.3 km away from the nuclear test site, with over 95% of the plutonium in the groundwater well being associated with colloidal particles. The plutonium species formation was a result of the alteration, under hydrothermal conditions, of the NNSS nuclear melt glass. Desorption rates of plutonium from colloids shaped at a temperature around 140°C can be predicted based on the kinetics of plutonium sorption and desorption onto montmorillonite. **The half-life of plutonium on colloids is estimated to be around 0.6–1.8 years**. Similarly, colloid transport of Pu from a lake site (Karachay) showed that a significant amount of plutonium is bound to colloids with a size of less than 15nm made of amorphous ferrihydrite (A. Yu. Romanchuk et al., 2020).

The sorption of plutonium onto mineral colloids is crucial to understand its transport. Recently, it was found that Pu(IV) stabilization onto mineral surfaces may result in Pu surface precipitation in the form of PuO_2 nanoparticles. The strong interaction of Pu with minerals and sediments ensures a stable association with no observed leaching even after a period of 32 years of ageing (Emerson et al., 2019).

Researches indicate that seasonal variations in redox conditions have potentially a significant impact on the movement of redox-sensitive actinides, especially to Pu (A. Yu. Romanchuk et al., 2020; Vázquez-Campos et al., 2017; Xie et al., 2018). Any variations in the properties of temperature and rainfall, or similar, all over the world may significantly affect the migration of redox-sensitive radionuclides. **The microbiological community plays a significant role in these biogeochemical processes and should be considered**. Microbiological activity affects the movement of radionuclides in groundwater. When Pu interacts with microorganisms, it undergoes reduction. However, other processes, including sorption onto cell surfaces, accumulation within the cells, biomineralization, and complexation, may also play a role.(Boggs et al., 2016). The exact mechanism of the interaction and its influence on Pu mobility is unclear. The interface and interaction of Pu(V) and Pu(IV) with cells in the presence of extracellular polymeric substances (EPS) or their absence were investigated by Boogs et al. (2016). It was actually found that cases of reduction for Pu(V) typically occur in the interaction with EPS. In all studied systems, till the end of the reaction, the cells immobilized Pu on their surface. However, in some other studies, the reduction of Pu(IV) to Pu(III) in the reaction with cells led to an increased mobility of those radionuclides (A. Yu. Romanchuk et al., 2020; Xie et al., 2018).

2.2. Iodine

While the determination of the salinity in groundwater has well-established routine methodologies, these methods are not able to distinguish salinity sources. The use of iodine-127 (^{127}I, stable isotope) and radioisotope, iodine-129 (^{129}I, long-lived radioisotope with half-life: 15.7 million years) can establish new methods to understand the movement and origin of salinity(Tan et al., 2020).

Iodine-129 is released into the environment in three ways, two of which occur naturally and one is caused by anthropogenic activities. Iodine-129 production can naturally occur in the atmosphere by (n,p) reaction on xenon-129 nucleus where the neutrons originate from the interaction of cosmic rays with the atmosphere (Tan et al., 2020). In the ground, ^{129}I is produced through spontaneous fission of uranium-238. On the other hand, human activities, such as nuclear fuel reprocessing plants, bomb testing and nuclear accidents, are responsible for the anthropogenic production of ^{129}I. Currently, the largest source of ^{129}I comes from nuclear fuel reprocessing plants (Hou and Hou, 2012; Tan et al., 2020). Factors that may affect the spatial distribution of ^{129}I and ^{127}I are seasonal variations, wind patterns, the equilibrium of iodine to the soil profile, and other sources of ^{129}I and ^{127}I. However, the chemistry of iodine in the biosphere is not fully understood (Moran et al., 1999;

Renaud et al., 2005). A log-log relationship between the $^{129}I/^{127}I$ ratio, the salinity and the original source should include the time scale and the incidents occurring in that period. Anthropogenic influence on atmospheric depositions and the increased evaporations in a semi-closed basin may significantly change the concentrations in each one of them and the final ratio after the interaction between them. Iodine isotope signatures from various sources such as natural rock, brine, seawater, and rain (both pre-nuclear era and modern) should be compiled and plotted together, including those affected by accidents.

In a study of the impact of sediment composition and conditions on the speciation of iodine (Price and Calvert, 1973) it was found that the iodine content in surface sediments can vary greatly, ranging from a few to thousands of parts per million (ppm). In marine shelves, there is a correlation between iodine and organic carbon. The ratio of iodine to carbon is expected to decrease from the shelf edge, where surface sediments are oxidizing, towards shoreward areas where sediments are reducing due to intense water upwelling. Similar types of surface sediments are expected in gulfs. The lowest iodine values are found in reduced sediments, while the highest values are found in oxidized sediments. The high iodine content in oxidized sediments is mainly due to iodine uptake by plankton settled on the seabed. In reduced sediments, the bulk of the iodine comes from planktonic matter in surface waters. When sediments are buried, most of the iodine in oxidized sediments is lost through the degradation of organic matter. This does not occur to the same extent in reduced sediments.

The behaviour of iodine during burial in oxidizing and reducing conditions may be reflected in ancient sediments. While most sedimentary rocks contain only small amounts of iodine, indicating significant loss from the original sediment during diagenesis, some Jurassic organic-rich sediments may have high levels of iodine (34-72 ppm) (Collins and Egleson, 1967). Is proposed that these sediments were likely deposited in a reducing environment (Price and Calvert, 1973).

The oxidation of iodide (I^-) to iodate (IO^-_3), (or iodide (I^-) to iodine (I_2) as we will see further below) for extraction to an organic form and back extraction through reduction is a common method used for iodine separation for analysis. Mass Spectrometry (MS) methods are considered the most favourable for isotopic analyses, with Accelerator Mass Spectrometry (AMS) being the top choice (Chen et al., 2014). For the AMS method, we will focus on it later in a separate chapter.

The distribution coefficient in trace-level isotopes should be carefully considered and estimated. The general description is written as:

$$Kd = \text{Concentration in organic (Bq/L)}/\ \text{Concentration in aqueous (Bq/L)}$$

Which for the sample itself should be described as:

$$Kd_{(s)} = \text{Concentration in sediments (Bq/kg)}/\text{Concentration in water (Bq/L)}$$

*referring to the sample before the frieze drying, or the leaching afterwards

2.3. Global Circulation

The thermohaline global circulation plays the utmost crucial role in the stability of climate and life in the whole spectrum of forms and variety. Besides the main global flow, it's important to examine and well preserve the maintenance of the functionality of those smaller parts which consist of the base for the overall global one.

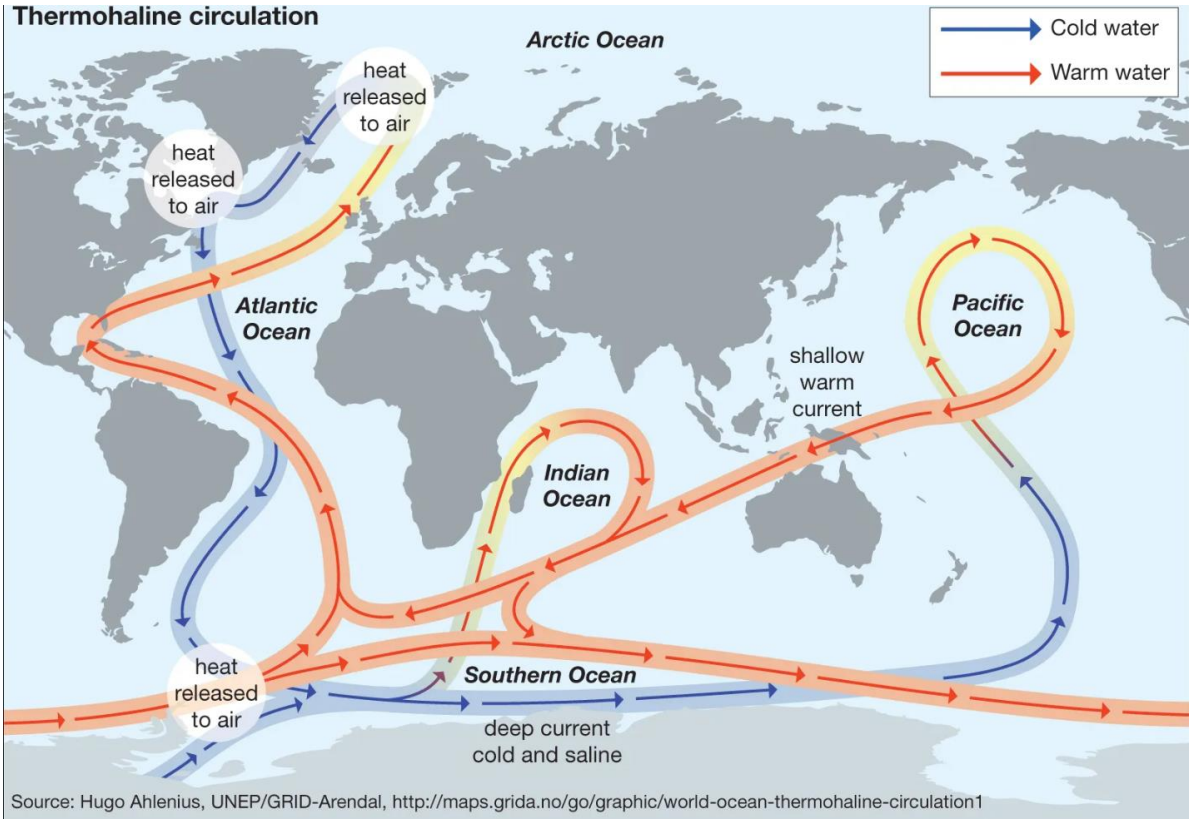

Graph. 2.3.1: Thermohaline global circulation, in a simplified version("Ocean current - Thermohaline, Circulation, Global | Britannica," 2024).

The thermohaline circulation, also known as the global conveyor belt ("The great ocean conveyor | AIP Conference Proceedings | AIP Publishing," n.d.; "The Great Ocean Conveyor on JSTOR," n.d.), is a large-scale oceanic circulation pattern driven by the combined effects of temperature and salinity variations. The Thermohaline Circulation system involves the movement of water masses based on their temperature (Greek-thermo aka warm) and salinity (Greek- haline from allas-salt) characteristics. It plays a crucial role in redistributing heat around the Earth, affecting climate and weather patterns ("Ocean circulation and climate during the past 120,000 years | Nature," n.d.). The primary driver is the sinking of cold, dense water in polar regions and the upwelling of warmer water in equatorial regions as well as the vertical movements of water masses and the reconstruction of their stratification in areas of dense water formation ("Descriptive Physical Oceanography: An Introduction - Lynne D. Talley - Google Books," n.d.; US Department of Commerce, n.d.; Wunsch, 2002).

2.4. Oceanographic tools

The main oceanographic parameters used to analyse an area are Salinity, Temperature, Dissolved Oxygen, and Density. Oceanographers mainly use Potential Temperature for this analysis. These factors are typically depicted on vertical polyparameter graphs, with the depth of observation or assignment being the most common correlation. For example, in the deep northern Cretan seas' basin, a graph depicted the total concentration of ^{137}Cs per litre alongside these parameters after sampling in 2014.

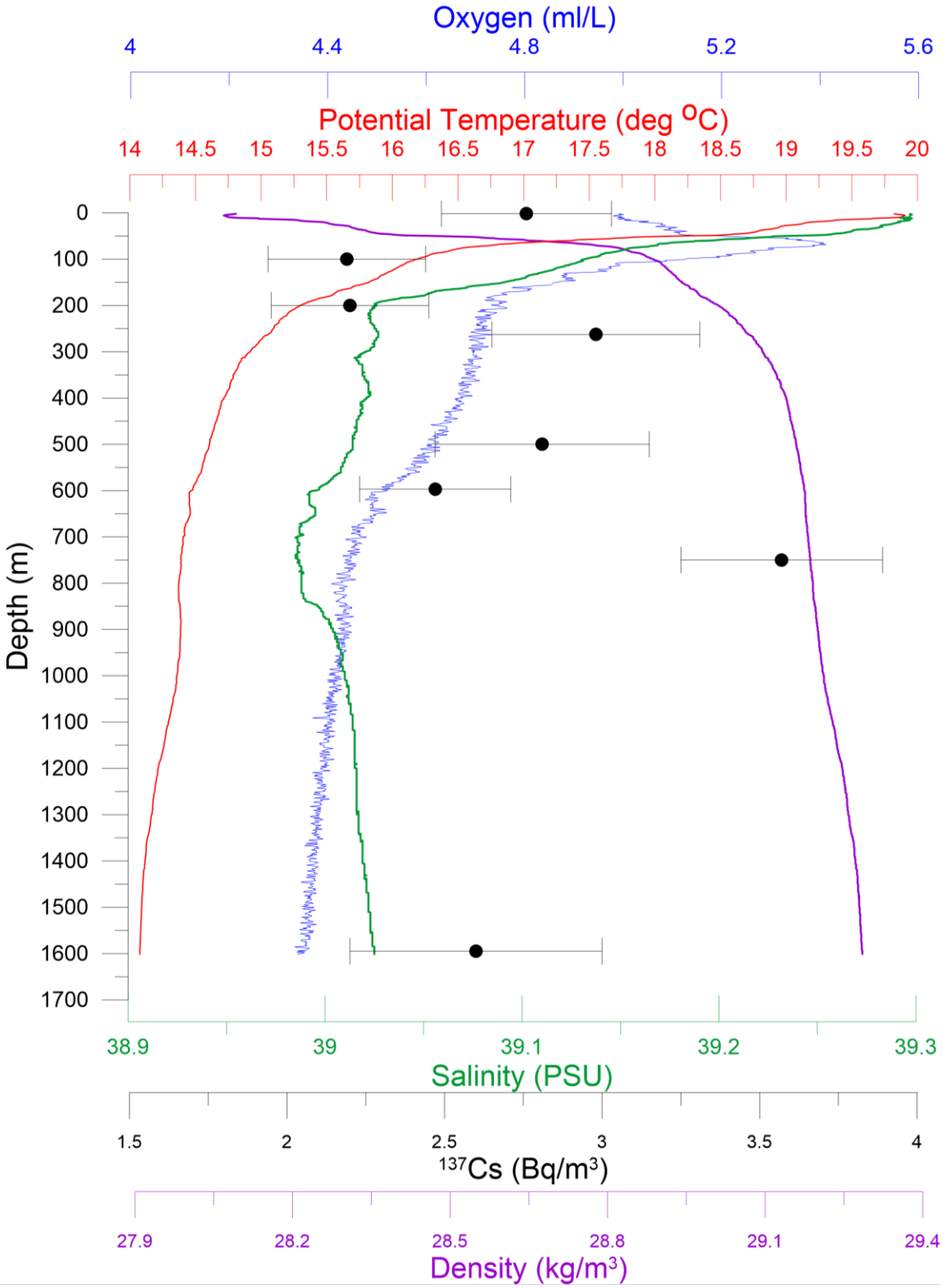

Graphic 2.4.1: Vertical graphic depiction of density, salinity, oxygen, potential temperature and ^{137}Cs (Bq/m^3) in correlation with the depth of observation. The graphic represents the Deep Cretan Basin observatory point known as M3A, and the data corresponds to sampling from 2014 (Tsabaris et al., 2019).

2.4.1. Mixing water types

A water type A, due to the homogeneity of T_A and S_A (where T and S stand for the temperature and salinity, respectively) that characterize it, is represented by a point in the T/S diagram. Water coming from another region will generally be characterized by different T_B temperature and S_B salinity.

Let a mass "α" of water type A come into contact with and mix completely with a mass "β" of water type B. Let water type A be characterized by temperature T_A and salinity S_A, and water type B is characterized by temperature T_B and salinity S_B. After the waters are completely mixed, the resulting mass "γ" of seawater will be equal to the sum of the two masses:

$$\alpha + \beta = \gamma$$ Mass conservation

Also, the thermal load of the resulting mass will be equal to the sum of the thermal loads of the two masses:

$$\alpha c_p T_A + \beta c_p T_B = \gamma c_p T_\Gamma$$ Heat conservation

Finally, the total salt contained in the resulting quantity ***γ*** will be equal to the sum of the salt contained in the two quantities ***α*** and ***β*** mixed:

$$\alpha S_A + \beta S_B = \gamma S_\Gamma$$ Salinity conservation

The above three equations define a linear system of equations:

$$\left.\begin{aligned} \alpha + \beta &= \gamma \\ \alpha T_A + \beta T_B &= \gamma T_\Gamma \\ \alpha S_A + \beta S_B &= \gamma S_\Gamma \end{aligned}\right\}$$ solved, gives us that the salinity values S_Γ and temperature T_Γ of the quantity γ that will result from mixing will define a point in the diagram Θ/S located on the straight segment joining the water types A and B (Figure 2.3.1.1):

$$\frac{T_A - T_B}{S_A - S_B} = \frac{T_\Gamma - T_B}{S_\Gamma - S_B}$$

The ratio of the lengths of the straight segments ΓA/ΓB is equal to the inverse of the proportions of the masses in which the two types were mixed, i.e. ΓA/ΓB = 0.7/0.3

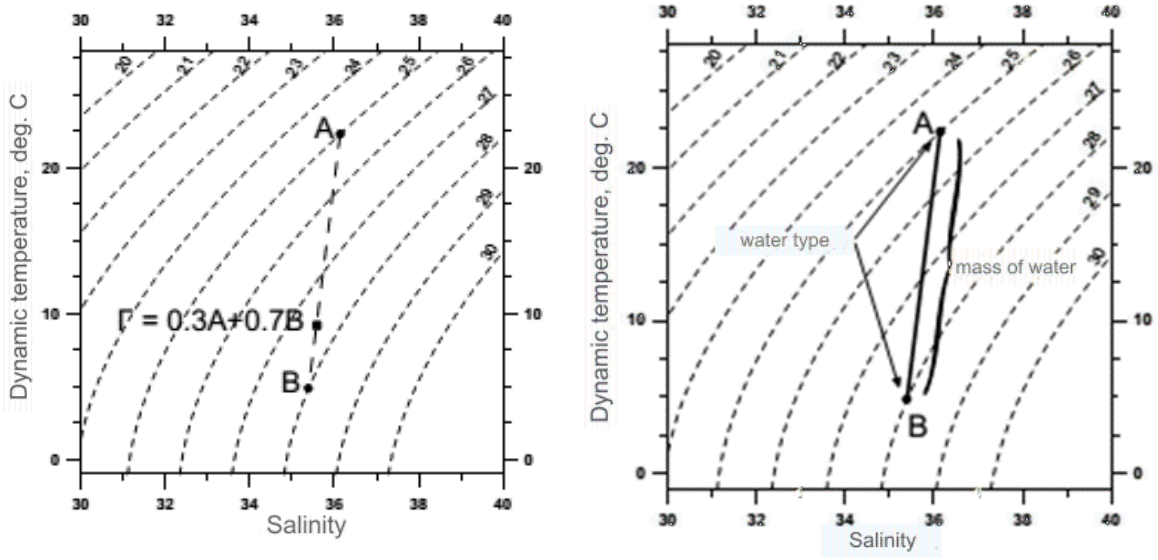

Graph. 2.4.1.1: Left: mixing ratios 0.3 of type A and 0.7 of type B in diagram Θ/S. *Right*: mixing of two types of water and creation of water mass in a Θ/S diagram (*Zervakis, notes from the undergraduate classes, 2016*)

Observe that T changed to Θ and that is because the temperature we mostly need and use in those diagrams is the dynamic temperature, which means that we use the temperature the mass would have if we take it from its' depth to the surface adiabatically (without transferring heat or mass between the thermodynamic system/sample and its environment).

In nature, if we have a layer of water of type A and a layer of type B, and there is mixing at the interface, then the mixing does not become completely homogeneous all the way toward the mixing mass, but there are depths richer in type A waters and others richer in type B waters. but in water whose properties are distributed over the straight segment joining the primary formulae in a Θ/S diagram. This rectilinear segment defines the mass of water resulting from the mixing of the two types (Figure 2.4.1.1).

In the case of mixing three types of water, the process is similar, although more complex. The three layers (Figure 2.4.1.2) respectively represent three types of water, represented in the Θ/S diagram by three points. The interfaces separating the water types are eroded through some mixing that causes diffusion of temperature and salinity and in the early stages of mixing the intermediate type is not completely corroded, hence the vertical distributions and the corresponding Θ/S diagram take the form shown in the left part of Figure 2.4.1.2. If mixing continues, and the intermediate water type is finite (or not recharged), this type will corrode, resulting in vertical distributions and the Θ/S diagram taking the form shown in the right-hand part of Figure 2.4.1.2.

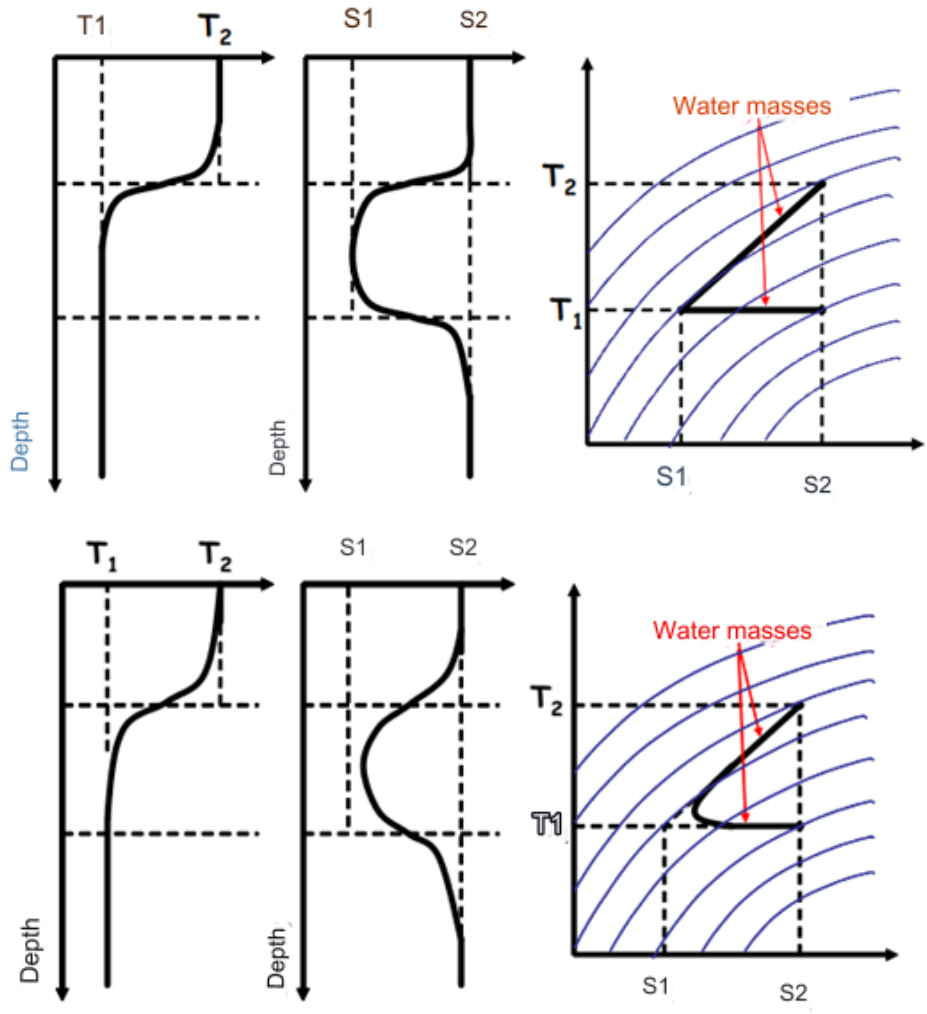

Graph. 2.4.1.2: *Top*: Vertical temperature and salinity distribution of three overlying water types, and corresponding Θ/S diagram for initial mixing stages and *Bottom*: for mature mixing stages.

To that end, Θ/S graphs may give us the most basic and important information.

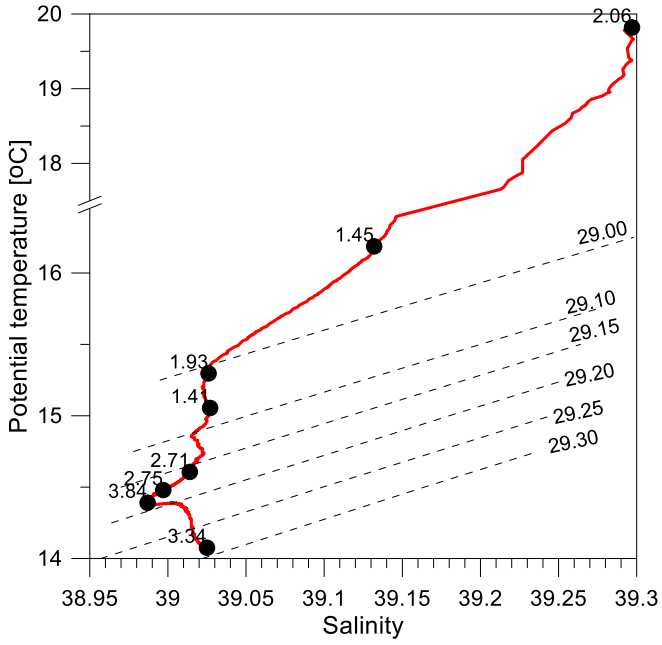

Graph. 2.4.1.3: Diagram θ/S from the data of the M3A station in the Cretan Sea in 2014. The circles refer to the values of the concentration of ^{137}Cs in Bq m^{-3}, the dashed curved lines correspond to the isodense ones.

The combination of Θ/S and the radioisotopic information in integrated graphs, the dynamic of water masses can be revealed in both geotopical and time vector (Leivadaros et al., 2022; Tsabaris et al., 2020). The physicochemical characteristics of water masses are influenced by factors such as deposition rate, time spent in deep basins, and phenomena like deep water formation following extreme weather events. Thinking backwards, all of these phenomena can be identified and mapped through this water investigation.

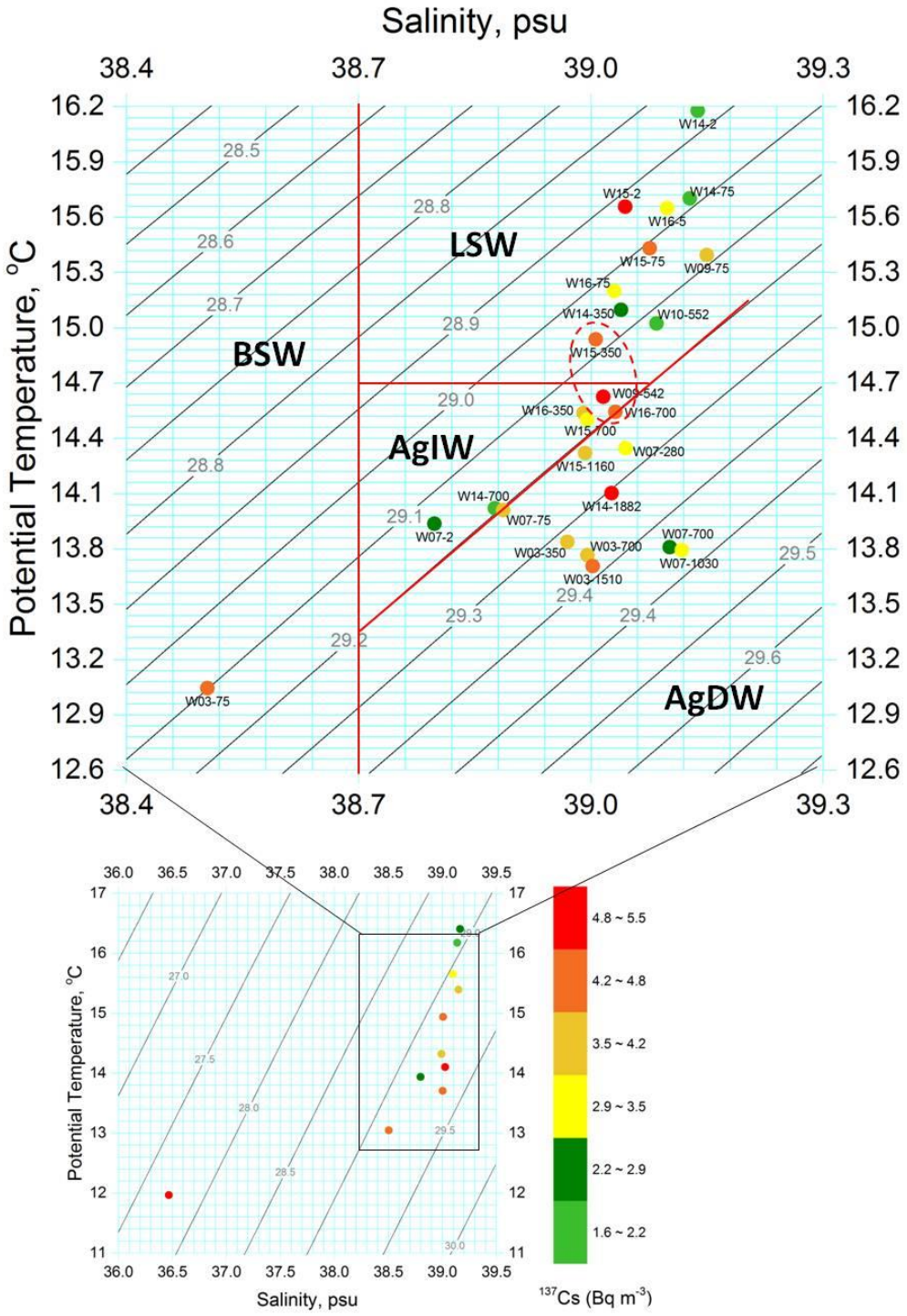

Graph. 2.4.1.4: combination Θ/S and radioisotopic information ($C_{(137\text{-}Cs)}$) in an integrated graph (Leivadaros et al., 2022)

2.4.2. Radionuclides and stable isotopes as an oceanographic tool

The use of both the radionuclides and stable nuclides can be combined in the same research approach, either measured by their radiation (e.g. Cs-137) in the case of radioactive isotopes or measured by mass-spectrometry (e.g. I-129 or U-236). Using the radionuclides as tracers – $^{129/127}$I, $^{137/134}$Cs, $^{226/224}$Ra, Rn, U and so on- or studying the fate of radionuclides in the oceans stresses the spectrum of application of isotopic ratios. As we see in other researches, isotopic ratios can be used for extended research, varying from dating to elemental tracing (McDaniel et al., 1992).
With high sensitivity limits, Accelerator Mass Spectrometry (AMS) is used for both radionuclide

dating and stable isotope trace element determination. It has a wider range of applications, including oceanography, and extended to terrestrial studies, glaciology, hydrology, meteorology, environmental studies in general, and furthermore to biomedical and more.

3. Radionuclides detection and measurement

In this research, we focus mainly on (radio)isotopes of 4 elements, specifically U, Pu & I and to a smaller extent on Cs. The Cs mostly interest us for the isotope 137-Cs which is typically measured by low-background gamma-ray spectrometry through its decay in 137m-Ba and its gamma emission, for that reason γ-spectrometric methods such as HPGe are used. Radioisotopes of the remaining three elements belong among the long-lived ones that are advantageously measured by mass spectrometry.

The techniques of analysis are usually distinguished based on their detection systems, in general, we can highlight two big microanalytical categories

Non-destructive - Microanalytical techniques

This category includes a series of techniques which have the advantage of not destroying the samples. However, they have a number of limitations such as accuracy and detection limit level. Such techniques are X-ray photoelectron Spectroscopy (XPS), X-ray fluorescence (XRF), micro X-ray fluorescence (conventional micro-XRF), Synchrotron radiation (SR)-based μ-XRF, SR-based μ-XANES & SR-based μ-XRD -, μ-tomography etc

Destructive - Microanalytical techniques

This category includes all the Mass Spectrometry (MS) techniques - AMS, ICP-MS etc-, and techniques such as liquid scintillation-based detecting systems. Even for HPGe (high-purity germanium systems), the very low-activity samples have to be decomposed and passed through a non-reversible procedure to be analysed.

Regarding the properties we detect, it is possible to categorize the techniques based on four big areas of detection: **α-spectrometry, β-counting, γ-spectrometry, and mass spectrometry**.

3.1. Radiation detection

Unstable nuclei transform into stable ones by minimizing their' absolute masses, this mass is expressed as a value which includes nucleon binding energy. During radioactive decay, radiation is sensed during its interaction with matter. For the identification (qualitative and quantitative) of radionuclides, radiation detection systems have been developed, as well as a mathematical-empirical method of analysis of the results (spectroscopy).
Charged particles, electrons, positrons and photons can be emitted during a decay or a decay chain (most often in some combination between them through the same decay or consecutive decays of the mother and the daughters).
Charged particles interact quite easily and fast with their surrounding environment, especially when those particles have a big size such as alpha particles (He^{2+}) and hence even if they are of the most ionizing ones their penetration and range is quite small. Those particles are easily detected by gas-filled detectors such as e.g. ionizing chambers or Geiger-Müller detectors.
Beta decay has a bigger range than alpha, and smaller than gamma and, at the same time is less ionizing than alpha, but more than gamma. In the same spirit, being an intermediate phenomenon between alpha and gamma, the radiometric detection of the ionizing or excitation effects of beta particles on matter is detected commonly through the ionization of gas in proportional or Geiger–Müller counters, or the excitation of scintillators in scintillation counters.

3.1.1. Interaction of gamma radiation with matter

Unlike charged particles, in gamma decay, a well-aligned monochromatic *gamma-ray* exhibits exponential absorption in matter. This is because photons are absorbed or scattered in a single event. This means that the parallel photons of the beam passing through the absorber had no interaction with it, while those that are absorbed or scattered have been expelled from the beam in a single event. The description of the probability of such an interaction It is determined by the active cross-section of the process. The attenuation that the gamma-ray beam undergoes as it passes through matter is exponential in nature and is equal to:

$$dN/N = -\sigma\alpha dx$$

where N is the number of gamma rays in the beam, αdx is the number of atoms per unit area, and σ is the effective cross-section of photon attenuation. If the above relation is completed for matter thickness from zero to x then it follows that

$$N = N_0 e^{-\sigma\alpha x} = N_0 e^{-\mu x}$$

which is a characteristic exponential attenuation relationship of a parallel gamma-ray beam entering a thin sheet of matter, where μ=σα is the linear attenuation coefficient in that material and N_0 is the initial number of gamma-rays in the beam.

For the energy range where nuclear transitions usually occur, from 0.01 to 10 MeV, all but a very small percentage of interactions are explained by the following processes: the photoelectric effect, Compton scattering and ion-pair formation.

Photoelectric effect

The photoelectric effect refers to the interaction of a photon with an atom of the absorber whenever it disappears completely. In place of the photon, an energetic photoelectron is emitted, that is, one of the bound electrons of the atom. It should be emphasized that the interaction takes place with the atom as a whole and not with free electrons. For high-energy gamma rays, the origin of photoelectrons is most likely to come from the most closely related shells of the atom, such as the K shell. The photoelectron appears with an energy given by the following relationship:

$$E_e = h\nu - E_b$$

where E_b represents the binding energy of the photoelectron in its initial layer and *hν*, the energy of the incoming photon. For gamma rays with an energy greater than a few hundred keV, the photoelectron carries most of the initial energy of the photons.

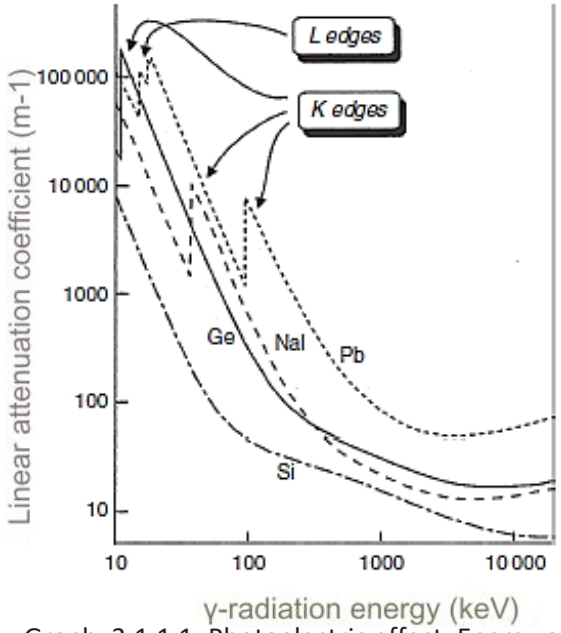

Graph. 3.1.1.1**:** Photoelectric effect. Energy attenuation, coefficient of gamma-ray, for various materials (Sousa, 2010).

The probability of the photoelectric effect to occur is given by the following relationship:

$$\tau \propto \frac{Z^n}{E_\gamma^m}$$

where *n* and *m* take values from 3 to 5 depending on the energy, clearly Z is the number of electrons in the absorber (equal to the proton number of the absorbing element).

Compton scattering

The Compton effect is an elastic scattering of a photon on an atomic electron in which the former is scattered at an angle θ from its original direction. The photon transfers some of its energy to the electron, known as the recoil electron. The energy of the scattered photon is given by:

$$hv' = \frac{hv}{1 + \frac{hv}{m_0 c^2}(1 - \cos\theta)}$$

where m_0c^2 is the resting mass of the electron (0.511 MeV) and *hv*, *hv'* the energy of incoming and scattered radiation respectively.

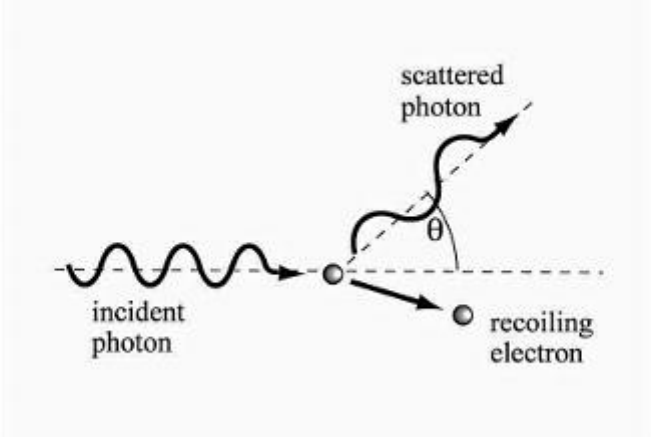

Graph. 3.1.1.2: Schematic representation of Compton scattering (with a free electron at rest) (Negm, 2014).

The probability of Compton scattering is given by the formula:

$$\sigma = constant + \frac{Z}{E_\gamma}$$

Compton scattering most likely occurs in photons with an energy of 0.6-4 MeV and is therefore the dominant interaction mechanism for the characteristic gamma rays of radioisotope sources in large Z absorbent materials.

Pair Production

For photon values exceeding twice the resting mass of the electron (1022 MeV), an electron-positron pair can form, where each particle holds a surplus of energy in the form of kinetic energy. The pair production effect takes place in the presence of a Coulomb field, the one created by the nucleus. The probability of producing a pair is related to the energy of gamma radiation and to the Z of the absorber and is approximated by the relationship:

$$\kappa \propto constant * f(E_\gamma, Z)$$

Figure 3.1.3.1 shows the relative contribution between the three processes of interaction of gamma radiation with matter:

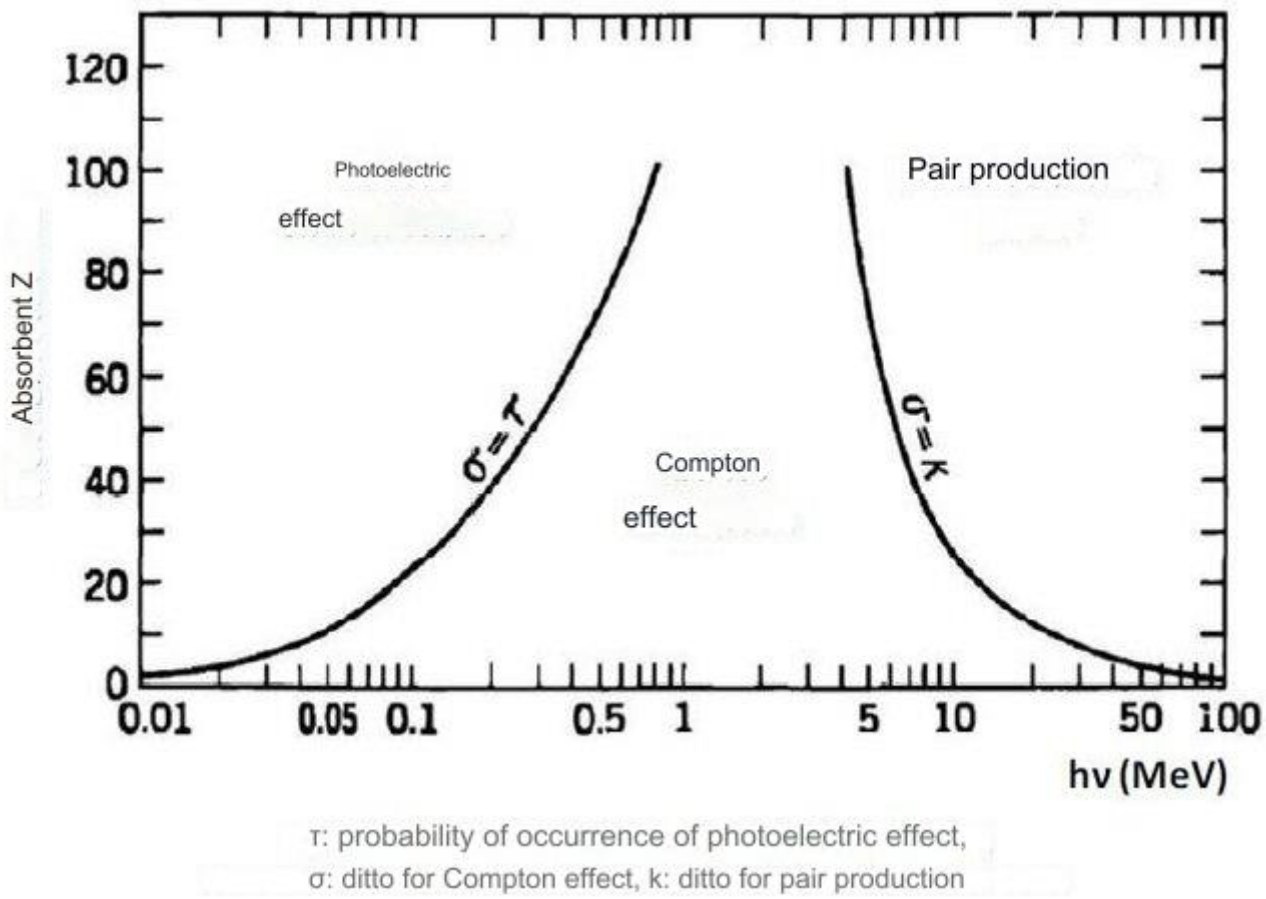

Graph 3.1.1.3 Relative contribution of photoelectric absorption, Compton scattering and pair production as a function of photon energy (Cabello, 2020).

3.1.2. Detection systems

Radiation detectors are specialized devices that convert the interaction of energetic photons or charged particles into a visible signal. Key factors for detector selection include performance, resolution, and dead time. Efficiency measures the detector's ability to detect radiation emitted from a source. The energy resolution capacity of a detector distinguishes individual photons or particles with neighbouring energies. Dead time is the duration needed for the system to recover after the incidence of one ray and respond to the next.

Two fundamental principles of function of ionizing radiation spectrometric systems can be distinguished – the wavelengths and the energy dispersive ones.
Radioactive materials are physically indistinguishable from other (non-radioactive) metals. Additionally, ionizing radiation is not detectable by one's senses. It cannot be seen, heard, smelled, tasted, or felt (exception is our skin which is able by producing melanin in direct association of the UV radiation absorbed by it, to behave as a biological radiation detector for that specific wavelength spectrum). For these reasons, radiation sources need special markings in order to be detected ("Detecting Radiation," n.d.). Personal Radiation Detectors (PRD), Handheld Survey Meters, Radiation Isotope Identification Devices (RIID), and Radiation Portal Monitors (RPM) are some varieties of detectors.

Regarding their characteristics and their operating process generally, **there are three most common types of detectors**:

- Gas-filled detectors
- scintillation counters

- semiconductor detectors

And of course, then the very same categories include the passive and active varieties of detective systems.

Gas-filled detectors are instruments that can identify and measure the presence and activity of radioactive substances in the air or other media. They are used for various purposes, such as environmental monitoring, nuclear security, medical diagnosis, and scientific research. Such detectors, like gas flow proportional counters are used mainly to detect longer wavelengths aka low energies. But they are also used for higher energies too. Gas flows continuously through the series of multiple detectors, and then leads to waste. The gas is usually 90% argon & 10% methane, (mostly in gas flow proportional counters) although the argon may be replaced with neon or helium where very long wavelengths (over 5 nm) are to be detected. Incoming photons ionise the argon, and the electric field multiplies this charge into a measurable pulse. Another subcategory is the sealed gas detectors, which are similar to the gas flow proportional counter, with one crucial difference, the gas does not flow through them, but they typically use krypton or xenon at high pressures and are mainly used for wavelengths in the 0.15–0.6 nm range. Although they could theoretically be used for longer wavelengths, their practical application is limited by the difficulty of manufacturing a thin window that can withstand the high-pressure difference.

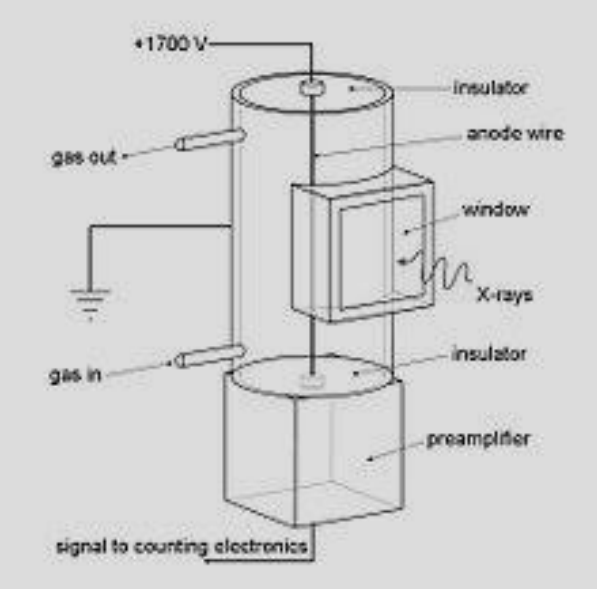

Graph. 3.1.2.1: Typical arrangement of gas flow proportional counter

There are different types of gas detectors for radionuclides, depending on the nature and energy of the radiation emitted by the radionuclides (“Quantification of Radionuclides, MARLAP, July 2004,” n.d.). Except *Proportional counters & Noble gas monitors another* well-spread gaseous ionization detective system is **Geiger-Müller detectors,** which uses the Townsend avalanche phenomenon to produce an effortlessly detectable electronic pulse from as little as a single ionizing incident from any radiation particle. It can be used for the detection of all the radiation spectrum, even neutrons. Usually in the form of some tube operates in the "Geiger" region of ion pair generation.

Some of the challenges and opportunities for gas detectors for radionuclides are:

Improving the sensitivity, resolution, and speed of the detectors, especially for low-level and short-lived radionuclides, such as radioxenon (Foxe et al., 2021). **Developing portable, robust, and low-cost** detectors that can be deployed in various environments and scenarios, such as field surveys, emergency response, and public health. **Integrating the detectors with other sensors and data sources** to provide comprehensive and reliable information on the origin, transport, and impact of radionuclides in the environment (Rodellas et al., 2023).

Scintillation counters as the name refers to, are systems that use scintillating materials that emit light when returning to the ground state after their excitation by the impact of able ionizing radiation, such as gamma rays or X-rays etc. Those detectors consisted of a scintillating crystal, typically made of sodium iodide doped with thallium, attached to a photomultiplier. When a photon is absorbed, the crystal produces a series of scintillations, with the number of scintillations being proportional to the energy of the photon. This results in a voltage pulse from the photomultiplier that is proportional to the photon's energy. The crystal is protected by a relatively thick aluminum or beryllium foil window, which limits the use of the detector to wavelengths below 0.25 nm. Scintillation counters are often connected in series with a gas flow proportional counter. The gas flow counter has an outlet window opposite the inlet, to which the scintillation counter is attached. This arrangement is commonly used in sequential spectrometers.(Hellborg and Siegbahn, 2005).

Semiconductor detectors create multiple electron-hole pairs along the paths charged particles travel through the band structured semiconductors. This process can be direct or indirect, and the particle generates high-energy electrons or secondary very fast (high energy) electrons (gamma rays that produce even further ionization) that produce more electron-hole pairs while losing their energy. The ionization energy (denoted by "e") is largely independent of the incident radiation's energy and type. In a semiconductor, radiation always leads to an equal number of holes and electrons. The low ionization energy of semiconductors allows for a greater number of charge carriers, resulting in improved energy resolution for detector applications. Same way equal numbers of free electrons and positive ions are produced in a gas, similarly every conduction electron created in a semiconductor must also lead to a hole in the valence band, resulting in an equal initial number of created charges (*Radiation Detection And Measurement Glenn F. Knoll 3rd Ed 1999*, n.d.). Some exceptional characteristic subcategories are:

Energy-dispersive spectrometers (EDX or EDS), consist of detective systems that allow the determination of the photons' energies when those are perceived. The detectors have been based on silicon semiconductors, in the form of lithium-drifted silicon crystals, or high-purity silicon "wafers".

Si(Li) detectors: Consisted principally of a silicon junction (only 3–5 mm thick) type p-i-n diode (same as PIN diode) with a bias of −1000 V across it. Including the lithium-drifted centre part that forms a non-conducting i-layer, where Li compensates the residual acceptors which would otherwise make a p-type layer. When an X-ray (or γ-ray) photon passes through, it causes the formation of a swarm of electron-hole pairs, concluding a voltage pulse. Low temperature is essential for the detective system to obtain sufficiently low conductivity. Liquid-nitrogen cooling is usually used for optimal resolution.

High-Purity Germanium (HPGe) Radiation Detectors: HPGe detectors are an important system technologically that has been evolving for over half a century. Initially, the detectors were based on lithium-drifted germanium (Ge(Li)) and lithium-drifted silicon (Si(Li)). However, Ge(Li) was later replaced with more advanced, high-purity germanium (HPGe) detectors. Cryogenic cooling is necessary for germanium semiconductor radiation detectors in any of the various counting geometries. HPGe radiation detectors have been used worldwide in diverse applications, in a wide

range of detectors that cover an extensive range of energies (Knoll, 2010; “Physics for Radiation Protection, 3rd Edition | Wiley,” n.d.).

3.2. Mass spectrometric methods

When it is needed to measure primordial radioisotopes, whose half-life would have forced us to extend the time of measurement to irrational and greatly costly levels, then it’s more efficient to use Mass Spectrometers instead of semiconductors or other spectrometers. Unlike radiation-based methods, by mass-spectrometers, we count mass-separated atoms rather than the radiation emitted during decay. Inductively coupled plasma mass spectrometry (ICP-MS) is commonly used today for this purpose. This makes mass spectrometry especially well-suited for measuring long-lived radionuclides, as its detection limit is lower than that of radiometric methods. For example, for ^{99}Tc ($t_{½}$ = 2.11 × 10^5 y)(“Technetium-99 - an overview | ScienceDirect Topics,” n.d.) The detection limits for Liquid Scintillation counters can reach in such low levels even less than 1 Bq of activity (Schubert and Kallmeyer, 2023). That would correspond to a detection limit lower than one per second, which could be more than efficient to most of the radioisotopic researches but in the case of ^{99}Tc, for example, that activity corresponds to a number of almost 9.6 10^{12} atoms. A smaller amount of atoms can be more easily detected and counted by mass spectrometry. In principle all radionuclides with half-lives longer than ca 100 years can be more sensitively measured by ICP-MS or even better (in particular when the matrix of our sample is more complex) by AMS.

3.2.1. Inductively coupled plasma mass spectrometry

ICP-MS (Inductively coupled plasma mass spectrometry) is a potent analytical tool for elemental determinations, with excellent detection capabilities, especially for trace and rare-earth elements (Barrat and Bayon, 2024; Herrmann et al., 2020). It has been further enhanced by the development of high-mass resolution systems, which can achieve lower detection limits, and resolving typical spectral interferences (Feldmann et al., 1994). The technique has also been applied to the analysis of metallic or metal-containing engineered nanoparticles, with the development of single-particle ICP-MS (SP-ICP-MS) (Abad-Álvaro et al., 2022). This method allows for the rapid detection and characterization of a large number of particles, as well as the determination of particle size and size distributions.

An ICP-MS system operates by using an argon (Ar) plasma (the ICP) to convert the sample into ions, which are then measured using a mass spectrometer (the MS). ICP-MS is similar to inductively coupled plasma optical emission spectroscopy (ICP-OES) and it also provides fast analysis of multiple elements in a sample. However, ICP-MS measures the elements (ions) directly, while ICP-OES uses an optical spectrometer to measure the light emitted from elements passing through the plasma. ICP-MS provides detection limits much lower than ICP-OES, making it a better choice for trace element analysis. A typical ICP-MS instrument mainly consists of the ICP (ion source), an MS (mass spectrometer), typically a scanning quadrupole mass filter, and finally a detector. The ICP operates at atmospheric pressure, while both the MS and the detector are in a vacuum chamber (consequently a vacuum pump is also required), also in the vacuum interface some electrostatic ion “lenses” are used to focus the ions through the system. Contemporary ICP-MS structures also typically contain some device or mechanism to resolve spectral interferences. Even though these machines are capable of distinguishing neighboring isotopes, a problem common to almost all mass-spectrometric techniques which is the isobaric interferences still persists.

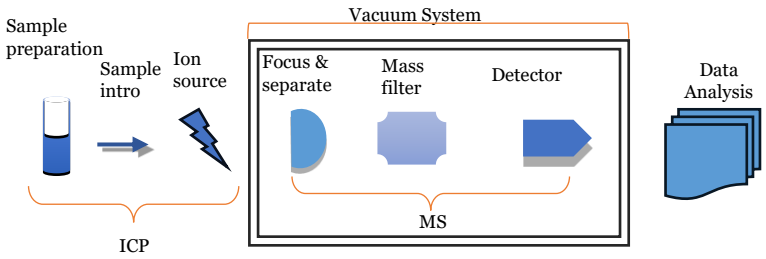

Graph. 3.2.1.1: graphic depiction of ICP-MS

3.2.2. Accelerator Mass Spectrometry

Accelerator Mass Spectrometry (AMS) enhances higher energy particle acceleration techniques to the fundamentals of Isotope Ratio Mass Spectrometry (IRMS) to provide extremely low detection capability (sub-1 femtogram) of rare isotope samples of natural materials as small as 1 mg. Depending on the selected element and equipment configuration, rare isotope sensitivities can reach less than one part in 10^{15} (Kieser, 2023). The system uses negative analyte ions, generated in the ion source, before being pre-accelerated and sent through two mass spectrometers separated by a molecule-dissociating accelerator stage. A variety of detectors may be used for the quantification of analyte ions

Advantages	**Disadvantages**
– Low background and detection limits – Significant suppression of molecular interferences – High abundance sensitivity	– Sample preparation – Analysis cost – Longer switching times between masses reduce precision

While AMS has diverse applications, here we focus on it due to its significant role in marine science:

Marine organic materials play a crucial role in understanding past climate changes and ocean dynamics. Accelerator mass spectrometry (AMS) is an immersive tool that helps researchers to date these materials accurately. Additionally, using AMS, precise measurements of stable isotopes such as carbon, nitrogen, and oxygen in marine samples can be made. This enables tracing the nutrient cycles, food web dynamics, and palaeoceanography. AMS also detects long-lived radioisotopes such as ^{14}C, ^{10}Be, and ^{129}I at ultra-low concentrations. These isotopes aid in the study of ocean circulation, sediment transport, and environmental pollution (Hain et al., 2022; Kieser, 2023; Young, 2023). AMS contributes significantly to sustainable marine research by unravelling historical processes, tracking pollutants, and advancing our understanding of Earth's oceans.

AMS provides information on both the concentration as well as the origin (through the isotopic ratios) of a relatively small obtained portion, making the fractional analysis of samples far more

detailed and precise. Due to its importance and applications, especially in this research AMS will be described further below in a separate chapter with some detail.

4. Sampling, chemical separation and bulk analysis

In this research, we focus mainly on 4 elements, mostly U, Pu & I and a bit less with Cs. The use of ion exchangers, solid extractants, or even activated carbon for extracting and concentrating uranium and/or plutonium from aqueous samples has a range of potential applications. The use of ion exchangers for purifying trace metal ions, including uranium & plutonium, from geological and water systems and the development of improved selective resins and adsorbents for their extractions, have potential applications in treating contaminated water (and not only) and preventing environmental contamination from uranium-plutonium mining/reprocessing activities (Aly and Hamza, 2013). Iodine has some unique handling necessities, therefore we will examine it separately. For Cs, the isotope 137-Cs mostly interests us which is typically detected through the decay of its daughter 137m-Ba and its gamma emissions, for that reason γ-spectrometric methods such as HPGe are used.

In this research, the main technique used for sample preparation and purification were chromatographic separation methods. For non-destructive bulk sample analysis, XRF was used. This is why these two techniques are described below in more detail.

4.1. Chromatographic separation methods

In many cases, when we want to analyze a sample using one of the destructive techniques, it's necessary to separate or purify the substances in the sample beforehand. Maybe the most commonly used for this purpose are the chromatographic methods.

Chromatography is a family of separation methods with a wide range of applications in chemical separation. In contrast to simpler techniques such as Liquid-liquid Extraction, Filtration, Sedimentation, Distillation, Evaporation, Sieving, Magnetic Separation, Crystallization, Centrifugation etc. Chromatography makes use of the distribution of the substances between the sample and a chromatographic resin (e.g. a mobile phase on a stationary phase – which doesn't have to be always "stationary" – in the case of extraction chromatography) often applying some of the pre-mentioned techniques too.

Liquid solution chromatography: A stationary and a mobile phase can be partitional or absorptional depending on the physical forces on the interface, in short description we could say that hydrophilic compounds stay in the aqueous phase and the hydrophobic stays in the organic phase (distribution depending on their active surface between them too). The previous for liquids was named liquid-liquid chromatography and regarding the mobile phase, we have got also **Gas-liquid and gas-solid chromatography**. In absorption, we have separation of the substances through absorption mainly by Van der Waals and hydrogen bonding interaction

Ion-exchange: In solids mostly, in some cases in column arrangement, too, ions are exchanged separated between the liquid sample and the ion exchanger. the less interacting ions pass through the exchanger column uninfluenced while the interacting ones are retained.

Extraction chromatography: In extraction chromatography, where the solution of extraction agent in an organic diluent is loaded onto an inert support to form a so-called solid extractant, the polarity is the main separation mechanism. The separation steps can be summarized as Conditioning-

Equilibration-Loading-Washing-Elution. The mobility of the substances changes regarding the interaction of the ions with the stationary phase in the prevailing condition at the time.

Size-exclusion chromatography: separates based on the size and specifically usually uses gels where the molecules act as stationary phase and restrict the mobility of the larger molecules, leading to extracting the bigger molecules in the first extracted portions.

Sheet methods such as paper and thin-layer chromatography: Similar to extraction chromatography the mobility changes due to the interaction between the ions and stationary phase due to polarity (bigger polarity, smaller distance covered at same time step). The difference is that in this case, the mobility moves from bottom to top or horizontally instead of vertically from top to bottom and that in this case, we have a small portion only moving between the thin layers or in the paper sheets. (used mostly for analytical control checks).

In **column chromatography** which is mostly used, we use a stationary phase "a resin" which most often will be coated with some substance which will work together with one of the above-mentioned techniques (Ion-exchange, liquid-liquid extraction, extraction chromatography) or a combination of them and their properties.

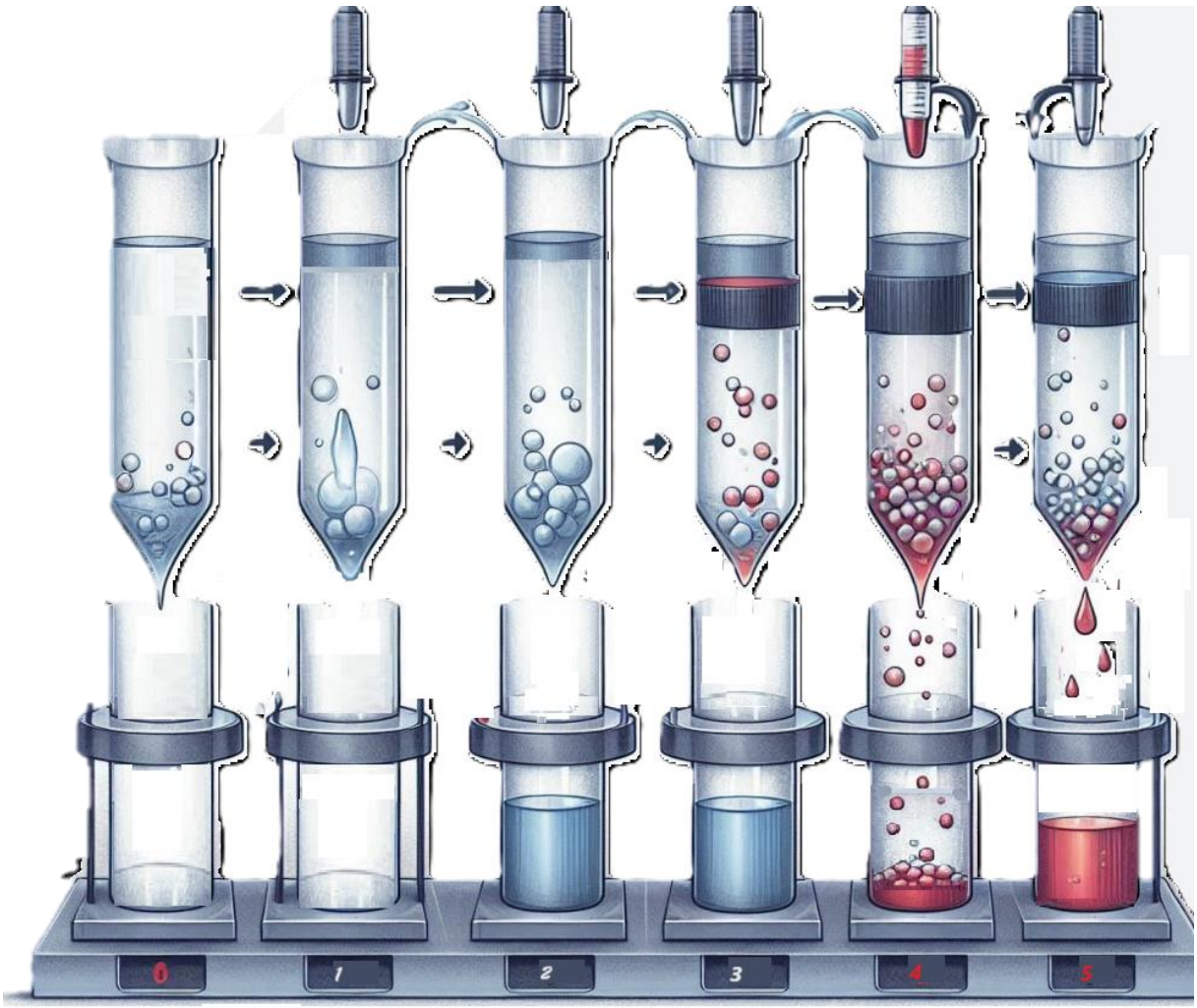

Graph. 4.1.1: Illustration of a general form of column preparation and elution, Column with resin(0)→conditioning(1)→equilibrium(2)→sample loading(3)→ washing(4)→elution(5)

The above may vary and some steps may excluded or repeated regarding the method we apply each time, but the general form is the same more or less.

Regarding elution, we have 3 main types of extractions:

The frontal: the sample acts as a mobile phase itself, there are no ion exchanges so the least absorbed component is eluted at first

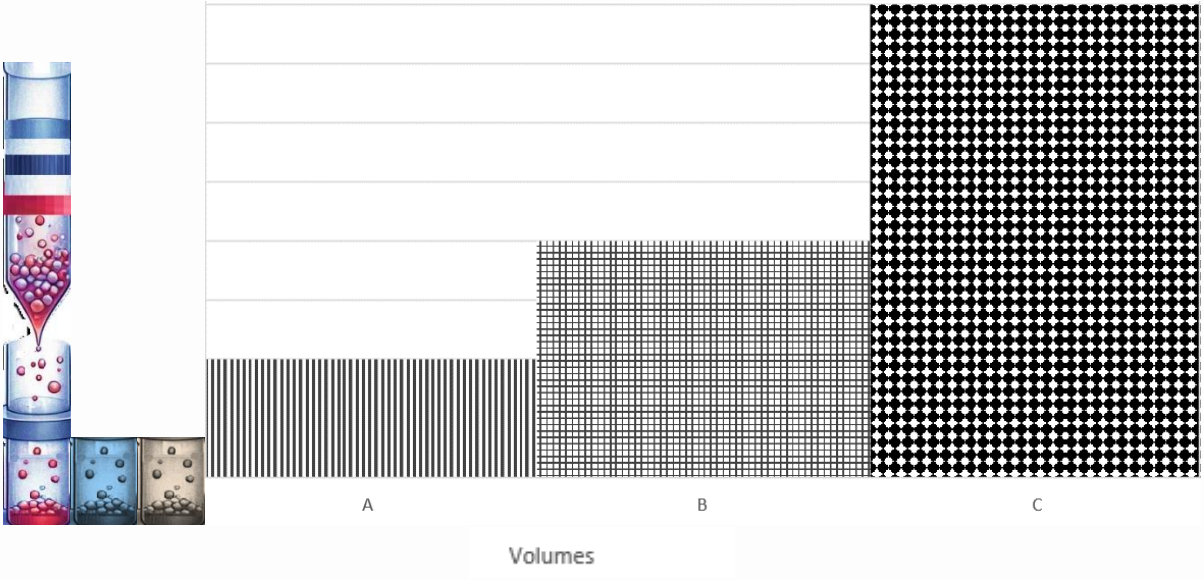

Graph. 4.1.2: Illustration of a frontal extraction and its results, where A,B,C are the separated substances, with A<B<C their reactivity with the resin

***Displacement*:** The difference here is that we add a displacement agent as a mobile phase after loading the sample, and we get a mixture of substances and the displacement agent at the outlet of the column, based on the strength of interaction between the absorbent and the substances.


Easiest absorbed from the resin: D>C>B>A

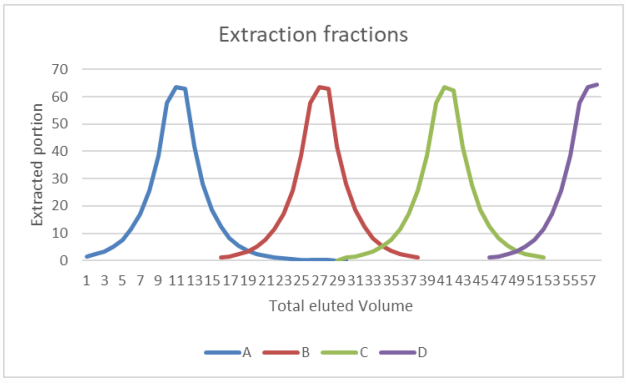

Graph. 4.1.3: Illustration of a displacement extraction and its results, where A,B,C are the separated substances, D the displacement agent with A<B<C<D their absorption from the resin.

***Elution*:** the only one that 100% distinguishes between eluted substances (based on their strong or light interaction and their being bound with the stationary phase). The elution that will be used should be the weakest bounded agent among the substances but in bigger concentrations than the rest so it will "push out" the other agents at different speeds.

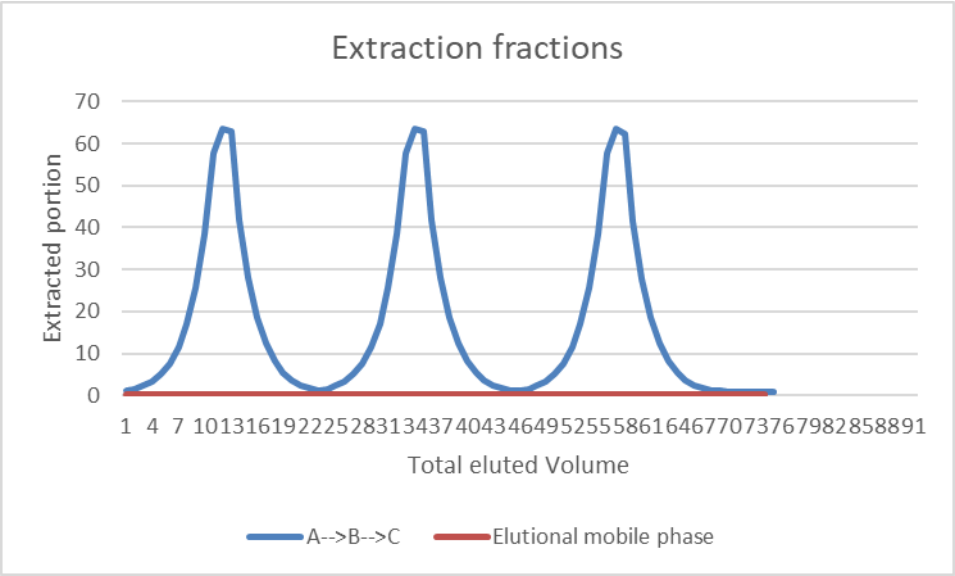

Graph. 4.1.4: Illustration of an elution chromatography and its results, where A,B,C are the separated substances, with A<B<C their reactivity with the resin and/or C<B<A their ability to complex with the elution (E)- mobile phase.

4.2. X-ray fluorescence (XRF) spectrometry

The working principle of an XRF spectrophotometer is summarised in three main parts: the X-ray production part (Source), the Detector and the electronics/data recording part. Compared to a classical spectrophotometer we can observe the absence of the monochromator and the angled arrangement (between initially detected radiation) as a consequence of the fact that in this spectroscopy we exploit the radiation emitted by the sample (and not the one absorbed). The primary rays (X1) from the source, produce characteristic secondary rays (X2) (fluorescence) caused by the samples' excitation, whose energies are lower than the energy of the primary rays, and they depend on the elements that the sample contains. These characteristic radiations are detected in the detector, where they are converted into an electrical signal, which is then amplified in the preamplifier and the system amplifier, converted from analogue to digital in the ADC (Analog to Digital Converter) and recorded in the computer. From their energy, the type of elements of the sample is determined (qualitative analysis) and from their intensity, the amount composition of the sample (quantitative analysis).

The phenomenon is not that simple in reality, the de-excitation can be accompanied by radiation or by an electron (Auger electron). For each element and each orbital layer, a characteristic ratio called fluorescence yield (ω) is measured

ω = (the number of produced x-rays) / (the number of ionizations)

and where ω varies between 0 and 1. The fluorescence yields for the various elements are given in special tables and start from minimal values, for the light elements (less than 0.01) to reach almost 1 for the heavy (high individual number).

This means that the lighter (low atomic number) an element is the more it "prefers" to be de-excited with Auger electrons and the heavier with X-rays.

The measurement time is usually a few minutes (<h). The results depend also on the number of X-rays recorded and can be improved by extending the measurement time. The statistical uncertainty S_N of the recorded X-rays is given as the square root of the X-rays' number N

$S_N=\sqrt{N}$

Minimum detection limits depend on both the element being measured and the sample's matrix and are typically in the ppm (parts per million) range.

5. Accelerator Mass Spectrometry (AMS)

Combining the principles of the **Isotope Ratio Mass Spectrometry** (IRMS)**, AMS is an analytical technique with higher energy-charged particle acceleration**.

Detection Capability: AMS allows for **extremely low detection** of isotopes in samples, even the very rare ones, of natural or/and non-natural materials, even as small as **1 milligram**. The sensitivity can reach, in some cases, even less than one part in 10^{15} parts (Kieser, 2023).

Accelerators have been used to increase the sensitivity of mass spectrometry since 1939. Alvarez and Cornog back then, used the Berkeley cyclotron to detect the existence of ^{3}He in a sample of ^{4}He at a ratio of $^3He/^4He \approx 1 \times 10^{-6}$. However, it was not before the development of the tandem electrostatic accelerators and the negative ion sources that the technique managed to become more widely used.

Around the same time, Libby developed the technique for determining measurements of the age of organic samples. Counting the β particles emitted in the radioactive decay of ^{14}C in samples could use a series of known-age samples for overall calibration. This technique gained popularity in Earth and environmental sciences, as well as in archaeology.

By the mid-1970s, the need for precise and rapid ^{14}C dating exceeded the capacity of the decay-counting method. However, mass spectrometry was still hindered by the presence of the isobar ^{14}N, which has a nearly identical mass. It was till 1977 when Purser and his team discovered that the negative ions of ^{14}N are unstable while those of ^{14}C are relatively robust (Purser et al., 1977). After that discovery, the way was paved for the spreaded use of tandem electrostatic accelerators and sputter ion sources to provide ^{14}C measurements with acceptable accuracy.

With the ion energy provided by tandem accelerators and high ion currents from the sputter source, the fortuitous instability of the ^{14}N anion could be exploited. Today, accelerator mass spectrometry is widely used for various applications, including measuring the age of organic samples and analyzing environmental samples.

Between 0.5 and 3 mg of materials are compressed inside the target. A reservoir of metallic Cs is heated up in the ionizers' area of the target to a temperature of around 130-145°C. Caesium has a low ionization energy (3.8939 eV), making it easy to remove the outer electron from the atom. When heated to 2500°C, Cs lose its electrons and can then accelerate and hit the sample, creating a cloud of molecular ions, including vapors of metallic Cs. At this stage, the excited ions and molecules pick up electrons from Cs, resulting in a cloud of negatively charged ions. These ions are extracted from the ion source by an electric field. Subsequently, the beam, which contains negatively charged ions, is

directed to the mass spectrometer. It is worth noting that only elements capable of forming negative ions can be analyzed by this technique.

The small sample sizes result in cost-effective collection, shipping, and preparation. Besides that, AMS allows precise analysis of specific chemical compounds within a sample and provides more accurate chronological information for radioactive isotopes.

5.1. AMS overall description

Graph. 5.1.1.: Graphic depiction of AMS, reproduced through “AI” graphic tool, from an actual photo of the AMS system operating in Rez.

A negative ion beam is formed inside the ion source (5.1.2), subsequently an electrostatic and a magnetic analyzer are analyzing this beam in the injector. The ion beam undergoes several steps of analysis and manipulation in the accelerator system. First, the beam is bent to become vertical using the electrostatic analyzer, and then it is bent back to the horizontal with the magnetic analyzer. Along the beamline, optical devices such as einzel lenses and quadrupole lenses are placed to maintain a small beam envelope.

The process continues as the negative ion beam is directed into the accelerator and propelled towards the positively charged high-voltage terminal of the tandem accelerator. Upon reaching the high-voltage terminal, the negative ions traverse a foil or a gas cell, shedding electrons in the process, thereby acquiring a positive charge and gaining significant energy. The foil or gas cell also serves to dissociate molecular ions, effectively preventing interference. Subsequently, the positively charged ions undergo additional acceleration towards ground potential through the second stage of the accelerator, further augmenting their energy level.

Subsequent to this stage, the positive ion beam is scrutinized by a magnetic analyzer, through which the ions of interest are methodically singled out. The beam then undergoes successive analyses by a velocity selector and once again by a magnetic analyzer. This careful selection process ensures that the identified ions possess precisely defined charge states, energy levels, and mass. These ions are then meticulously detected, identified, and quantified one by one through the use of a detector. It is of paramount importance to note that the identification of ions based on their energy level is essential in order to prevent potential interference from undesired ions that may reach the detector (Hellborg and Skog, 2008). Both decay counting and conventional mass spectrometry have some

essential limits compared to Accelerator Mass Spectrometry, particularly for rare and long-lived radioisotopes. A characteristic example is the one of MS that can only be used for an isotopic ratio of $^{14}C/^{12}C$ which is approximately 10^{-7} **or higher**. The AMS as an alternative, drops the $^{14}C/^{12}C$ detection limit even lowered (at approximately 10^{-15}). 1 mg carbon sample, only, is sufficient for AMS measurements, and that is the one-thousandth of the material needed for a decay counting analysis. That 1 mg sample will be completely sputtered (inside the ion source) within one or two hours and most typically $6{\cdot}10^5$ atoms can be counted in the AMS detector, which corresponds to 1% of the total ^{14}C content (Hellborg and Skog, 2008).

For the actinides, the setup of the accelerator was modified regarding their special need. In general, as shown below, is formed in a very similar structure as (Christl et al., 2023a). All AMS measurements described here were conducted using the compact 300 kV AMS system called MILEA. To measure actinides, a terminal voltage of around 260 kV is applied, which is limited by the bending capability of the HE-magnets. Taking into account the sum of ion source and sample potential of 46 kV, and the molecular breakup from the oxide injection, the stripping energy of actinide ions is about 285 keV. By selecting the three-plus charge state, the final actinide ion energy is slightly above 1 MeV. The signal from the first anode of the GIC is used for the detection of rare actinide isotopes. Actinide analyses utilize a 3 × 3 mm² or a 4 × 4 mm² SiN detector entrance window of 30 nm thickness.

The process involves compressing a sample (0.5 to 3 mg) in a sphere-shaped target with a hole, which is then placed in an array in a special case. A magazine containing the targets is inserted into the first area with an ionizer, where a single target sample is chosen each time for ionization. The first part of an AMS is the ionizer and ion source, which operates at very high temperatures and contains a reservoir with metallic Cs (stable). When heated to 2,500 °C, caesium loses its electrons due to its low electron ionization potential, and, as a result of a potential difference between the ionizer and the sample, it is accelerated and hits the sample stuffed into a cathode.

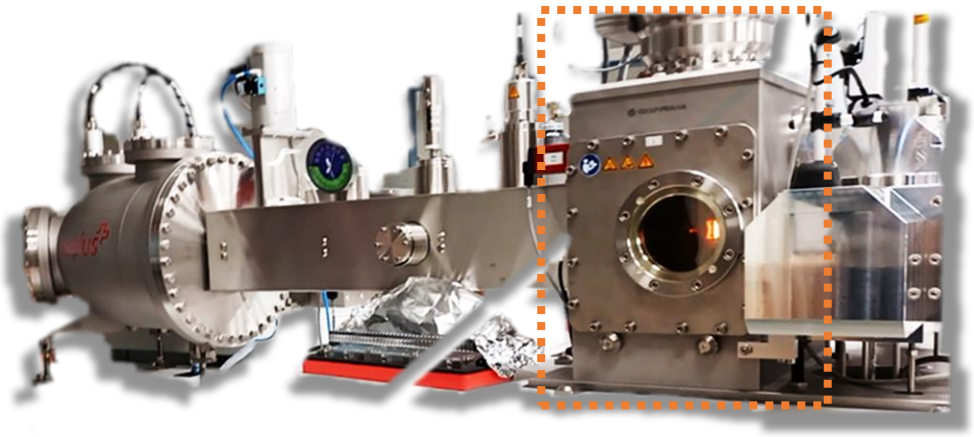

Graph. 5.1.2.: Graphic depiction of the ion source (orange rectangular) before the first magnet of AMS.

The process begins with the formation of atomic and molecular ions through a collision with metallic Cs vapours. The excited atoms and molecules take electrons from Cs, which has the lowest electronegativity of all metals, creating a cloud of negatively charged ions. These ions are then extracted from the ion source, ideally by evaporating everything inside the cathode.

The unpurified ion beam passes through an array of splitters and cutters before entering the first electrostatic analyzer. Inside this tube, two electrodes allow only ions with the correct potential to

follow their exact bending trajectory. This allows us to select ions and molecules with specific charge-to-mass ratios, leading them into the first magnet based on their energy charge relation.

When a charged particle is moving in an electric field it bends depending on the fields' energy and its atomic mass. Furthermore, after the Magnet, the first Faraday Cups measure the current from the beam, so we can have a first glance at its consistency. The beam then accelerates. Negative ions enter in an array of two accelerator tubes left and right and a "terminal" in the middle connected with a capillary with helium. The terminal (connected in the middle) has a max of +300 kVolt.

Graph 5.1.3.: "AI" generated, from a real photo, graphic depiction of the terminal with the helium capillary.

When negatively charged molecules are accelerated towards a small chamber filled with helium, they collide with the helium atoms, causing the molecules to break and release electrons into the surrounding environment, while producing positively charged atoms. These positively charged atoms then accelerate away from the center, resulting in the generation of positively accelerated ions.

After this acceleration, ions exhibit different energies and velocities, thus we need a photon line both before and after the magnet to ensure that the ions are properly focused into a single well-formed "beamline." Different masses of ions are bent in varying degrees by magnets and are led to different Faraday Cups, where precise mass-count events are measured. A specialized injector continuously introduces specific isotopes into the system to analyze their ratios. Following the second analysis by the magnet, we use Faraday Cup detectors to observe the positions of the ions, from the most bent to the least bent, through the top window. Due to their lighter mass, lighter isotopes bend more and consequently end up on the inner side.

A Faraday detector collects and measures the charge of the beam hitting inside the cup over time, providing accurate data. Heavier atoms possess greater kinetic energy, resulting in less bending of their trajectory. In theory, the number of Faraday cups available determines the total number of different isotopes that can be measured.

Uranium, for example, ^{236}U straight-line measured from the charge, including the slightly lighter ^{235}U. In the Faraday cups, you can measure the most abundant ones, and for the rear ones you need to use the detector. Normally located after the last magnet, at the very end of the AMS array, an electrostatic analyzer cleans the beam to leave only the isotopes of interest and the magnet leads the beam to the gas detector. There, different particles decelerate differently in interaction with the gas and an additional distinguishing between them occurs (different atomic and mass numbers decelerate once again at different speeds).

From the magnets and after the isotopes separated, and the beam is tuned by moving from an open curve to a closed one, in order to clear and specialize what is coming into the final detector. A second electrostatic analyzer depicts what the detector receives in real-time.

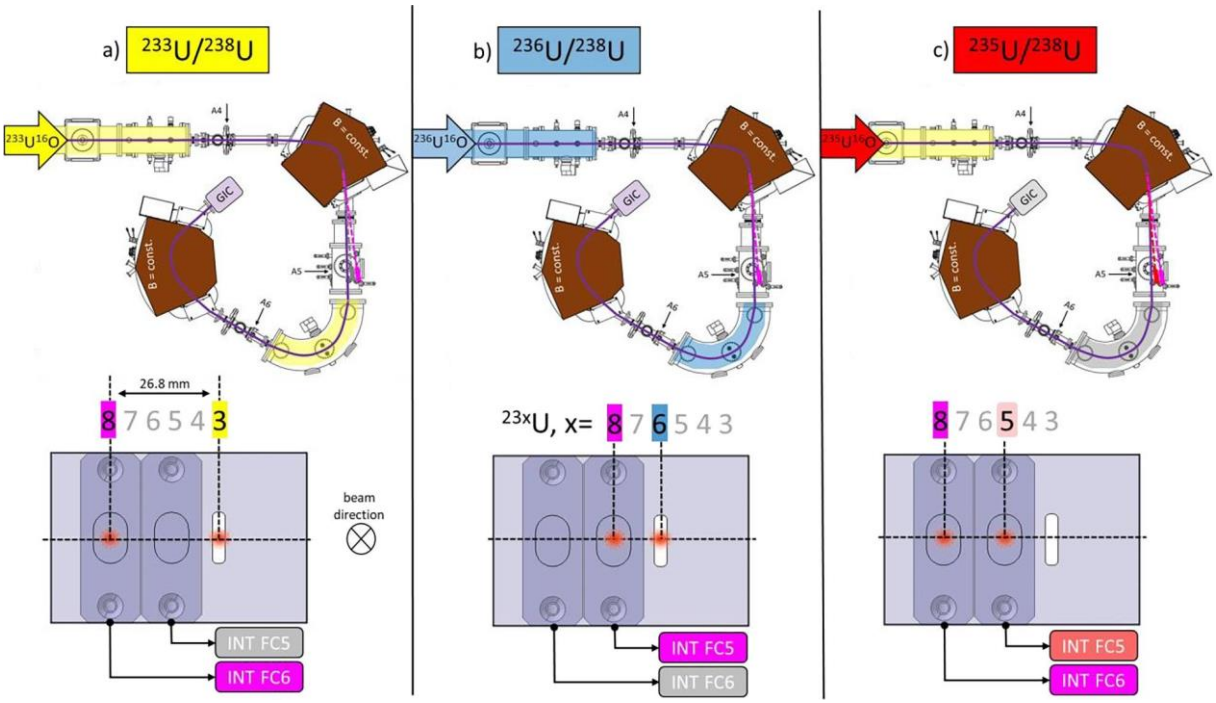

Graph. 5.1.4: **Measurement cycles for uranium isotopes** (Christl et al., 2023b)

The MILEA system has two main components: the low energy (LE) side and the high energy (HE) spectrometer.

The LE side features a multi-cathode MICADAS-type Cs-sputtering negative ion source, which operates at voltages of up to 50 kV. It also includes a 90° electrostatic analyzer (LE-ESA, r = 534 mm) and a 90° magnet (LE-magnet, r = 450 mm) that allows for achromatic injection of the negative ion beam into the accelerator and stripper. The LE-magnet has a fast-bouncing system that enables the fast, sequential injection of different masses into the accelerator. There are two movable Faraday cups on the LE-side, which are positioned on each side of the beam axis in front of the accelerator. These Faraday cups allow for the monitoring of the negative ion current and the determination of ion beam transmission through the accelerator.

The HE spectrometer consists of two momentum (p/q) filters: the 90° HE1 magnet (r = 600 mm) and the 110° energy (E/q) filter: the 120° HE2 magnet (r = 600 mm) and an ESA (r = 620 mm) placed between them. There are also seven moveable Faraday Cups (HE FC) in the analysis chamber after the HE1 magnet, allowing for the measurement of the ion currents of stable or abundant nuclides for the various AMS setups. HE FC 1 – 4, which are located on the right-hand side of the rare isotope beam axis, are used for the stable nuclide(s) detection during ^{14}C, ^{10}Be, ^{41}Ca, and ^{129}I measurements. FC 5 – 7 are placed on the left-hand side for U-isotopes and Al measurements. To account for the spatial separation of different isotopes, two versions of FCs have been designed with an opening width of 14 mm (HE FC 1,2,3 & 7) and 8 mm (HE FC 4, 5 & 6). The smaller FCs are used for current measurements, such as ^{235}U.

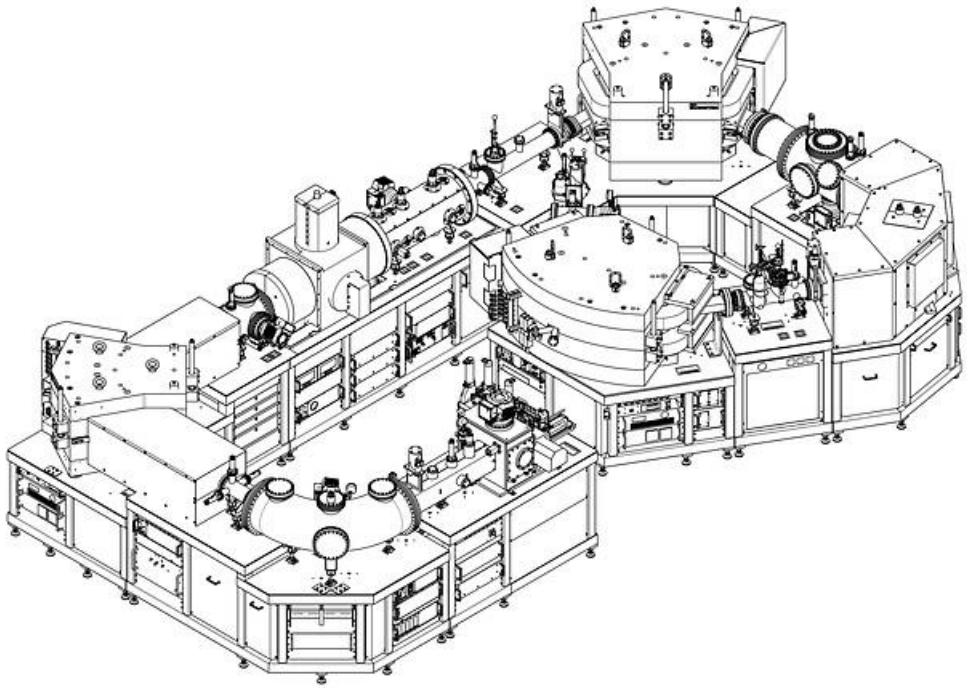

Graph. 5.1.5.: Graphic depiction of MILEA - Multi-Isotope Low-Energy AMS, from Ionplus. It's an accurate graphical representation of the AMS detector elaborated in Nuclear Physics Institute of the CAS, Ústav jaderné fyziky AV ČR, Řež.

The following equation gives the total apparent detection efficiency, with Y representing the isotope of interest (Christl et al., 2023b):

$$eff_{def}(Y) = \frac{\Sigma counts(Y)}{spikedatoms(Y)} \times \frac{\sum_{sputtertime}(target)}{\sum measuretime(Y)}$$

A total ionization efficiency was calculated assuming 33 % transmission (LE to the HE side) and 85 % HE-transmission:

$$eff_{ion}(Y) = eff_{det}(Y) \times \frac{1}{tra(LE-HE)} \times \frac{1}{tra(HE)} = eff_{det}(Y) \times 3.6$$

6. Areas of research

The main object of this research focused on the development of an optimum way for environmental radioactivity research in Vefsnfjord sampling area (Norway). Sampling took place from the scientific team of Norwegian University of Life Sciences - NMBU. Furthermore, and after discussion, a small number of samples were collected from North Cretan Island (Kolpos Almirou), and one opportunistic sample from Copenhagen (Denmark). All together were and still are under proper treatment for a number of measurements, for a series of isotopes for elements of iodine, plutonium, and uranium.

The research performed so far touched three areas:

- Vefsnfjord, Norway
- North Cretan Island
- Christiania, Copenhagen

Vefsnfjord, Norway

This area was selected in a collaboration project with the Norwegian University of Life Sciences (Norges miljø- og biovitenskapelige universitet – NMBU, Ås). The final aim of the study is to determine the interaction of the contaminated land with rivers, fjords and open sea. The Vefsnfjord area belongs among the areas contaminated most heavily by the fall-out from the Chernobyl NPP disaster. The target nuclides / nuclidic ratios for the study have been $^{236}U/^{238}U$, $^{129}I/^{127}I$, and plutonium isotopes.

A total of 97 samples (including tests, blanks + one from Denmark) were collected, 51 samples were mailed to Czechia, 46 were handled at NMBU in Ås including tests and blanks.

Picture 6.1: Geographically marked areas where samplings occurred from.

The sampling was held by the Isotope Laboratory / Centre for Environmental Radioactivity (CERAD) research team of the Norwegian University of Life Sciences (NMBU) from the Environmental Chemistry Section and included a large number of sediment and soil samples from vertical cores (“carrots”).

Two sampling sites have been chosen based on an overall observation of ^{137}Cs concentration on the surface of the understanding area.

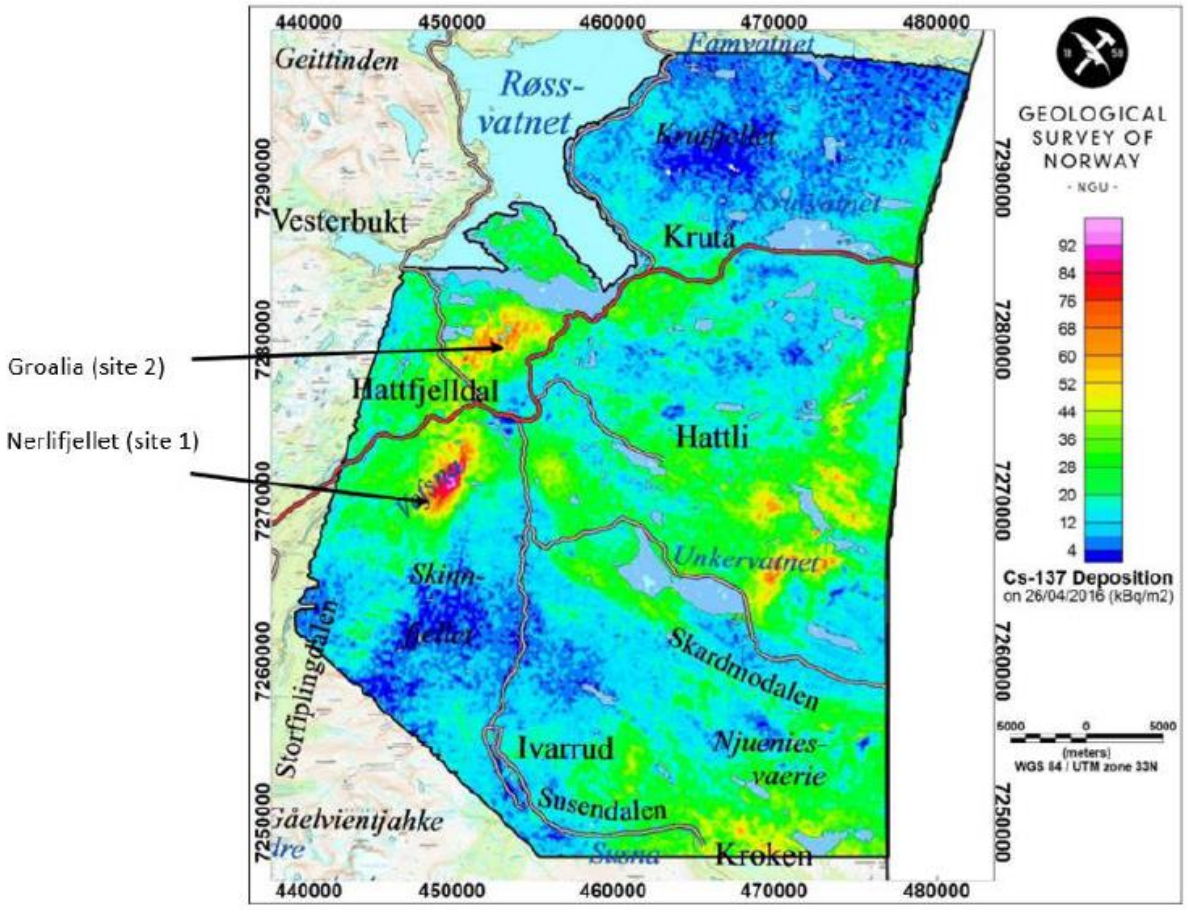

Picture 6.2: Sampling sites within the fjord, with widespread ^{137}Cs concentrations, for their surficial depositions (provided by the Geological Survey of Norway through NMBU)

North Cretan Island

The bays of Souda and Almyros represent an area of particular ecological and radiological interest. There, the southern arm of the estuary of the river Almyros, flows to the south of Kalyvaki beach, while its northern arm represents a second section of the same river complex and forms a very clear stratification of fresh, semi-sweet & salt waters which are separated by their densities due to their large difference in salinity and temperature differentiation, especially in spring when the sampling took place (May 2022). The overall area includes one of the biggest NATO bases in Europe and, at the same time, there is an output of a water flow possibly carrying a load of remains of old mining activity in the central area of Crete.

Similarly to the Vefsnfjord area, the target nuclides / nuclidic ratios for the study have been ^{236}U/^{238}U, ^{129}I/^{127}I, ^{137}Cs, and plutonium isotopes. In addition, bulk analysis of the samples by XRF was performed.

Three water sampling points and two for sediment exact on the coastline, double samples from every water sampling spot were collected for uranium and iodine separation procedure 10 litres for iodine and 5 litres sample for uranium, the very same day the chemical number one added on the samples for iodine and chemical number two on the samples for uranium, finally the cores collected from both sides separated into 4 parts the first double core kept intact for further analysis and the second core into the upper layer(A) and the lower layer (B) with the centimetres depicting the depth of the core layers.

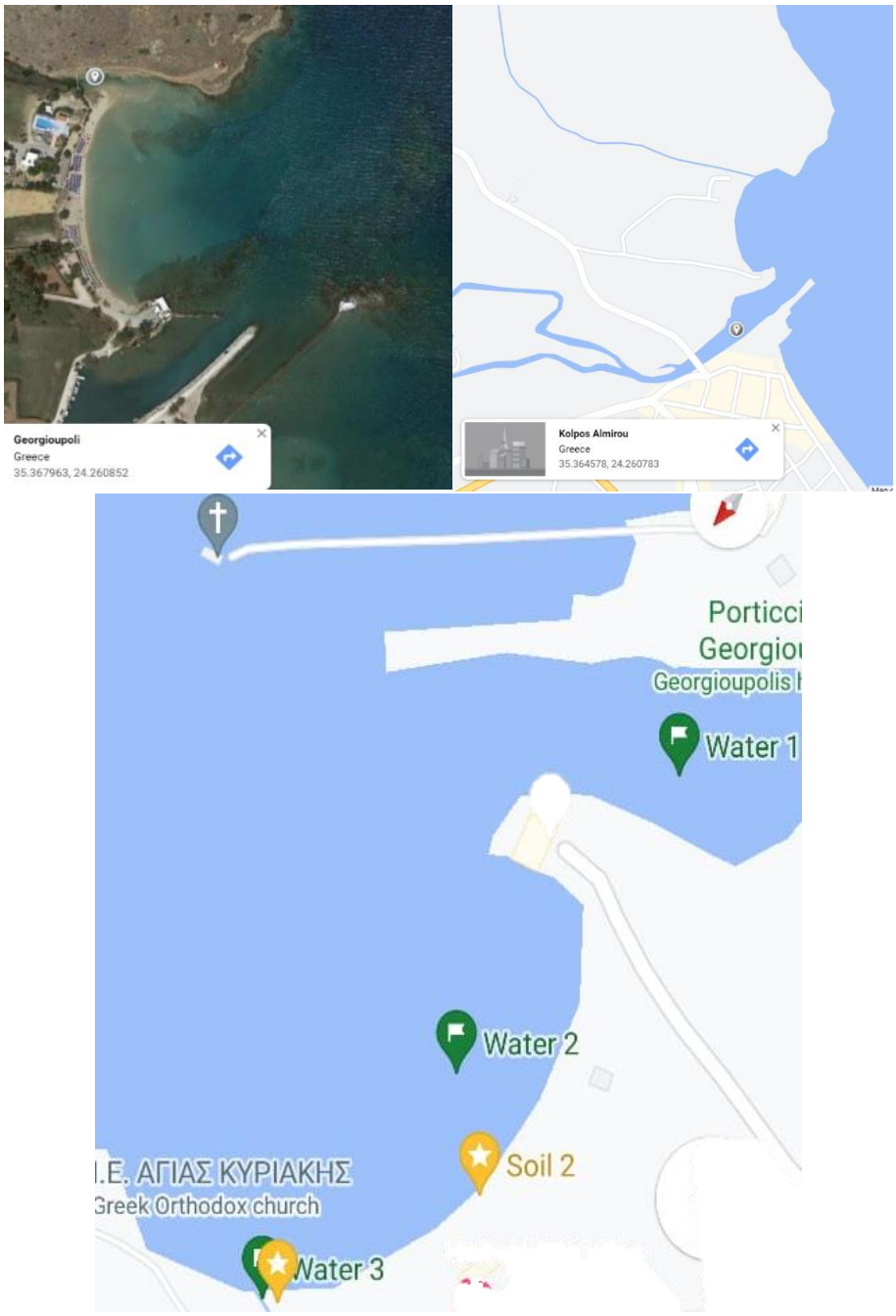

Picture 6.3.: Kolpos Almirou and pointed sampling points for water (⚑) and for sediment (★).

Christiania, Denmark

Only one sample (sediment) from the inner lake of Christiania was collected, in a sample tube of approximately 10cm high.

7. Research approach

The research approach involves a threefold analysis of samples from various regions with diverse thermodynamic and geodynamic geological characteristics. Additionally, samples will undergo γ spectroscopy using high-purity germanium detectors, with main-sample analysis conducted using an Accelerator Mass Spectrometer in conjunction with measurements from ICP-MS. General screening

using X-ray fluorescence spectrometry (XRF) will also be performed for select samples (Cretan). The AMS analysis will outline the isotopic ratios of uranium, plutonium, and iodine. Approximating the concentration of caesium provides insight into the expected radiochemical background and characteristics of our sampling sites (e.g. Vefsnfjord).

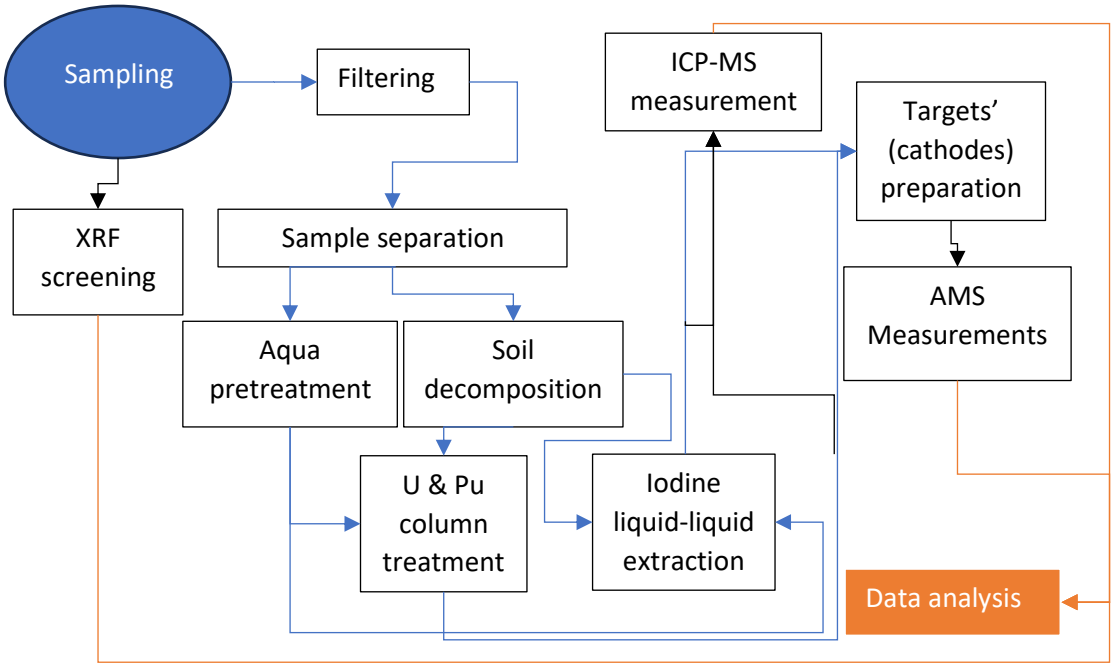

Graph. 7.1: schematic depiction of the overall methodological approach in steps

Iodine due to its nature, being very volatile in most of its forms, needs to be treated carefully under different handling steps for each one of the fractions that contain it. In the soils and sediments, where iodine can be present in a broad scale of chemical forms, a general sequential analysis may have the design to identify the abundance of iodine in the following species:

- Fraction 1: Water-soluble Iodide, Iodate and polar organics
- Fraction 2: Exchangeable Iodide
- Fraction 3: Iodine in reducible Fe, Al, Mn oxides & oxyhydroxides
- Fraction 4: Iodine in carbonates
- Fraction 5: Iodine in non-polar organics and natural organic matter
- Fraction 6: Iodine in resistant oxides and sulfides

Up to the present time, no soil or sediment samples have been treated for the above fractions. This is because a suitable leaching method needs to be found, which involves microwave digesting systems, in order for the process to be efficient in terms of both separation and time. Although we have studied relevant bibliography on the subject, (Gómez-Guzmán et al., 2011; Victoria et al., 2022), successful trials still need to be conducted.

However, in Czech Technical University in Prague a less inconvenient approach if currently used and optimised for its' efficiency as described below.

7.1. Methodologies

In this research, 2 main methodologies were followed for iodine and U/Pu, as described below, nonetheless, 2 more treatments were examined for a smaller sampling number from the Mediterranean region. All treatments (examined and studied for future treatment) are noted below

in some detail. The data for ^{137}Cs and its measurements were provided by the research team of NMBU, no pretreatment details are given in this text.

7.1.1. Iodine

Sediments:

For ICP-MS determination of ^{127}I:

1) 1 g of soil into the 50 mL plastic centrifuge tube.
2) 25 mL of 10 % TMAH (tetramethylammonium hydroxide) solution.
3) Incubate at 90 °C for 2 hours.
4) Centrifugate and transfer the aqueous phase into the new centrifuge tube.
5) 0.1 mL aliquot of TMAH should be taken out and diluted with 0.01 % $(NH_4)_2SO_3$.

The aliquot from step 5) can be measured on ICP-MS. A sufficient carrier is mandatory to determine $^{129}I/^{127}I$ by ICP-MS or AMS. The rest of the procedure above can be used as follows.

1) 0.03 g $K_2S_2O_8$ into the solution.
2) Incubate at 60 °C overnight.
3) Centrifugate and discard the precipitation.
4) Add 5 mL of CCl_4, 1.5 mL of 1 % $(NH_4)_2SO_3$ and 9 mL of 6 M HNO_3 to adjust pH < 3.
5) Shake for 2 minutes, centrifuge and discard the organic layer between CCl_4 and TMAH.
6) Add 0.4 mL of 5 % $NaNO_2$ under acidic conditions.
7) liquid-liquid extraction.
8) Then, a portion can be measured on ICP-MS again or continue to the liquid-liquid extraction for AMS as described in the next subchapter.

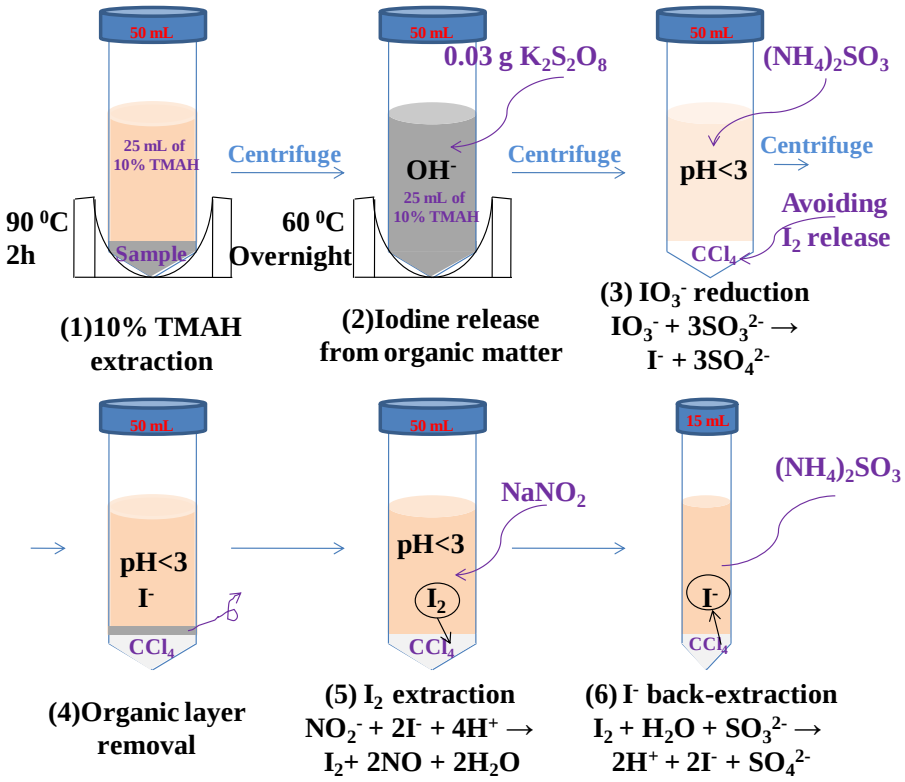

Graph. 7.1.1.1: Graphical depiction of iodine extraction approach described by (Yang et al., 2018)

Liquid-liquid extraction:

In this chapter, we will describe the methodology followed for two different types of aqueous samples (fresh and saltwater), as have been established so far.

1) Water samples should be filtered through a 0.45 µm filter within 2 days of sampling. For transportation or storage, pretreat samples by adding 12.6 g Na_2SO_3 per 1 dm^3 (1 dm^3=1 L).

2) 0.5 – 0.8 dm^3 of freshwater (or 100 ml of seawater) into a beaker, and then weigh the mass of the water. Next, $K_2S_2O_8$ was added to reach a final concentration of 30 $mg \cdot cm^{-3}$.

3) Following, 1.0 mg of stable iodine carrier (or 2.0 mg if using seawater) with the Woodward iodine isotope ratio $^{129}I/^{127}I$ less than $2 \cdot 10^{-14}$ into the sample. To determine the chemical yield, add 5 kBq of ^{125}I tracer (with a half-life of 59.4 days, γ-energy 35.5 keV, and yield of 6.68%). Alternatively, ^{131}I can be used (with a half-life of 8.0252 days, γ-energy 364.5 keV, and a yield of 81.5%). The pH should be adjusted to 1 by adding a few drops of concentrated HNO3. Beaker covered with a glass watch and heat the solution on a hotplate at 60 °C for 20 hours to decompose organic matter and convert all iodine to inorganic forms. Finally, allow the solution to cool down naturally.

4) 3 cm^3 *(1 cm^3 for seawater)* of 1 $mol \cdot dm^{-3}$ $NaHSO_3$ to the freshwater sample, concentrated HNO_3 (few drops) should be added to pH 1 – 2. Wait at least 5 minutes to convert iodine (I_2) to iodide (I^-).

5) The solution can be transferred to a 500 cm^3 separation funnel. Adding 10 – 15 cm^3 of $CHCl_3$ and shaking the phases. If a third phase is formed, it must be removed together with $CHCl_3$. Then, fresh 10 – 15 cm^3 of $CHCl_3$ is added to the aqueous phase. Adding dropwise 1 – 2 cm^3 of 1 $mol \cdot dm^{-3}$ $NaNO_2$, until a pink colour appears in the organic phases. In this step, $NaNO_2$ oxidize I^- to I_2. I_2 extracted to the organic phase by shaking.

6) Separate the $CHCl_3$ phase (down) to the beaker. A new portion of $CHCl_3$ is added to the separation funnel to extract the remaining I_2, organic phases can be combined afterwards. Extraction repeated 2 – 3 times (or more), till the pink colour disappears. During the last extraction, add 5 drops of 3 $mol \cdot dm^{-3}$ HNO_3 and 1 drop of 1 $mol \cdot dm^{-3}$ $NaNO_2$.

7) The organic phase is then transferred to a washed and clean 50 cm^3 separation funnel. Add 20 – 30 cm^3 ultrapure water (18 MΩcm). Then, 0.3 cm^3 of 0.05 $mol \cdot dm^{-3}$ $NaHSO_3$ added to back extract iodine to the water phase by reducing I_2 to I^-. Wait ~2 minutes to see whether adding reducing agent is sufficient – both phases must be colourless. In case, that the water phase is yellow or organic phase is pink, it is necessary to add more $NaHSO_3$. Separate and discard the organic phase to a waste bottle.

8) Adding to the water phase in the funnel, 10 cm^3 $CHCl_3$, 5 drops of 3 $mol \cdot dm^{-3}$ HNO_3, and 0.1 cm^3 $NaNO_2$ (1 drop should be enough) to oxidize I^- to I_2. I_2 extracting to $CHCl_3$, separate the organic phase to the beaker. Adding 10 cm^3 of fresh $CHCl_3$ to the separation funnel, repeat the extraction, combine the organic phases. Repeat extraction if necessary.

9) The organic phase can be transferred to a new separation funnel and 3 cm^3 of ultrapure water (as less as possible) and 0.2 cm^3 of 0.05 $mol \cdot dm^{-3}$ $NaHSO_3$ are added afterwards to back extract iodine to the water phase. Both phases must be colourless. Afterwards, organic phase can be discarded to the waste bottle. If the solution becomes coloured, add 1 drop of 1 $mol \cdot dm^{-3}$ $NaHSO_3$.

10) Finally, the water phase is transferred to a 10 mL centrifuge tube (max volume for the sample should be ~ 7.5 mL). Fill the free volume with water which was used for cleaning of the separation funnel. In case the precipitation is done later (or the solution is not yellow), after a few hours or the next day, add 1 drop of 1 $mol \cdot dm^{-3}$ NaHSO3 into the sample in the tube.

11) For precipitation, to the water phase in the centrifuge tube, add 1 cm^3 of 3 $mol \cdot dm^{-3}$ HNO_3 and 1 cm^3 of 1 $mol \cdot dm^3$ $AgNO_3$. Mix it well (using a Pasteur pipet) to let the AgI to precipitate. Centrifuge at 2300 rpm for 2 minutes.

12) The precipitate washed with 0.5 – 1 cm^3 of 3 $mol \cdot dm^{-3}$ HNO3, adding again water, mix and centrifuge. Repeating the washing step with water only, 2 – 3 times. Then, transferring the precipitate with a Pasteur pipet into a weighed 1.5 cm^3 centrifuge tube with the help of water. Remove the excess of water with the pipette. Centrifuge, and remove the water rest. Dry the precipitate in the centrifuge tube in an oven at 60 – 80 °C for not longer than 2 hours.

Following the precipitation with silver to form AgI, we can utilize this resultant precipitation for AMS targets and measurements. More precisely, we will combine a 1:1 ratio of Niobium to AgI, with the combined portion not greater than 1-2 mg.

7.1.2. Uranium and plutonium

For sediment samples chosen for uranium and plutonium determination, partially treated also for organic matter determination (mainly for the needs of acid compositional decisions during the decompositional process). All samples were very carefully freeze-dried, and then small portions (1-2 grams) were separated to burn in a pyrolytic procedure in order to measure the organic matter (calculated from the difference of mass before and after pyrolysis). The rest portion from every sample was carefully treated in order to measure $^{236/235/238}U$, $^{129/127}I$ and $^{234/240/241/242}Pu$. Expected ratios for uranium isotopes were for ^{238}U > 99%, ^{235}U~0.72%, and for ^{236}U the concentrations are expected so low that only AMS measurements could actually provide us with some detectable measurements.

To around 2 grams of every sample, 1ml of tracer (^{233}U) and between 15-20 ml of HNO_3 was added, and then digested in an ultra-CLAVE digesting system. After carefully separating the solution from any remaining precipitates, it is best to minimize the addition of distilled water or filters *(may use them if necessary)*, although they may be used if necessary. Teflon vessels are recommended for effective separation. The remaining solids should be dried and then subjected to a second digestion in a mixture of HNO3 and HF solution. The amount of HF required depends on the quantity of non-organic material present, and the addition of nitric acid is crucial to enhance the effectiveness of HF in dissolving the remaining substances.

Following the second digestion, the solutions should be combined and the process continued with the resin columns as detailed below.

Dissolution for soils & sediments

The process for the case of uranium and plutonium differs slightly between water samples and soil-sediment sample treatment (in essence only in digestion), the acids used to dissolve the sediment and soil could be used to acidify the starting sample solution (in the case of water sample – but then precipitate again). In general, the solutions from soils/sediments are formed according to their content of organic carbon and minerals.
The more the organic the more concentrated HNO_3 we need in the solution, the overall volume should carefully be considered in order to avoid possible explosions from the formation of nitro-glycerine $C_3H_5N_3O_9$ during ultra-CLAVE digestion.
The minerals' breakdown by HF, usually has reactions like the following example:

$$^{IV}SiO_2 + 4HF \rightarrow SiF_{4(g)} + 2H_2O$$
$$Al_2O_3 + 12HF + 3H_2O \rightarrow 2AlF_6 + 6H_2O + 3H_2$$

Tracers for uranium and plutonium should be introduced into the sediment or soil first. If we are specifically investigating the ratio of plutonium isotopes (such as $^{240}Pu/^{239}Pu$) to determine the source, then the plutonium tracer may be excluded from the process. It is important to prepare one reference sample/material and one blank concurrently.

The digestion process should ideally take place using ultraCLAVE digestion in two steps: first with HNO_3 to break down organic matter, and then a second digestion of the residue with HF to dissolve the minerals. Alternatively, this can be done on a hot plate with a higher concentration of acid (mixed HNO_3 + HF) at a temperature range of 100-180 ^oC.

Following digestion, a column procedure is performed to separate uranium and plutonium.

Of the final solution, the majority, around 1ml, should be retained for AMS measurements, while the remainder should be diluted to approximately 5 ml for ICP-MS measurements.

The necessary equipment and chemicals for this process include: concentrated nitric acid, concentrated hydrochloric acid, concentrated hydroiodic acid, 6 M nitric acid, 1 M nitric acid, 0.1 M nitric acid, 9 M hydrochloric acid, 9 M hydrochloric acid containing hydroiodic acid, 200 $mg \bullet ml^{-1}$ ferrous ammonium sulphate, 0.7 M sodium nitrite solution, AG1-×8 resin column, UTEVA resin column, plastic pipettes, glass and Teflon beakers, and a hot plate.

Column treatment

1.1 Redissolve material in 18 mL 1M Nitric acid.

1.2 Add 1 mL of 200 mg mL-1 ferrous ammonium sulphate. Allow to stand for 30 minutes

1.3 Prepare tandem AG1-×8 and UTEVA columns by washing with 10 mL 6 M nitric acid mixed with 1 mL 0,7 M sodium nitrite solution.

1.4 Add 1 mL 0,7 M sodium nitrite solution to solution from 1.2

1.5 Add 10 mL of concentrated nitric acid

1.6 Load solution onto tandem columns prepared in 1.3 and collect the eluate

1.7 Wash the column with 3×5 mL 6M nitric acid and combine eluate with that from 1.6.

1.8 Reserve eluates if necessary.

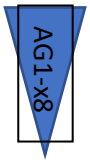

At this point, we reached the separation of Uranium and Plutonium, and from that here on we separated the columns

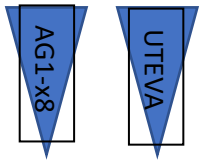

Pu-Solution U-Solution

For AG-x8 columns, we follow:

2.1 Wash the AG1-×8 column from 1.9 with 5 mL 9 M hydrochloric acid, and collect the eluate, which may be retained for thorium measurements.

2.2 Wash the AG1-×8 column with 20 mL 9 M hydrochloric acid (HCl) containing hydroiodic acid (HI).

2.3 Evaporate the combined eluates to <5 mL, but do not allow to dry. Add 1 mL concentrated nitric acid and heat.

2.4 Repeat 2.3 until no further iodine is outgassed and the solution remains colourless.

2.5 Evaporate the remailing solution to <5 mL, but do not allow to dry. Transfer to a suitable container for measurement solution preparation.

For UTEVA columns we follow:

3.1 Wash the UTEVA column from 1.9 with 15 mL 0,1 M nitric acid, and collect the eluate.

3.2 Wash the UTEVA column with 10 mL water, and combine the eluate with that from 3.1

3.3 Evaporate the combined eluates to <5 mL, but do not allow them to dry. Transfer to a suitable container for measurement solution preparation.

From that step on, the solution for ICP-MS will be treated differently, specifically a portion of that will further dilute and transfer for measurement. The rest portion will be combined with the AMS solution to be treated properly for the U and Pu preconcentration.

For the AMS targets:
1ml of Fe(III) nitrate nonahydrate (5mg Fe/ml) should be sufficient for every 0.5 ml from the U fraction. The mixture should evaporate to dryness on a hotplate and 1mol/dm^3 HNO_3 (15ml) can be added to remove any residual chlorides. This should be then taken and baked to a hotplate for approximately 1h at about 300^{o}C to convert $Fe(NO_3)_3 \rightarrow Fe_2O_3$. The oxide residue goes to a furnace at 450^{o}C for at least 4 h to ensure the complete conversion to oxide & the evenly distribution of uranium within iron oxides.
Eventually, the oxide should mix with aluminium powder in a 1:1 ratio and then packed into the targets.

7.1.3. Cretan samples pretreatment

During the sampling of water and sediment from Cretan Island, a different approach was chosen. 132g Sodium sulfite (Na_2SO_3) was added to preserve the iodine in the sample solution, and 6 ml of Titanium(IV) Butanolate (TBOT) to precipitate uranium. The iodine solutions followed the liquid-liquid extraction as described above and the ones for uranium were filtered in order to separate the TBOT precipitate from the aqueous phase, then treated similarly with the sediment procedure mentioned first.

Table 7.1.3.1: **Water and sediment sampling from Creta**

Sample	Site	Volume/depth / Core layer	addition	Temperature (°C)	Type
1st Water A	*W1*	*10 L*	*Na_2SO_3*	*6*	*Fresh sub surface*
2nd Water A	*W2*	*10 L*	*Na_2SO_3*	*19*	*Salty deeper*
3rd Water A	W3	*10 L*	*Na_2SO_3*	6	*Fresh sub surface*
1st Water B	W1	5 L	***TBOT***	*6*	*Fresh sub surface*
2nd Water B	W2	5 L	***TBOT***	*19*	*Salty deeper*
3rd Water B	W3	5 L	***TBOT***	6	*Fresh sub surface*
1st soil	S1	6 cm	-		*surface full diameter*
2nd soil	S1	20 cm	-		*surface and sub, thin*
3rd soil A	S2	12 cm	-		*surface thin*
3rd soil B	S2	~18	-		*subsurface broken*

132g Na_2SO_3 was added to the 10 litres samples of water in order to preserve iodine inside them till they ended up in CTU and proceeded to the liquid-liquid extraction process.

5-6 ml TBOT on the other hand added to the 5 litres samples to precipitate uranium in all its forms as white precipitation and leached out later in the lab, following the column treatment described above.

XRF measurements demanded a pretreatment as described in (Kallithrakas-Kontos et al., 2018)

8. First Data

Following the methodologies mentioned above for U/Pu (Norway, Denmark) in sediments and water samples (Crete), and I for water samples from Crete, the following first estimations are provided. For the sediment digestion, a mixture of HNO_3 & HF is used, for that reason and due to the fact that we use it for the majority of the samples with microwave digesting systems, where acids and samples, decompose under high pressures, it is important to know precisely the content of organic matter for every single sample. A bigger concentration of organic matter would suggest a bigger ratio of HNO_3/HF, the HF should be handled with extreme care, only for the decomposition of hard inorganic minerals.

The organic matter is estimated as follows:

Simplified method for determination of dry matter and organic matter in soil/sediment samples (Øien and Krogstad, 1987) .

Weigh 3-5 g air-dried soil or sediment into a pre-weighed porcelain crucible. Dry for at least 6 hours or overnight at 105°C. After drying, the samples were transferred into a desiccator for cooling. Weight of the samples measured (= M_1)

$$\%\ Dry\ matter = \frac{M_1(g) * 100}{Total\ air\ dried\ sample\ (g)}$$

Result in % Dry matter

The porcelain crucibles with the dried samples are placed in a furnace. Increasing temperature gradually until 550°C is reached. The samples glowed overnight, and the door opened in the morning. When the temperature is a little lowered, the samples can be transferred to the desiccator for cooling. Weigh the cooled samples (= M_2).

$$\%\ Loss\ on\ ignition\ = \frac{(M_1 - M_2) * 100}{M1}$$

Result in % Loss on ignition (LOI) (one digit)

LOI = organic matter

Org. C (TOC)= ~58% of LOI

Table 8.1: Example of Dry matter, Loss of ignition, organic matter and TOC for the sample site 3B 4-5 first cm.

% Dry matter	% Loss on ignition	LOI	Org. C (TOC)= ~58% of LOI	no/name
99.9751002	0.799402256	0.0995	0.05771	271/siteB 4-5

8.1. First measurements

Uranium measurements

The first series of measurements came for uranium sediment samples. Graphically represented below are the results for all the measured parameters, aka total ^{236}U, ^{238}U and their ratio. Unfortunately, we were not able to measure ^{233}U, due to the lack of an appropriate test sample for the calibration of our AMS system.

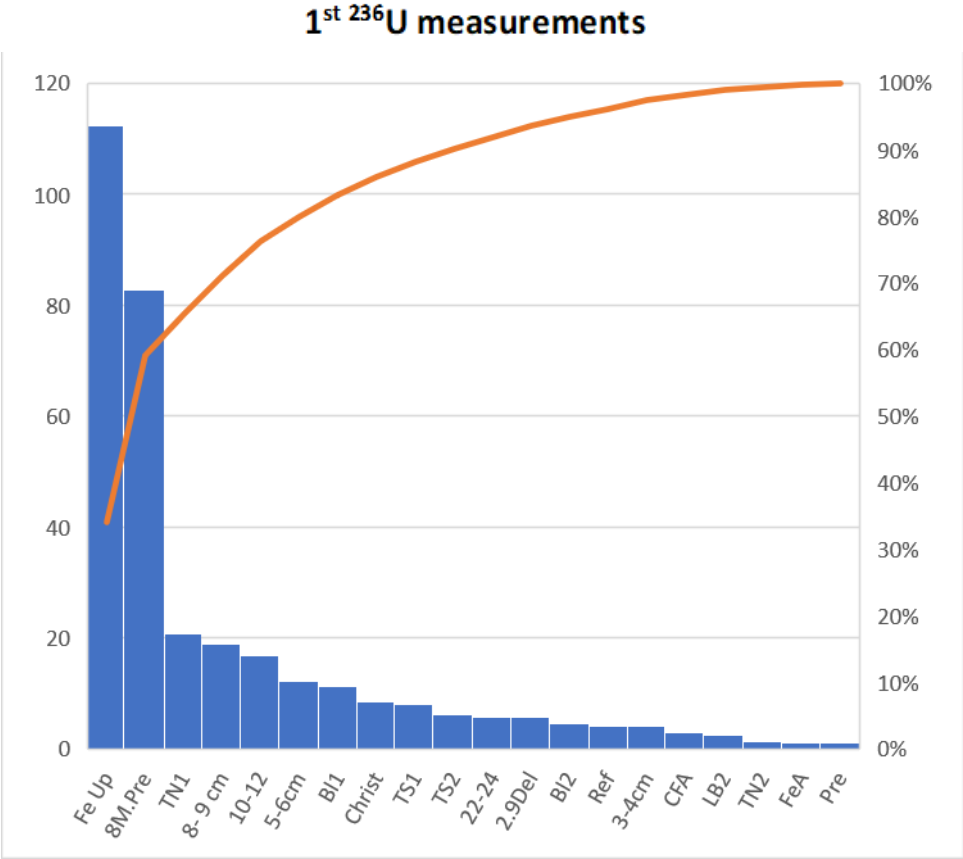

Graph. 8.1.1: Graphic representation of a total ^{236}U per round (counts in the left Y-axis) and the % of the total contribution (right Y-axis), for every each one measurement (X-axis has the names of the samples measured).

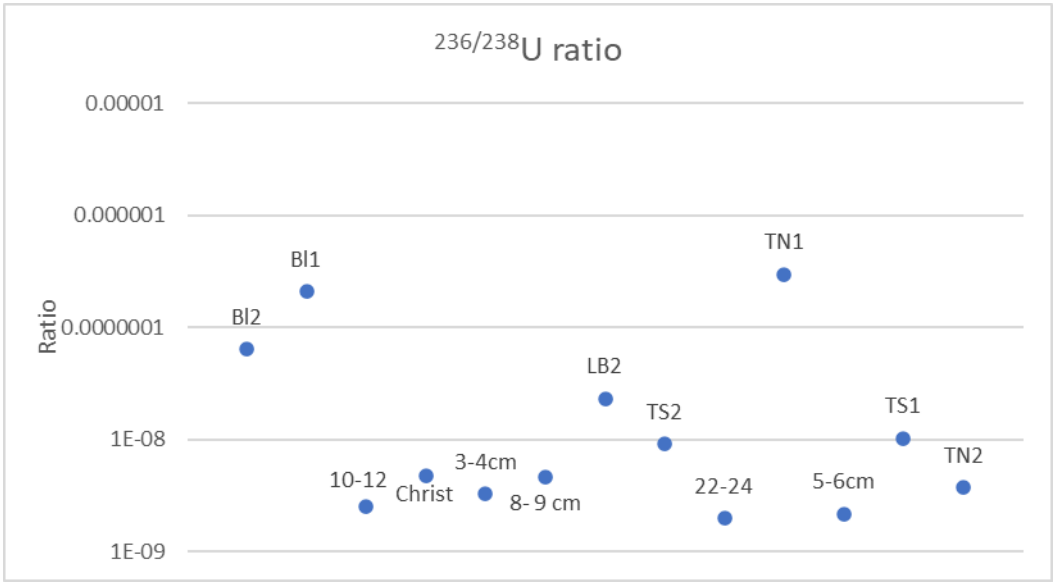

Graph. 8.1.2: Ratio of $^{236}U/^{238}U$ for all the Norweigian and Denmark samples from the first measurement campaign. The samples "FeUp" and "8M.Pre" have the highest ^{236}U counts in the previous figure, but they are missing from this figure because were too contaminated to be used for any U precipitations (they were referring to old iron compounds from another lab and a piece of iron stored from pre-WorldWar2 times, respectively).

Several blank test samples and background samples from both labs (NMBU & CTU) as well as carrier samples (Fe) from the laboratories of CTU were chosen for the first series of measurements. It is interesting to observe that, compared to the majority of the sediment samples, both Blank samples from NMBU (Bl1 & Bl2) have somewhat increased both the total ^{236}U counts and in particular the ratio of $^{236/238}U$. Considering that, we can assume some contamination from outer sources. Contaminated distilled water or contamination during lab procedures, if acids or any other material was contaminated then we should have observed similarly high ^{236}U counts.

In the sampling area with the code name "site 3B" an agreement between $^{236/238}U$ ratios and previous ^{137}Cs data is observed. It is once again the case of what we could call "the past depicted on the core". The rate of the sedimentation process can be easily estimated from those data and the other way around, by knowing the sedimentation rates, it is effortlessly possible to connect our observations to the historical events of global impact (such as the Chernobyl accident in 1986). Unfortunately, the ^{137}Cs data are still unpublished and even if I have used them for some sampling decision making, I am not able to present the values here.

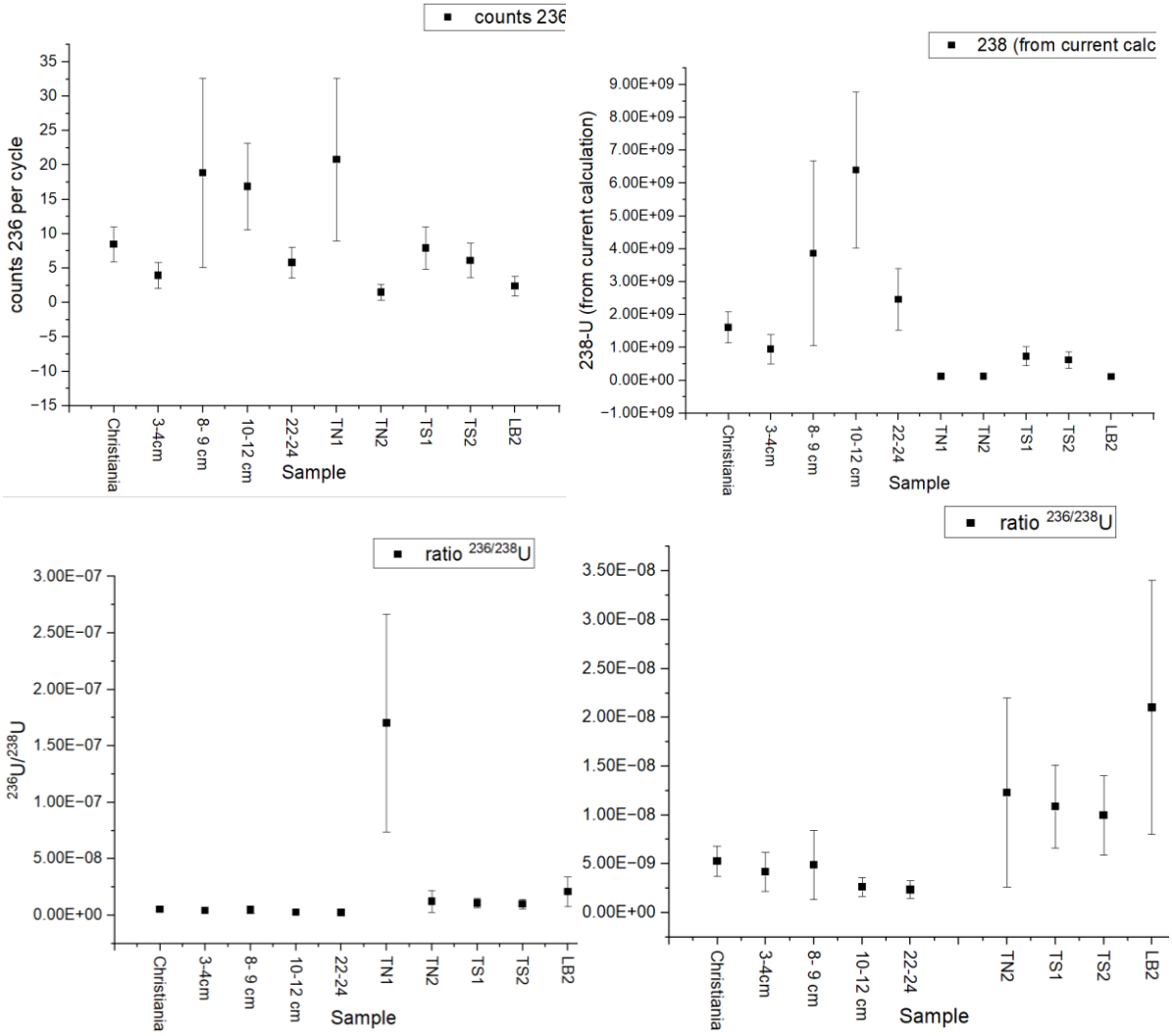

Graph. 8.1.3: Uranium data for both isotopes (^{236}U & ^{238}U), for CPS and ratios.

Iodine measurements

The first series of iodine measurements originated from water samples from Crete. Graphically represented below are the results for all the measured parameters. Unfortunately, we had to deal with several unexpected circumstances and failures as we will see further below.

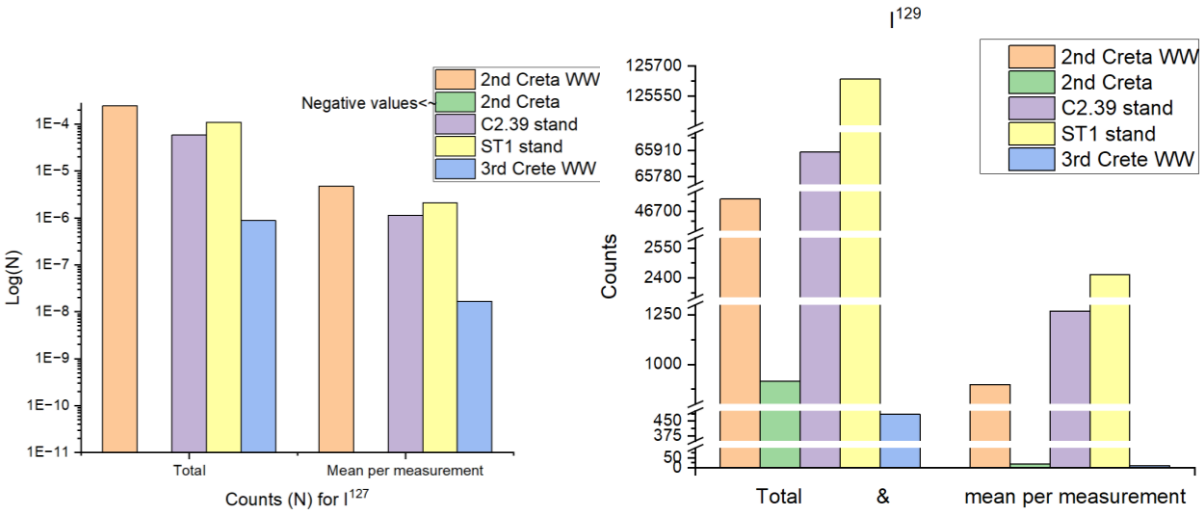

Graph. 8.1.4: An overview of iodine measurements for ^{127}I (left) and ^{129}I (right) for the successfully measured samples.

The only successfully measured samples were the two samples with Woodward carrier added and one made from 2L- sample of the bottom layer at the middle of the site from Crete (which corresponds to open sea salt water).

The 2nd Cretan sample proved maybe the clearest evidence regarding the Woodward carrier needs and effectiveness for this methodology. From the same sample 100ml with the addition of Woodward carrier (0.5 ml of 2.082 mg ^{127}I per ml Woodward iodine (I2) solution) gave more info for both isotopes than the 2 litres without Woodward, while the 200ml without Woodward led to failure. As for the ratio it will be discussed separately in encountered problems' chapter due to its complicated nature during preparation and mea

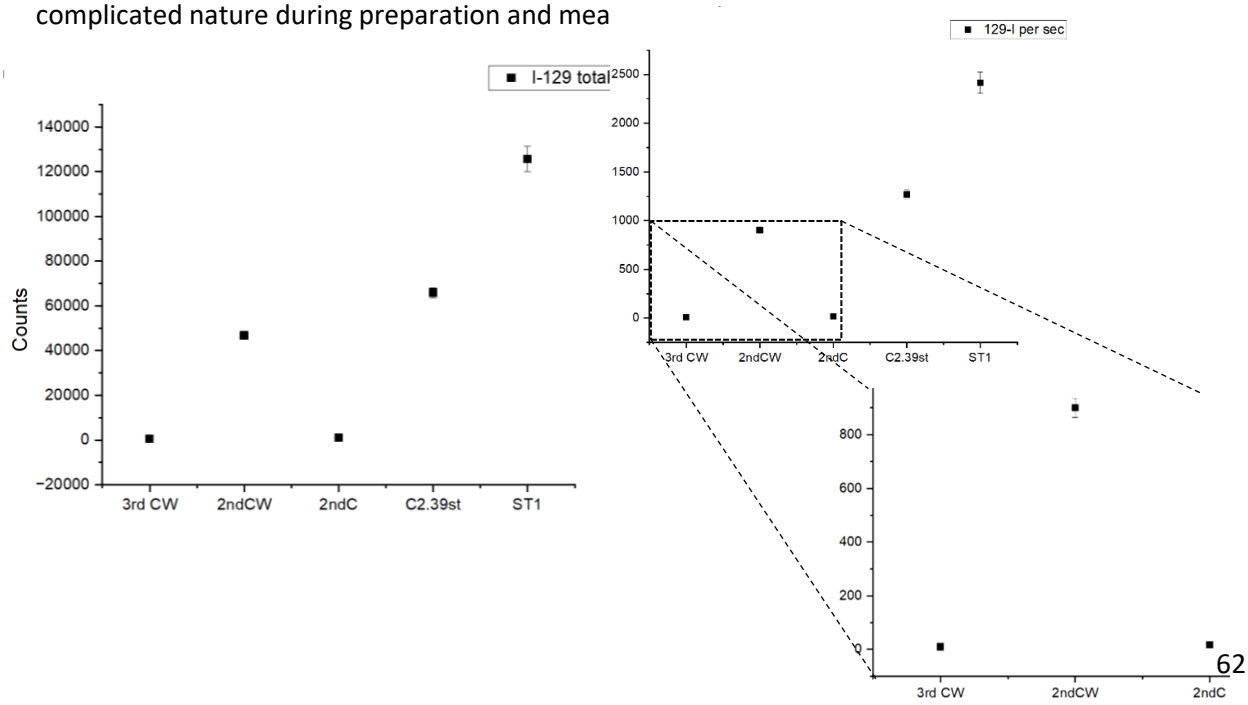

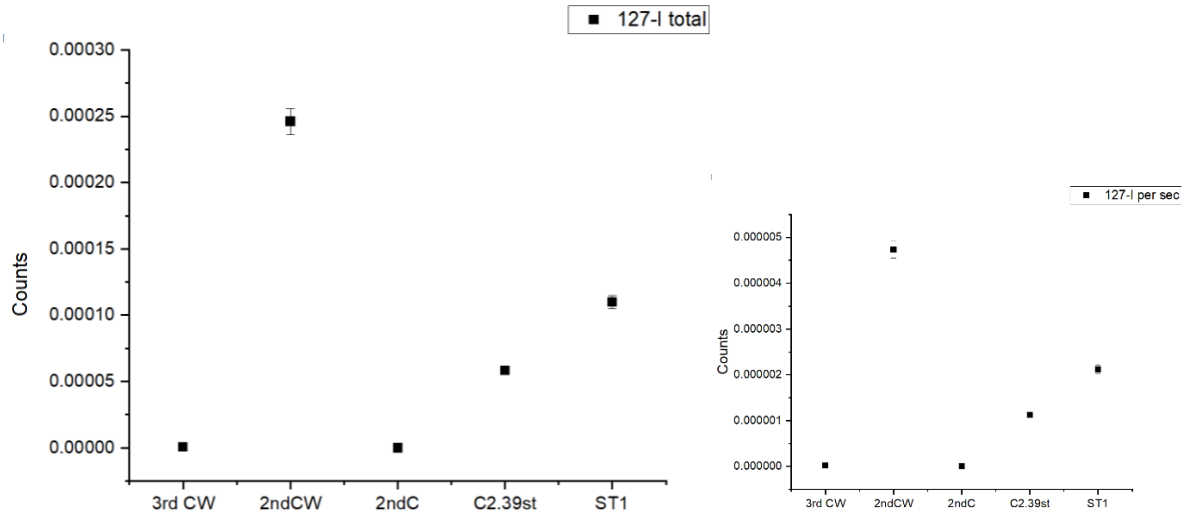

Graph. 8.1.5: Iodine measured data. ^{129}I total counts and cps (top ones) & ^{127}I total counts and cps (bottom ones).

8.2. XRF screening

The overall screening for the water samples gave a very general result for their chemical composition. Since sodium could not be correctly detected by the system used, due to its very large absorptions (of sodium), its analysis is very unsecure. A possible way to overcome this obstacle is to roughly assume that the chlorine detected is due to the presence sodium chloride and approximation of the sodium concentration based on the chlorine concentration. Using this approach, it was demonstrated that more than 94% of the elemental composition (dissolved salts) is represented by Na-Cl<Br<Sr with ~90, ~3 & ~1 % abundance, respectively.

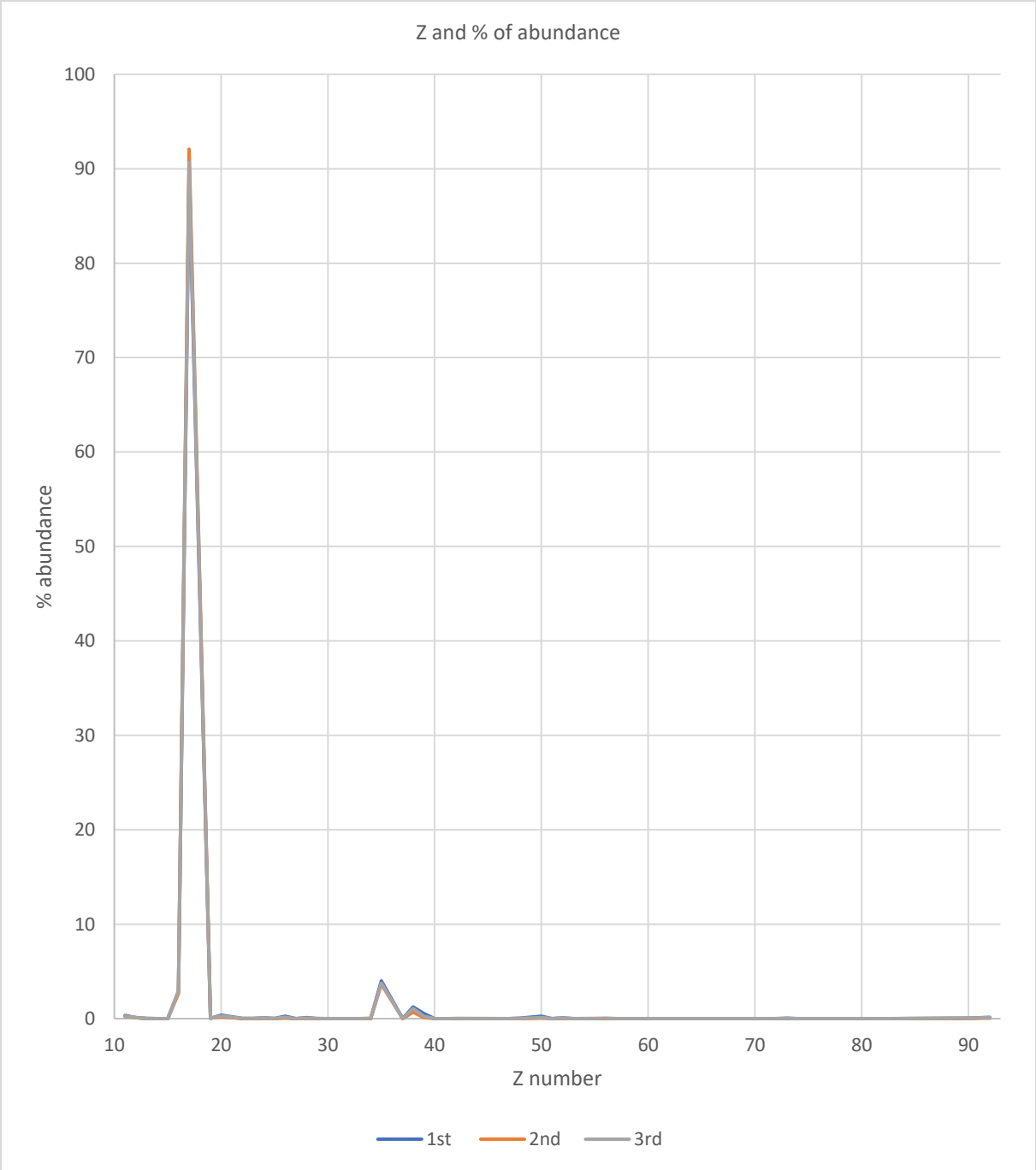

Graph. 8.2.1: Abundance graph for elements presented in the 3 water samples.

The abundance of macro-elements in sediment was quite similar in all our samples, for examples see the following figures:

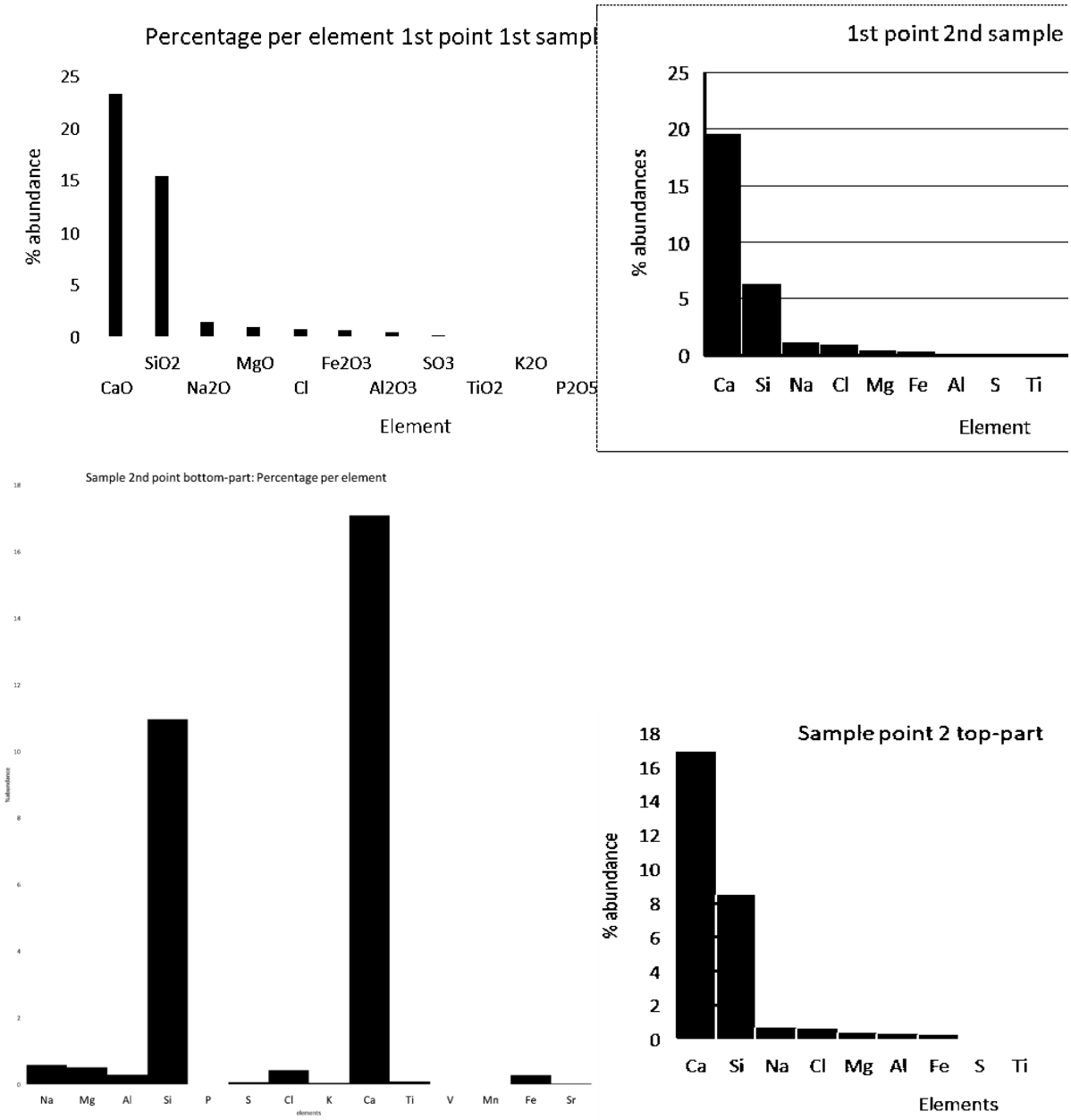

Graph. 8.2.2: Graphics for the 4 different sediment XRF screenings on the sedimental samples. First graph left with the “oxide forms” to state the original form of data we receive in an XRF analysis

To summarize, there were huge similarities in results of the screening of the same type of salt water samples and the detection limits were not low enough to spot any tracing or even low-concentrated elements. The elemental detection in sediments was significantly better though, and could provide some information regarding the composition of them.

8.3. Encountered problems and their mitigation

A crucial problem we have to deal with in samples treated for U/Pu separation is the accidental loss of samples during the final drying procedure. Those samples were washed a couple of times with ultrapure water before being placed in a special oven to get dry entirely at high temperature, thus they would stripe out entirely from any ammonia remaining. Ammonia which may not wash out properly, or (in some cases) be trapped in the sample in air bubbles, may violently decompose and the resulting gasses escape out of our sample. A white crystal formation seen around our final crucibles is probably ammonium chloride, the same chloride that expands and leads the sample in

some cases even to an “explosive” behavior which may spread the sample all over the area of the oven contaminating on top of that the rest of the samples too.

Pic.8.3.1: Crucibles with different undesirable outcomes.

The white crystal flakes seen around the crucibles are most probably ammonium chloride (NH_4Cl) which may cause problems inside the oven if they stay trapped underneath the sample's surface. During the measurement for one series of samples, the final samples inside the AMS measurement targets were still quite volatile, causing the accelerator to overload. Due to this, an entire series of samples got wasted when the “**Nista 27ila” sample** (IAEA standard prepared in Norway) and one more from the same series overloaded the ion source and crashed the AMS. Possible causes are unclear at this moment but we could suggest (additionally to the NH_4Cl) the existence of carbonates in undesirable concentration, possibly leftovers of the overall sampling procedure, both “**Nista 27ila”´s composition nature and lab procedures should be investigated furthermore to avoid similar failures in the future.**

While waiting for the ICP-MS results, it's important to clarify the problematic parameters in this analytical system. One key factor is the need to clearly understand the composition of the matrix while ensuring thorough homogenization and dilution. It's crucial to effectively distinguish between and manage the overlapping elements in our samples during laboratory procedures before conducting any analysis.

Iodine

The samples from the Cretan region which have been planned to be examined for iodine measurements were separated into 2 parts, those in which Woodward reference material was added and those to which it was not. The starting point here was to investigate if we could overcome the lack of Woodward material by performing more efficient extraction from a bigger sample volume.

For example, from the 1st sample, 100 ml was treated with Woodward in parallel with 200 ml naked sample. Even before the measurements, it became obvious that the presence of the Woodward standard proved to be essential for the precipitation of iodine. As expected, only the 2nd sample (Salt deeper) which corresponds to Mediterranean open sea water, proved to contain enough iodine to

precipitate, and after a bigger portion treated, to form sufficient iodine precipitate for some measurements. The characteristic indicator in those cases was the distinctive purple-pink colour during extraction with the addition of $NaNO_2$.

And even the amount of Woodward seemed to be crucial and cannot be decreased below a certain limit. As a support for this statement, in 100ml of **less salty** water 0.5ml of Woodward failed to catalyse the reaction (1ml is the minimum suggested to be used).

Summarizing the iodine ratio results and taking into consideration the Woodward AMS measurements and composition *(Woodward iodine: 2.082 mg ^{127}I per g of the solution)* we could conclude at the following:

Considering that the ^{127}I in our samples is negligible compared to the amount added from us through Woodward (as the measurement on samples without Woodward proving) total concentrations for ^{129}I could calculated for two samples, 2nd Cretan $WW_{extr.}$ (100ml sample + 0.5ml Woodward) & 3rd Cretan $WW_{extr.}$ (100ml sample + 1ml Woodward). 1.2431×10^{-16} mol/L & 2.83705×10^{-16} mol/L respectively.

Ratios $^{129/127}$I, calculated as ^{129}I counts(R) from the AMS measurements after subtraction of the background, divided by the number of ^{127}I atoms, calculated from the actual measured current.

Table 8.3.1: Ratios ^{129}I/^{127}I for the two successfully measured samples from Crete

	Ratios $^{129/127}$I
2nd	1.51541E-12
3rd	1.72927E-12

Any other attempt to calculate the ratio of $^{129/127}$I for the rest of the samples would result in failure or even worse in false results since the current in the background measurements is very close to ^{127}I current from our natural samples, so it can't be distinguished. Any attempt gave irrational results with negative values for the ratios, which would mean that in some unrealistic way, there were some negative measurements, in any of the two isotopic measurements, which of course is absurd. A measurement without Faraday cups (non-current measurements) is needed (most efficiently ICP-MS).

9. Conclusions and future plans

The first samples indicate that high $^{236/238}$U isotopic ratios and Cs depth concentrations' pics correlate well with each other in Vefsnfjord sampling area.

The horizon around 10cm depth in Vefsnfjord (point of agreement between ^{137}Cs and $^{236/238}$U should be representative of the timeline depiction of the Chernobyl fallout. Other nuclear tests could also have affected the area, but then again due to the fact that we know well that **Chernobyl's accident affected greatly the north and central area of Norway back in 1986 (and after), some clear signs of this event in the core are expected**, especially after depths with almost zero/or "clear" background signal.

The ratio of $^{236/238}$U was unexpectedly high in the case of a sample from Christiania from Denmark. So, a more comprehensive sampling may be planned for future measurements and research to confirm and explain this finding. In a recent study, researchers used the two man-made

radionuclides, ^{129}I and ^{236}U, to figure out how long it takes for North Sea saltwater to move into the Baltic Sea (Lin et al., 2024). Studies like these demonstrate how man-made radionuclides can help us understand how water moves and mixes in different regions, and how to achieve solid evidence that pollutants stay in the sea even for decades.

In the case of Cretan samples iodine did not give us any insight and unfortunately, the malfunction of the ionizer in the second measurement series resulted in the loss of some of them. **If no sample will be retrieved from the remaining portions maybe a second sampling would be useful for additional measurements.**

At the time of writing this report, we are waiting for the results from ICP-MS measurements from NMBU. Besides that, in NMBU with Dr. Karl Andreas, we tried with success to precipitate Iodine in solutions using ozone (O_3) as an oxidizing agent ozone. It is in my interest to try similar precipitation in a gas-formed reaction using the volatility of iodine (I_2), as a methodological mechanism drive factor.

9.1. Further discussion

51 sediment samples from Norway have been stored for future iodine measurements. It is very important for AMS, in combination with other radioanalytical techniques, to provide information on both the concentration and the origin (through isotopic ratios) of the crucial radionuclides such as Pu in obtained fractions with quite small concentrations or chemical separation yield (due to their matrix).
Several cases demonstrated that Pu isotopes exhibited different environmental behaviour depending on the source and the scenario during which they were released, and those releases can be identified and back-tracked using those radio-isotopic ratios.
The combination of techniques can provide a significant improvement in the integrated analysis of the collected data and their sampling sources.
While the failure during measurement may cost a whole series of samples, a sufficient size of samples could prevent the final loss of information. On top of that some of the analytical techniques, can be combined into a series of processes to obtain data for several elements from the very same portion of the sample.

A tracer that exhibits conservative behaviour in the marine environment (in the aqua phase), meaning it remains evenly distributed and suspended in the water phase, should be suitable for water samples' analysis. On the other hand, a nonconservative tracer is more likely to adhere to particles or end up bound to bottom sediments, hindering accurate measurement of the analyte concentration in water samples, but perfectly adequate for sediment measurement. Both parameters must be combined to draw integrated conclusions for water transport, time of residence, and precipitation processes.

Repeated samplings in some easily accessible regions could provide us with some control of the repeatability of our methodologies as well as a chronological mapping of the physicochemical conditions of our environment. So, a repeat of some samplings is considered to be conducted and parallel examination of various methodologies to be tested upon the same sampling bodies.

Sampling from the exactly same area and in a similar period of the year in Crete should have been planned and should be carried out for both uranium and iodine measurements, this time ICP-MS should definitely contribute to measurements, mostly for the Iodine measurements, so we would be able to overcome the problem with the ^{127}I low currents. In this way, we will be able to sufficiently

provide data for the status quo of the area, in respect of its radiochemical conditions. Woodward has already been acquired in the department of CTU, for future separations. Nominal values should be calculated carefully again and correspond to the measurements for the specific solutions that may be used in the future and for every different method change step that may be applied then.

Bibliography

Abad-Álvaro, I., Vázquez, E., Bolea, E., Bermejo-Barrera, P., Castillo, J., Laborda, F., 2022. ICP - Mass Spectrometry.

Aly, M.M., Hamza, M.F., 2013. A Review: Studies on Uranium Removal Using Different Techniques. Overview. Journal of Dispersion Science and Technology 34, 182–213. https://doi.org/10.1080/01932691.2012.657954

Barrat, J.-A., Bayon, G., 2024. Practical guidelines for representing and interpreting rare earth abundances in environmental and biological studies. Chemosphere 352, 141487. https://doi.org/10.1016/j.chemosphere.2024.141487

Bhaumik, B., 2014. Radioactivity. This article is written for earth science students who intend to take a course on crustal radioactivity. https://doi.org/10.13140/RG.2.1.4813.2649

Blanco-Quintero, I.F., Gerya, T.V., García-Casco, A., Castro, A., 2011. Subduction of young oceanic plates: A numerical study with application to aborted thermal-chemical plumes. Geochemistry, Geophysics, Geosystems 12. https://doi.org/10.1029/2011GC003717

Boggs, M.A., Jiao, Y., Dai, Z., Zavarin, M., Kersting, A.B., 2016. Interactions of Plutonium with Pseudomonas sp. Strain EPS-1W and Its Extracellular Polymeric Substances. Applied and Environmental Microbiology 82, 7093–7101. https://doi.org/10.1128/AEM.02572-16

Bugai, D., Smith, J., Hoque, M.A., 2020. Solid-liquid distribution coefficients (Kd-s) of geological deposits at the Chernobyl Nuclear Power Plant site with respect to Sr, Cs and Pu radionuclides: A short review. Chemosphere 242, 125175. https://doi.org/10.1016/j.chemosphere.2019.125175

Cabello, F.M., 2020. Optimization of 6Li-based Scintillators for Neutron Imaging and Flux Monitors. https://doi.org/10.13140/RG.2.2.22989.24802

Chen, N., Hou, X., Zhou, W., Fan, Y., Liu, Q., 2014. Analysis of low-level 129I in brine using accelerator mass spectrometry. J Radioanal Nucl Chem 299, 1965–1971. https://doi.org/10.1007/s10967-013-2915-y

Christl, M., Gautschi, P., Maxeiner, S., Müller, A.M., Vockenhuber, C., Synal, H.-A., 2023a. 236U analyses with the ETH Zurich MILEA prototype system. Nuclear Instruments and Methods in Physics Research Section B: Beam Interactions with Materials and Atoms 534, 61–71. https://doi.org/10.1016/j.nimb.2022.11.009

Christl, M., Gautschi, P., Maxeiner, S., Müller, A.M., Vockenhuber, C., Synal, H.-A., 2023b. 236U analyses with the ETH Zurich MILEA prototype system. Nuclear Instruments and Methods in Physics Research Section B: Beam Interactions with Materials and Atoms 534, 61–71. https://doi.org/10.1016/j.nimb.2022.11.009

Clark, D.L., Hecker, S.S., Jarvinen, G.D., Neu, M.P., 2006. Plutonium, in: Morss, L.R., Edelstein, N.M., Fuger, J. (Eds.), The Chemistry of the Actinide and Transactinide Elements. Springer Netherlands, Dordrecht, pp. 813–1264. https://doi.org/10.1007/1-4020-3598-5_7

Collins, A.G., Egleson, G.C., 1967. Iodide Abundance in Oilfield Brines in Oklahoma. Science 156, 934–935. https://doi.org/10.1126/science.156.3777.934

Deng, C., Liang, J., Sun, R., Wang, Y., Fu, P.-X., Wang, B.-W., Gao, S., Huang, W., 2023. Accessing five oxidation states of uranium in a retained ligand framework. Nat Commun 14, 4657. https://doi.org/10.1038/s41467-023-40403-w

Descriptive Physical Oceanography: An Introduction - Lynne D. Talley - Google Books [WWW Document], n.d. URL https://books.google.cz/books?hl=en&lr=&id=Chb14jomm08C&oi=fnd&pg=PP1&dq=Talley,+L.+D.+(2013).+Descriptive+Physical+Oceanography:+An+Introduction.+Academic+Press&ots=fCdKTZurxc&sig=HykwjyQepdvTnhT1SWBkHoKcwKg&redir_esc=y#v=onepage&q&f=false (accessed 5.25.24).

Detecting Radiation [WWW Document], n.d. . NRC Web. URL https://www.nrc.gov/about-nrc/radiation/health-effects/detection-radiation.html (accessed 7.8.24).

Dragović, S., Janković, Lj., Onjia, A., Bačić, G., 2006. Distribution of primordial radionuclides in surface soils from Serbia and Montenegro. Radiation Measurements 41, 611–616. https://doi.org/10.1016/j.radmeas.2006.03.007

Dresel, P.E., Wellman, D.M., Cantrell, K.J., Truex, M.J., 2011. Review: Technical and Policy Challenges in Deep Vadose Zone Remediation of Metals and Radionuclides. Environ. Sci. Technol. 45, 4207–4216. https://doi.org/10.1021/es101211t

Emerson, H.P., Kaplan, D.I., Powell, B.A., 2019. Plutonium binding affinity to sediments increases with contact time. Chemical Geology 505, 100–107. https://doi.org/10.1016/j.chemgeo.2018.11.009

Emerson, S., Hedges, J., 2008a. Chemical Oceanography and the Marine Carbon Cycle. Chemical Oceanography and the Marine Carbon Cycle, by S. Emerson and J. Hedges. Cambridge: Cambridge University Press, 2008. https://doi.org/10.1017/CBO9780511793202

Emerson, S., Hedges, J., 2008b. Chemical Oceanography and the Marine Carbon Cycle. Cambridge University Press.

Feldmann, I., Tittes, W., Jakubowski, N., Stuewer, D., Giessmann, U., 1994. Performance characteristics of inductively coupled plasma mass spectrometry with high mass resolution. J. Anal. At. Spectrom. 9, 1007. https://doi.org/10.1039/ja9940901007

Foxe, M., Bowyer, T., Cameron, I., Cooper, M., Hayes, J., Haas, D., Lidey, L., Mayer, M., Mendez, J., Slack, J., 2021. Design and Operation of the U.S. Radionuclide Noble Gas Laboratory for the CTBTO. Pure Appl. Geophys. 178, 2741–2752. https://doi.org/10.1007/s00024-020-02591-0

Gartman, B.N., Qafoku, N.P., Szecsody, J.E., Kukkadapu, R.K., Wang, Z., Wellman, D.M., Truex, M.J., 2015. Uranium fate in Hanford sediment altered by simulated acid waste solutions. Applied Geochemistry 63, 1–9. https://doi.org/10.1016/j.apgeochem.2015.07.010

Gómez-Guzmán, J.M., Enamorado-Báez, S.M., Pinto-Gómez, A.R., Abril-Hernández, J.M., 2011. Microwave-based digestion method for extraction of 127I and 129I from solid material for measurements by AMS and ICP-MS. International Journal of Mass Spectrometry 303, 103–108. https://doi.org/10.1016/j.ijms.2011.01.006

Hain, K., Martschini, M., Gülce, F., Honda, M., Lachner, J., Kern, M., Pitters, J., Quinto, F., Sakaguchi, A., Steier, P., Wiederin, A., Wieser, A., Yokoyama, A., Golser, R., 2022. Developing Accelerator Mass Spectrometry Capabilities for Anthropogenic Radionuclide Analysis to Extend the Set of Oceanographic Tracers. Frontiers in Marine Science 9.

Hellborg, R., Siegbahn, K., 2005. Electrostatic Accelerators: Fundamentals and Applications. Springer London, Limited.

Hellborg, R., Skog, G., 2008. Accelerator mass spectrometry. Mass Spectrometry Reviews 27, 398–427. https://doi.org/10.1002/mas.20172

Herrmann, W., Cornils, B., Zanthoff, H., Xu, J. (Eds.), 2020. ICP-MS. https://doi.org/10.1002/9783527809080.cataz08742

Hou, X., Hou, Y., 2012. Analysis of ^{129}I and its Application as Environmental Tracer. JAST 3, 135–153. https://doi.org/10.5355/JAST.2012.135

Huang, S.-X., Zhang, J.-P., Yang, W.-D., Wang, Z.-F., Hu, F., Liu, F., Sheng, L., Zeng, Q.-C., 2016. Predicting and Controlling Nuclear Accident Hazards: Issues and Challenges. Aerosol Air Qual. Res. 16, 417–429. https://doi.org/10.4209/aaqr.2014.12.0320

Jeandel, C., Oelkers, E.H., 2015. The influence of terrigenous particulate material dissolution on ocean chemistry and global element cycles. Chemical Geology 395, 50–66. https://doi.org/10.1016/j.chemgeo.2014.12.001

Jo, Y., Kirishima, A., Kimuro, S., Kim, H.-K., Yun, J.-I., 2019. Formation of CaUO2(CO3)32− and Ca2UO2(CO3)3(aq) complexes at variable temperatures (10–70 °C). Dalton Trans. 48, 6942–6950. https://doi.org/10.1039/C9DT01174A

Joseph, C., Balboni, E., Baumer, T., Treinen, K., Kersting, A.B., Zavarin, M., 2019. Plutonium Desorption from Nuclear Melt Glass-Derived Colloids and Implications for Migration at the Nevada National Security Site, USA. Environ. Sci. Technol. 53, 12238–12246. https://doi.org/10.1021/acs.est.9b03956

Kallithrakas-Kontos, N.G., Xarchoulakos, D.C., Boultadaki, P., Potiriadis, C., Kehagia, K., 2018. Selective Membrane Complexation and Uranium Isotopes Analysis in Tap Water and Seawater Samples. Anal Chem 90, 4611–4615. https://doi.org/10.1021/acs.analchem.7b05115

Kieser, W.E., 2023. Accelerator mass spectrometry: an analytical tool with applications for a sustainable society. EPJ Techn Instrum 10, 1–8. https://doi.org/10.1140/epjti/s40485-023-00088-3

Knoll, G.F., 2010. Radiation detection and measurement, 4th ed. ed. Wiley, Hoboken, N.J.

Leivadaros, P., Tsabaris, C., Patiris, D.L., Eleftheriou, G., Pappa, F.K., Androulakaki, E., Dasenakis, M., Krasakopoulou, E., Zervakis, V., 2022. Recent 137Cs Distribution in the Aegean Sea, Greece. Journal of Marine Science and Engineering 10, 1719. https://doi.org/10.3390/jmse10111719

Levchuk, S., Kashparov, V., Maloshtan, I., Yoschenko, V., Van Meir, N., 2012. Migration of transuranic elements in groundwater from the near-surface radioactive waste site. Applied Geochemistry, 25 years after the Chernobyl power plant explosion: Management of nuclear wastes and radionuclide transfer in the environment 27, 1339–1347. https://doi.org/10.1016/j.apgeochem.2012.01.002

Li, H., Wang, L., Zhang, J., Li, C., 2016. Research on and application of deep-sea environmental radioactivity online monitoring technology, in: OCEANS 2016 - Shanghai. Presented at the OCEANS 2016 - Shanghai, pp. 1–4. https://doi.org/10.1109/OCEANSAP.2016.7485579

Lin, M., Qiao, J., Hou, X., She, J., Murawski, J., 2024. Deciphering the Ages of Saline Water in the Baltic Sea by Anthropogenic Radiotracers. Journal of Geophysical Research: Oceans 129. https://doi.org/10.1029/2023JC020621

McDaniel, F.D., Matteson, S., Weathers, D.L., Duggan, J.L., Marble, D.K., Hassan, I., Zhao, Z.Y., Anthony, J.M., 1992. Radionuclide dating and trace element analysis by accelerator mass spectrometry. Journal of Radioanalytical and Nuclear Chemistry, Articles 160, 119–140. https://doi.org/10.1007/BF02041663

Mehta, V.S., Maillot, F., Wang, Z., Catalano, J.G., Giammar, D.E., 2016. Effect of Reaction Pathway on the Extent and Mechanism of Uranium(VI) Immobilization with Calcium and Phosphate. Environ Sci Technol 50, 3128–3136. https://doi.org/10.1021/acs.est.5b06212

Moran, J.E., Oktay, S., Santschi, P.H., Schink, D.R., 1999. Atmospheric Dispersal of 129Iodine from Nuclear Fuel Reprocessing Facilities. Environ. Sci. Technol. 33, 2536–2542. https://doi.org/10.1021/es9900050

Negm, H.H., 2014. Studies on the Optimum Geometry for a Nuclear Resonance Fluorescence Detection System for Nuclear Security Applications (doctoral thesis). Kyoto University.

Nuclear and Radiochemistry: Fundamentals and Applications, 4th Edition | Wiley [WWW Document], n.d. . Wiley.com. URL https://www.wiley.com/en-us/Nuclear+and+Radiochemistry%3A+Fundamentals+and+Applications%2C+4th+Edition-p-9783527349050 (accessed 6.18.24).

Ocean circulation and climate during the past 120,000 years | Nature [WWW Document], n.d. URL https://www.nature.com/articles/nature01090 (accessed 5.25.24).

Ocean current - Thermohaline, Circulation, Global | Britannica [WWW Document], 2024. URL https://www.britannica.com/science/ocean-current/Thermohaline-circulation (accessed 8.17.24).

Øien, A., Krogstad, T., 1987. Øvelser i jordanalyser. NLH: Institutt for jordfag.

OpenStax, 2016. 19.3 Radioactive Decay.

Physics for Radiation Protection, 3rd Edition | Wiley [WWW Document], n.d. . Wiley.com. URL https://www.wiley.com/en-us/Physics+for+Radiation+Protection%2C+3rd+Edition-p-9783527411764 (accessed 7.9.24).

Price, N.B., Calvert, S.E., 1973. The geochemistry of iodine in oxidised and reduced recent marine sediments. Geochimica et Cosmochimica Acta 37, 2149–2158. https://doi.org/10.1016/0016-7037(73)90013-6

Priest, C., Tian, Z., Jiang, D., 2016. First-principles molecular dynamics simulation of the Ca2UO2(CO3)3 complex in water. Dalton Trans. 45, 9812–9819. https://doi.org/10.1039/C5DT04576B

Primordial Radionuclides | nuclear-power.com [WWW Document], n.d. . Nuclear Power. URL https://www.nuclear-power.com/glossary/primordial-matter/primordial-radionuclides/ (accessed 6.28.24).

Purser, K.H., Liebert, R.B., Litherland, A.E., Beukens, R.P., Gove, H.E., Bennett, C.L., Clover, M.R., Sondheim, W.E., 1977. An attempt to detect stable N- ions from a sputter ion source and some implications of the results for the design of tandems for ultra-sensitive carbon analysis. Revue de Physique Appliquée 12, 1487. https://doi.org/10.1051/rphysap:0197700120100148700

Qiao, J., Casacuberta, N., Ginnity, P.MC., 2023. Editorial: Natural and artificial radionuclides as tracers of ocean processes. Frontiers in Marine Science 10.

Quantification of Radionuclides, MARLAP, July 2004, n.d.

Radiation Detection And Measurement Glenn F. Knoll 3rd Ed 1999, n.d.

Renaud, R., Clark, I.D., Kotzer, T.G., Milton, G.M., Bottomley, D.J., 2005. The mobility of anthropogenic 129I in a shallow sand aquifer at Sturgeon Falls, Ontario, Canada. Radiochimica Acta 93, 363–371. https://doi.org/10.1524/ract.93.6.363.65641

Rodellas, V., Roca-Martí, M., Puigcorbé, V., Castrillejo, M., Casacuberta, N., 2023. Radionuclides as Ocean Tracers, in: Blasco, J., Tovar-Sánchez, A. (Eds.), Marine Analytical Chemistry. Springer International Publishing, Cham, pp. 199–273. https://doi.org/10.1007/978-3-031-14486-8_4

Romanchuk, A.Y., Vlasova, I.E., Kalmykov, S.N., 2020. Speciation of Uranium and Plutonium From Nuclear Legacy Sites to the Environment: A Mini Review. Front. Chem. 8. https://doi.org/10.3389/fchem.2020.00630

Romanchuk, A.Yu., Vlasova, I.E., Kalmykov, S.N., 2020. Speciation of Uranium and Plutonium From Nuclear Legacy Sites to the Environment: A Mini Review. Frontiers in Chemistry 8.

Schubert, F., Kallmeyer, J., 2023. Liquid scintillation counting at the limit of detection in biogeosciences. Front. Microbiol. 14. https://doi.org/10.3389/fmicb.2023.1194848

Sousa, M.A. de, 2010. Cálculo do Kerma no Ar no Interior de uma Residência e em Campo Aberto a partir de Dados de Espectrometria Gama Aérea na Província Urinífera de Lagoa Real (Caetité BA). [WWW Document].

Tan, S.P.V., Bautista, A.T., Mendoza, N.D.S., Racadio, C.D.T., Puthenpurekal, M., Resurreccion, A.C., Matsuzaki, H., 2020. Iodine-129 for determining the origin of salinity in groundwater in Pampanga, Philippines. Journal of Environmental Radioactivity 218, 106239. https://doi.org/10.1016/j.jenvrad.2020.106239

Technetium-99 - an overview | ScienceDirect Topics [WWW Document], n.d. URL https://www.sciencedirect.com/topics/chemistry/technetium-99 (accessed 5.7.24).

The great ocean conveyor | AIP Conference Proceedings | AIP Publishing [WWW Document], n.d. URL https://pubs.aip.org/aip/acp/article-abstract/247/1/129/743821/The-great-ocean-conveyor?redirectedFrom=fulltext (accessed 5.25.24).

The Great Ocean Conveyor on JSTOR [WWW Document], n.d. URL https://www.jstor.org/stable/43924572 (accessed 5.25.24).

Tsabaris, C., Kaberi, H., Pappa, F.K., Leivadaros, P., Delfanti, R., Krasakopoulou, E., Zervakis, V., 2020. Vertical distribution and temporal trends of 137Cs at Lemnos and Cretan deep basins of the Aegean Sea, Greece. Deep Sea Research Part II: Topical Studies in Oceanography 171, 104603. https://doi.org/10.1016/j.dsr2.2019.06.011

Tsabaris, C., Kaberi, H., Pappa, F.K., Leivadaros, P., Delfanti, R., Krasakopoulou, E., Zervakis, V., 2019. Vertical distribution and temporal trends of 137Cs at Lemnos and Cretan deep basins of the Aegean Sea, Greece. Deep Sea Research Part II: Topical Studies in Oceanography 171. https://doi.org/10.1016/j.dsr2.2019.06.011

US Department of Commerce, N.O. and A.A., n.d. Thermohaline Circulation - Currents: NOAA's National Ocean Service Education [WWW Document]. URL https://oceanservice.noaa.gov/education/tutorial_currents/05conveyor1.html (accessed 1.4.24).

Vázquez-Campos, X., Kinsela, A.S., Bligh, M.W., Harrison, J.J., Payne, T.E., Waite, T.D., 2017. Response of Microbial Community Function to Fluctuating Geochemical Conditions within a Legacy Radioactive Waste Trench Environment. Applied and Environmental Microbiology 83, e00729-17. https://doi.org/10.1128/AEM.00729-17

Vértes, A., Nagy, S., Klencsár, Z., Lovas, R.G., Rösch, F., 2010. Handbook of Nuclear Chemistry: Vol. 1: Basics of Nuclear Science; Vol. 2: Elements and Isotopes: Formation, Transformation, Distribution; Vol. 3: Chemical Applications of Nuclear Reactions and Radiation; Vol. 4: Radiochemistry and Radiopharmaceutical Chemistry in Life Sciences; Vol. 5: Instrumentation, Separation Techniques, Environmental Issues; Vol. 6: Nuclear Energy Production and Safety Issues. Springer Science & Business Media.

Victoria, L.-T., Unai, A., María, V.-A., Jessica, K., Natalie, H., José María, L.-G., 2022. 129I in sediment cores from the Celtic Sea by AMS through a microwave digestion process. Nuclear Instruments and Methods in Physics Research Section B: Beam Interactions with Materials and Atoms 529, 61–67. https://doi.org/10.1016/j.nimb.2022.08.016

Wakabayashi, J., 2017. Structural context and variation of ocean plate stratigraphy, Franciscan Complex, California: insight into mélange origins and subduction-accretion processes. Prog Earth Planet Sci 4, 18. https://doi.org/10.1186/s40645-017-0132-y

Wu, W., Priest, C., Zhou, J., Peng, C., Liu, H., Jiang, D.-E., 2016. Solvation of the Ca2UO2(CO3)3 Complex in Seawater from Classical Molecular Dynamics. J Phys Chem B 120, 7227–7233. https://doi.org/10.1021/acs.jpcb.6b05452

Wunsch, C., 2002. What Is the Thermohaline Circulation? Science 298, 1179–1181. https://doi.org/10.1126/science.1079329

Xie, J., Liang, W., Lin, J., Zhou, X., Li, M., 2018. Humic acids facilitated microbial reduction of polymeric Pu(IV) under anaerobic conditions. Science of The Total Environment 610–611, 1321–1328. https://doi.org/10.1016/j.scitotenv.2017.08.184

Yang, G., Tazoe, H., Yamada, M., 2018. Improved approach for routine monitoring of 129I activity and 129I/127I atom ratio in environmental samples using TMAH extraction and ICP-MS/MS. Analytica Chimica Acta 1008, 66–73. https://doi.org/10.1016/j.aca.2017.12.049

Young, C.-C., 2023. Recent Advances in Marine Environmental Research. Water 15, 462. https://doi.org/10.3390/w15030462

Appendix

Table A.1: Dry matter, Loss of ignition, organic matter and TOC for the sample site 3B (first NMBU samples).

% Loss of ignition	LOI	Org. C (TOC)= ~58% of LOI	no/name
0.799402	0.0995	0.05771	271/siteB 4-5
0.877973	0.1135	0.06583	282/siteB 8-9
0.822324	0.1088	0.063104	294/siteB 5-6
0.871513	0.107	0.06206	274/siteB 7-8
0.993893	0.1258	0.072964	269/siteB 10-12
0.790848	0.1028	0.059624	305/siteB 9-10
1.092764	0.154	0.08932	302/siteB 14-16
0.764999	0.0901	0.052258	254/siteB 6-7
1.570532	0.2212	0.128296	299/siteB20-22
0.749574	0.0902	0.052316	292/siteB12-14
1.007195	0.1236	0.071688	260/siteB 3-4
1.055574	0.1333	0.077314	256/siteB 22-24
0.956659	0.128	0.07424	255/siteB16-18
0.549468	0.0677	0.039266	263/siteB 0-3

Table A.2: ***First samples from Norway and Christiania***

Soils	**General comments and details**	**Samples' Notes**
L:BI	Digested on a hot plate for two days in HNO_3 and one day with ~3ml solution of 5% (V/V) HNO_3+ 0.1% (V/V) HF at around 125+ ^oC. Diluted once again with 6 ml of a solution of 5% nitric acid and 0.1% hydrofluoric acid. From the final elution, 1ml was taken for ICP-MS measurements.	**~12g sample**
L:BII		**done for U**
Sediments	**E7/21 site 3B**	
0-1 cm	Digested on hot plate for two days in HNO3 and one day with ~3ml solution of 5% (V/V) HNO3+ 0.1% (V/V) HF at around 125+ ^oC	2g +1.06 from ^{233}U
1-2 cm		2.01g (+1.06g ^{233}U tracer)
2-3 cm		1.98g (+1.06g)
18-20 cm		2g(+1.05g)
20-22 cm		2.01g (+1.06g)
6-7 cm	Normal Procedure followed.	2+1 g
9-10 cm		2+1 g
4-5 cm	Normal Procedure, but with leftovers in the Teflon columns of the 2nd digestion with the HF (should take into account later).	~2+1.068g
7-8 cm		~2+1.066g
12-14 cm		2+1 g
16-18 cm		~2+1.065g
14-16 cm	Normal Procedure followed.	~2+1.068g
3-4 cm		~2+1.063g
5-6 cm		**done for U**

8-9 cm	Normal Procedure Separated for ICP-MS (only U) and AMS (U & Pu) measurements. Diluted once again with 5-6 ml of a solution of 5% nitric acid and 0.1% hydrofluoric acid --> 1ml separated for ICP-MS.	**done for U**
10-12 cm		**done for U**
22-24 cm		2.01g +1.05g ^{233}U
0-3	sediment mix, not treated	
Christiania's	Normal Procedure	**done for U**
Nista 27ila	Normal Procedure (caused problems in the second measurement row)	1.0061+1.0657g
Tests		
S1	Refer. Mat. IAEA384 (CaC) + tracers ^{242}Pu 2020-02-046 & ^{233}U 2020-02-089 (1ml of each to each in T&S) - B&T 14ml Dwater. Ready and separated for ICP-MS measurements (U & Pu) and AMS preparation (U & Pu). Diluted once again with 5-6 ml of a solution of 5% nitric acid and 0.1% hydrofluoric acid --> 1 ml separated for ICP-MS. Normal Procedure followed.	**~2+2**
S2		**~2+2**
T1		**Only tracers**
T2		**Only tracers**
B1		**Only H2O**
B2		**Only H2O**
Sediments E7/21 site 2B		
0-1 cm	Normal Procedure followed.	0.995+1.067g
1-2 cm		1.913+1.063g
2-3 cm		1.958+1.066g
10-12 cm		1.821+1.064g
3-4 cm	soil face to get treated in CTU	
4-5 cm		
5-6 cm		
3 test samples		
Test samples 1-6	4353a Rocky Flats Soil Number 2 6X~1gr +1 ml tracer ^{233}U--> 15ml of 15,8M HNO_3--> warm up for couple of minutes +15 ml after, parts of sediment remaining should digest in HF. 1.821+2.885	
1		1.89g sum weight
2		1.918g sum weight
3		1.879g sum weight
4		1.87g sum weight
5		1.852g sum weight
6		1.952g sum weight

Στον πολυαγαπημένο μου καθηγητή Γιώργη Βώδινα,
που αποχώρησε νωρίς από τις ζωές μας
το 2023…

ΠΟΛΥΤΕΧΝΕΙΟ
ΚΡΗΤΗΣ /
TECHNICAL
UNIVERSITY
OF CRETE